



**HAL**  
open science

# Power Enhancement of Piezoelectric Technology based Power Devices by Using Heat Transfer Technology

Yu-Hao Su

► **To cite this version:**

Yu-Hao Su. Power Enhancement of Piezoelectric Technology based Power Devices by Using Heat Transfer Technology. Electronics. École normale supérieure de Cachan - ENS Cachan, 2014. English. NNT : 2014DENS0025 . tel-01215031

**HAL Id: tel-01215031**

**<https://theses.hal.science/tel-01215031>**

Submitted on 13 Oct 2015

**HAL** is a multi-disciplinary open access archive for the deposit and dissemination of scientific research documents, whether they are published or not. The documents may come from teaching and research institutions in France or abroad, or from public or private research centers.

L'archive ouverte pluridisciplinaire **HAL**, est destinée au dépôt et à la diffusion de documents scientifiques de niveau recherche, publiés ou non, émanant des établissements d'enseignement et de recherche français ou étrangers, des laboratoires publics ou privés.



**ENSC-2014n°523**

**THESE DE DOCTORAT  
DE L'ECOLE NORMALE SUPERIEURE DE CACHAN**

Présentée par

Monsieur Yu-Hao Su

**pour obtenir le grade de**

**DOCTEUR DE L'ECOLE NORMALE SUPERIEURE DE CACHAN**

Domaine :

**ELECTRONIQUE –ELECTROTECHNIQUE-AUTOMATIQUE**

**Sujet de la thèse :**

**Power Enhancement of Piezoelectric Technology based Power  
Devices by Using Heat Transfer Technology**

Thèse présentée et soutenue à Taipei le 4 juillet 2014 devant le jury composé de :

Wei-Hsin Liao	Professeur-CUHK, Hong Kong	Rapporteur
Marc Lethiecq	Professeur-Université Francois Rabelais, France	Rapporteur
Yuan-Ping Liu	Chief Executive Officer - Miézo Inc., Taiwan	Examinateur
Jay Shieh	Professeur-NTU, Taiwan	Examinateur
Faa-Jeng Lin	Professeur-NCU, Taiwan	Examinateur
Chih-yi Lin	Senior Manager-DELTA, Taiwan	Examinateur
Chih-Kung LEE	Professeur-NTU, Taiwan	Directeur de thèse
Wen-Jong WU	Professeur-NTU, Taiwan	Encadrant
Dejan VASIC	Maître de conférences HDR U. Cergy-Pontoise	Directeur de thèse
François COSTA	Professeur-ENS Cachan, France	Encadrant

Laboratoire Système et Application des Technologies de l'Information et de l'Energie  
ENS CACHAN/CNRS/UMR 8029  
61, avenue du Président Wilson, 94235 CACHAN CEDEX (France)

# ABSTRACT

The objective of this study was to increase the output current and power in a piezoelectric transformer (PT) based DC/DC converter by adding a cooling system. It is known that the output current of PT is limited by temperature build-up because of losses especially when driving at high vibration velocity. Excessive temperature rise will decrease the quality factor  $Q$  of piezoelectric component during the operational process. Simultaneously the vibration energy cannot be increased even if under higher excitation voltage. Although connecting different inductive circuits at the PT secondary terminal can increase the output current, the root cause of temperature build-up problem is not solved. This dissertation presents the heat transfer technology to deal with the temperature build-up problem. With the heat transfer technology, the threshold vibration velocity of PT can be increased and thus the output current and output power (almost three times).

Furthermore, a comparison between heat transfer technology and current-doubler rectifier applied to the piezoelectric transformer based DC/DC converter was also studied. The advantages and disadvantages of the proposed technique were investigated. A theoretical-phenomenological model was developed to explain the relationship between the losses and the temperature rise. It will be shown that the vibration velocity as well as the heat generation increases the losses. In our design, the maximum output current capacity can increase 100% when the operating condition of PT temperature is kept below  $55^{\circ}\text{C}$ . The study comprises of a theoretical part and experimental proof-of-concept demonstration of the proposed design method.

**Keywords:** Piezoelectric transformer, Cooling system, DC to DC converters, Smart structure, Power enhancement

## **Amélioration de la puissance des transformateurs piézoélectriques par gestion de l'échauffement**

L'objectif de cette étude est d'améliorer les performances des transformateurs piézoélectriques en terme de courant de sortie et de puissance pour des applications d'alimentation DC/DC, grâce à la gestion de l'échauffement. Le courant de sortie des transformateurs piézoélectriques, et donc la puissance transmise, sont directement liés à la vitesse de vibration qui pour des valeurs élevées engendre des pertes et une forte élévation de température. Cette élévation excessive de la température a comme conséquence le changement des caractéristiques du transformateur et plus particulièrement la diminution du facteur de qualité  $Q$ . Ainsi cela entraîne une limite structurelle de la puissance transmise du transformateur. Une solution pour augmenter le courant de sortie est l'utilisation d'un redresseur doubleur de courant, qui grâce à 2 inductances permet, à courant de charge donné, de diminuer la vitesse de vibration du transformateur, mais ne permet pas de régler le problème d'échauffement du transformateur.

Dans cette thèse nous proposons des moyens d'évacuation de la chaleur ainsi que le choix de l'environnement dans lequel le transformateur devra fonctionner. L'influence de différents systèmes de refroidissement d'un convertisseur DC/DC à base transformateur piézoélectrique est étudiée. L'étude thermique du transformateur piézoélectrique multicouche polarisé en épaisseur et ayant des électrodes circulaires met en évidence un comportement non linéaire. Une plaque vibrante piézoélectrique est d'abord envisagée pour créer un flux d'air qui augmente l'évacuation de chaleur par convection, puis un module de refroidissement utilisant l'effet thermoélectrique. Les mesures montrent que la première solution est plus avantageuse car elle améliore sensiblement les performances du transformateur pour un coût énergétique très faible. Une étude thermique par éléments finis complète cette étude, montrant que l'approche par schéma électrique est pertinente. La puissance que peut délivrer le transformateur sur une charge optimale est encore augmentée.

Enfin, ce travail montre qu'en combinant les dispositifs de refroidissement tout en respectant la condition de température inférieure à  $55^{\circ}\text{C}$ , le rendement du convertisseur reste raisonnable (70%) et la puissance disponible peut doubler dans le meilleur des cas.

**Mots clés:** Transformateur piézoélectrique, Système de refroidissement, Convertisseurs DC/DC, Smart structure, Augmentation de la puissance.

# CONTENTS

ABSTRACT .....	ii
CONTENTS .....	iv
LIST OF FIGURES .....	vii
LIST OF TABLES.....	xi
<b>Chapter 1 Introduction.....</b>	<b>1</b>
1.1 Backgrounds and Motivations .....	1
1.2 Literatures Review.....	2
1.2.1 Thermal Issues in Piezoelectric Materials.....	2
1.2.2 Thermal Limits of Piezoelectric Materials.....	3
1.2.3 Power Limits of Piezoelectric Transformers.....	4
1.3 Framework of the Dissertation .....	6
<b>Chapter 2 Basic Theory of the Piezoelectric Transformer.....</b>	<b>8</b>
2.1 Fundamentals of Piezoelectricity.....	9
2.1.1 Piezoelectric Materials .....	9
2.1.2 Piezoelectric Actuation Mechanisms .....	10
2.2 Different Configurations of Piezoelectric Transformers .....	13
2.2.1 Common Configurations of Piezoelectric Transformers .....	13
2.2.2 High Power Piezoelectric Transformers .....	16
2.3 The Equivalent Circuit of the Piezoelectric Transformer.....	18
2.4 Equivalent Circuit Extraction for the Piezoelectric Transformers .....	25
2.5 Losses in Piezoelectric Transformers .....	29
2.6 Characteristics of the Piezoelectric Transformers Connected with a Linear Load.....	35

2.7	Summary .....	39
<b>Chapter 3</b>	<b>Thermal Analysis of Multi-Layer Piezoelectric Transformer .....</b>	<b>40</b>
3.1	Introduction.....	40
3.2	Analysis of Heat Generation and Temperature Rise for Multi-layer Piezoelectric Transformers .....	40
3.3	Analysis of Temperature-Dependent Nonlinear Resistance in PT Equivalent Circuit .....	42
3.4	Heat Flowchart of the PT and PT's Control Loop of the Energy Losses .....	45
3.5	Experimental setup .....	49
3.6	Experimental results of PT with thermal dissipation layers .....	52
3.7	Summary .....	56
<b>Chapter 4</b>	<b>Power Enhancement of PT by Using Heat Transfer Equipment .....</b>	<b>58</b>
4.1	Introduction.....	58
4.2	Different Mechanisms of Heat Transfer Equipment .....	58
4.3	Experimental setup .....	62
4.4	COMSOL Simulation Result of Heat Generation and Temperature Rise for Multi-layer PT .....	71
4.5	Experimental Results and Discussion.....	73
4.6	Summary .....	76
<b>Chapter 5</b>	<b>Application: PT-Based DC/DC Converter with Planar Heat Transfer Equipment .....</b>	<b>78</b>
5.1	Introduction.....	78
5.2	Converter Topologies and Control Considerations .....	78
5.3	PT-Based Converter Circuit Diagram and Its Operation.....	80
5.4	Study of PT-Based DC/DC Converter with Cooling System and	

Current-Doubler Rectifier.....	83
5.5 Experimental Results and Discussion.....	85
5.6 Summary.....	94
<b>Chapter 6 Summary and Conclusion .....</b>	<b>96</b>
REFERENCE .....	100

# LIST OF FIGURES

Figure 2-1. Designation of the direction and axes of PT actuation mechanisms .....	12
Figure 2-2. The equivalent circuit of the piezoelectric structure.....	19
Figure 2-3. The simplified equivalent circuit of the piezoelectric layer. ....	20
Figure 2-4. (a) Equivalent circuit of the PT by connecting two piezoelectric layers (b) simplified format of physics-based equivalent circuit model for PTs.....	23
Figure 2-5. Final format of physics-based equivalent circuit model for PTs.....	23
Figure 2-6. 4294A impedance analyzer and PT equivalent circuit model .....	26
Figure 2-7. Input impedance of the “Type A” PT with resonant frequency (marker 0) and anti-resonant frequency (marker 1).....	27
Figure 2-8. Equivalent circuit of the electrostatic capacitor.....	31
Figure 2-9. Current in the equivalent circuit of capacitor .....	31
Figure 2-10. Equivalent circuit with dielectric losses .....	32
Figure 2-11. Simplified equivalent circuit.....	33
Figure 2-12. Equivalent circuit of PT connected to a load.....	35
Figure 2-13. (a) Reflecting the output capacitance $C_2$ and load $R_L$ from secondary side to primary side (b) reflecting the parameters from primary side to secondary side.....	36
Figure 2-14. Generic operational characteristics of piezoelectric transformers [63] .....	39
Figure 3-1. Nonlinear equivalent circuit of piezoelectric transformer. ....	43
Figure 3-2. The method of shortening the output terminal to measure the mechanical current and nonlinear resistance .....	45
Figure 3-3. Structure of PT and thermal layers .....	46
Figure 3-4. Heat flowchart of the PT associated with or without the heat dissipation	



device.....	47
Figure 3-5. (a) PT thermal feedback loop and (b) PT with cooling system thermal feedback loop.....	48
Figure 3-6. Experimental setup. ....	49
Figure 3-7. Characteristics between $Y$ (thermal conductance) and temperature rise.....	53
Figure 3-8. Relationship between the square of mechanical current and the $R_{NL}$ at different temperatures .....	53
Figure 3-9. Relationships between temperature and input voltage. ....	55
Figure 3-10. Relationships between mechanical current and input voltage.....	55
Figure 3-11. Output power enhancement in different methods.....	56
Figure 4-1. (a) Air cooling without any cooling device (b) Heat transfer equipment (HTE) (c) HTE and planar piezoelectric fan (d) HTE and thermoelectric cooling module .....	59
Figure 4-2. Nonlinear resistance $R_{NL}$ as a function of the square of mechanical current and at different temperatures .....	60
Figure 4-3. A comparison of the mechanical quality factor varied with temperature rise of PT between: PT with aluminum pad and PT without the aluminum pad.....	61
Figure 4-4. The half-bridge driving circuits with a piezoelectric transformer .....	62
Figure 4-5. The production of switching loss in the power MOSFET .....	63
Figure 4-6. The corresponding waveforms of the ZVS-mode half-bridge circuit.....	64
Figure 4-7. The operation of the ZVS-mode half-bridge circuit with a PT during mode 165	
Figure 4-8. The operation of the ZVS-mode half-bridge circuit with a PT during mode 266	
Figure 4-9. The operation of the ZVS-mode half-bridge circuit with a PT during mode 366	
Figure 4-10. The operation of the ZVS-mode half-bridge circuit with a PT during mode 4 .....	67

Figure 4-11. The operation of the ZVS-mode half-bridge circuit with a PT during mode 5 .....	67
Figure 4-12. The operation of the ZVS-mode half-bridge circuit with a PT during mode 6 .....	68
Figure 4-13. Experimental setup of PT based DC/DC converter.....	69
Figure 4-14. Total displacement plot at 89.73 kHz longitudinal frequency.....	72
Figure 4-15. Temperature distribution of PT and HTE (Driving by a sinusoidal input voltage with a peak of 25V after 300 seconds).....	73
Figure 4-16. Characteristics between temperature, mechanical current and input voltage	74
Figure 4-17. Characteristics between mechanical resistance $R_m$ , temperature and mechanical current.....	75
Figure 4-18. Characteristics between loop gain $\alpha(T^{\circ}\text{C})$ , mechanical current and temperature. ....	75
Figure 4-19. Output power and efficiency as a function of load in different cooling structures.....	76
Figure 5-1. The schematic diagram of piezoelectric transformer based DC/DC converter. ....	80
Figure 5-2. (a)The schematic diagram of PT fed full-wave rectifier (b) theoretical voltage and current waveforms of the PT fed full-wave rectifier (c) experimental waveform of PT input voltage $v_{in}$ (blue, 20V/div), PT input current $i_{in}$ (yellow, 1A/div), voltage at PT output terminal $v_{rec}$ (green, 5V/div) and current at PT output terminal $i_{rec}$ (purple, 0.5A/div). ....	81
Figure 5-3. Equivalent circuit of a (a) PT fed full-wave bridge rectifier (b) PT fed current-doubler rectifier.....	83
Figure 5-4. (a) Theoretical waveforms of the PT fed full-wave bridge rectifier and PT	

fed current-doubler rectifier (non-overlapping mode) (b) enhanced rectifier current limitation of full-wave bridge rectifier by using HTE and piezoelectric fan.....84

Figure 5-5. Experimental waveforms of PT input voltage  $v_m$  (C1, 50V/div), PT input current  $i_{in}$  (C2, 1A/div), voltage at PT output terminal  $v_{rec}$  (C3, 50V/div) and current at PT output terminal  $i_{rec}$  (C4, 1A/div) for (a) full-wave bridge rectifier (b) full-wave bridge rectifier with HTE and piezoelectric fan (c) current-doubler rectifier (d) current-doubler rectifier with HTE and piezoelectric fan.....86

Figure 5-6. Characteristics between (a) input voltage and temperature in optimal load condition  $R_{CD}^*$  (b) input voltage and mechanical current in optimal load condition  $R_{CD}^*$  (c) input voltage and temperature in optimal load condition  $R_{FB}^*$  (d) input voltage and mechanical current in optimal load condition  $R_{FB}^*$ .....88

Figure 5-7. Result of the  $R_{NL}$  as a function of the square of mechanical current at different temperatures and in optimal load conditions: (a)  $R_{CD}^*$  (b)  $R_{FB}^*$ ...90

Figure 5-8. Characteristics between mechanical current and temperature. (a) in optimal load condition  $R_{CD}^*$  (b) in optimal load condition  $R_{FB}^*$  .....91

Figure 5-9. Characteristics between loop gain  $\alpha$  and temperatures (a) in optimal load condition  $R_{CD}^*$  (b) in optimal load condition  $R_{FB}^*$  .....92

Figure 5-10. (a)Output power enhancement in different heat transfer structures (b) efficiency enhancement in different heat transfer structures.....94

# LIST OF TABLES

Table 1-1. Classification of piezoelectric materials .....	2
Table 2-1. The comparison of design between different piezoelectric transformers [36].	15
Table 2-2. Different types of power piezoelectric transformers [41].	17
Table 2-3. Coefficients of different vibration type piezoelectric layer at first mode [60].	20
Table 2-4. Relationships between dimension factors and electric equivalent components for various kinds of PTs [60] .....	23
Table 2-5. The relationship between 4294A and PT equivalent circuit model. ....	26
Table 2-6 Size and structure of PTs in this dissertation .....	27
Table 2-7. Properties and key parameters of the piezoelectric material.....	28
Table 2-8. The experimental result obtained by impedance analyzer .....	29
Table 3-1. Size and structure of experimental cases .....	50
Table 3-2. Properties of the PTs .....	50
Table 4-1. Picture, size and properties of the PT.....	69
Table 4-2. Experimental data of the thermoelectric cooling module specimen .....	70
Table 4-3. Properties of the piezoelectric fan and thermoelectric cooling module.....	70
Table 4-4. Merit and demerit of the piezoelectric fan and the thermoelectric cooling module .....	77
Table 5-1. Characteristics of the PT fed rectifier. ....	82
Table 5-2. Characteristics of the PT fed rectifier [14][21]. ....	84

# Chapter 1 Introduction

Considering the case of large current ( $>1A$ ), the piezoelectric transformer (PT) easily becomes unstable or even crack with temperature rise because of the excessive internal losses. The output current of PT is also limited by temperature build-up effect owing to the heat generated by mechanical and electrical losses especially when driving at high vibration velocity. Once the PT exceeds a threshold vibration velocity, the temperature rise of PT would significantly increase and lead to instability. PT based power converters are therefore used commonly in high voltage and low current applications with a frequency-tracking mechanism adaptive to loading conditions. It should be noted that the restricted range of PT's output current leads to the limitation of output power. However, it is possible to increase the threshold vibration velocity, as well as the limitation of mechanical current, by using heat transfer technology. Once the threshold vibration velocity caused by the temperature rise can be increased, it represents the enhancement of the PT's maximum output current and output power.

## 1.1 Backgrounds and Motivations

Compared with an electromagnetic transformer, PT have several inherent advantages such as better efficiency, low profile, no EMI radiation, high power density, and easier for mass production. Accordingly, PTs are good substitutes of electromagnetic transformers especially in high voltage/low current applications, such as electronic ballasts or LCD (liquid crystal display) backlight inverters. However, the temperature build-up problem due to excessive internal losses is the predominant limitation of the piezoelectric transformers on high passing current applications [1]-[3]. Considering the case of large current ( $>1A$ ), the piezoelectric transformer easily becomes unstable or even crack with temperature rise because of the excessive internal

losses. In fact, internal heat generation in piezoelectric transformers represents internal losses in steady-state. Since internal loss, as well as heat generation, is the physical limitation of the piezoelectric transformers, several researches focused on modeling and explaining internal losses of piezoelectric transformers at high power condition.

## 1.2 Literatures Review

### 1.2.1 Thermal Issues in Piezoelectric Materials

Piezoelectric materials possess many advantages, such as reversible, easy integration, easy manufacture, low power requirements, abilities of low-profile and low weight, etc. Considering the stiffness and actuation response for different application areas, such as actuators and sensors, piezoelectric materials can be simply classified as follow three groups: single crystal, piezo-ceramic materials and piezo-polymer materials. Three widely-used piezoelectric materials are arranged in Table 1-1:

Table 1-1. Classification of piezoelectric materials

<b>Piezoelectric Materials</b>	<b>Typical Martial</b>	<b>Merit and Demerit</b>
1. Single crystal	Quartz	<ul style="list-style-type: none"> <li>● Higher electromechanical coupling</li> <li>○ Difficult to enlarge the size</li> <li>○ High manufacturing cost</li> </ul>
2. Piezo-ceramic	PZT (Lead Zirconate Titanate)	<ul style="list-style-type: none"> <li>○ Medium electromechanical coupling</li> <li>● Easy to mass manufacture</li> <li>○ Easy crack</li> </ul>
3. Piezo-polymer	PVDF (Polyvinylidene fluoride)	<ul style="list-style-type: none"> <li>○ Lower electromechanical coupling</li> <li>● Thinnest profile (piezoelectric)</li> </ul>

$\text{PbZr}_{1-x}\text{Ti}_x\text{O}_3$  (PZT) ceramics with morphotropic phase boundary (MPB) compositions have anomalously high dielectric and piezoelectric properties. As a result, PZT ceramics have been used for high power density applications because high coercive field is desirable [3][5]. However, non-linear effects caused by heat become significant in high power applications. Hysteresis losses caused by cyclic fields tend to intensify under high electric field and thus the thermal stress and heat generation [6]. Thermal problem leads to the result that the material properties no doubt will be changed. Furthermore, high intensification of the temperature gradient may cause rapid crack or thermal shock fracture growth [7]. It should be noted that the fracture behaviors of piezoelectric materials are more complex than that in conventional materials owing to the complicated coupling relationship between mechanical and electric behaviors [8]. Except the fracture problem, thermal depolarization condition cannot be avoided when the component temperature exceeds one-half the Curie temperature [9]. The thermal problems in piezoelectric materials become as the physical limitation and need to be dealt with especially in the high power applications.

### 1.2.2 Thermal Limits of Piezoelectric Materials

During operation, losses of the piezoelectric components are usually converted into thermal energy that leads to the temperature rise as the temperature build-up effect. Hirose *et al.* and Uchino *et al.* investigated the internal loss of high-power piezoelectric transducers and they divided internal loss of piezoelectric transducers into three parts: dielectric losses, mechanical losses, and piezoelectric losses. They also modeled losses in an equivalent circuit [10]-[12]. Generally, thermal limits are directly linked to the internal losses. It should be noted that thermal limits not only concentrate on the depolarization due to the overheating problem, but also the temperature build-up effect

that may lead to changes of piezoelectric material properties as the constrain of the output power and performance. For instance, excessive temperature rise will decrease the quality factor  $Q$  of piezoelectric component during the operational process. Simultaneously the vibration energy cannot be increased even if under higher excitation voltage [13]. This phenomenon can be regard as the physical limitation of the piezoelectric materials.

Although there are many other constrains as the limit of piezoelectric material such as electric breakdown strength, maximum surface charge density, maximum stress and maximum strain [3]. Temperature build-up problem arising from excessive internal losses is the predominant limitation of piezoelectric components especially in high vibration level condition. As to the piezoelectric transformer made with PZT materials, the theoretical power density of piezoelectric transformers calculated by stress boundary can reach  $330 \text{ W/cm}^3$  [3], but no piezoelectric transformer has ever reached such a high power density in practice. The power density of piezoelectric transformers is limited to  $33 \text{ W/cm}^3$  in practical applications. The underlying reason is that the maximum passing current of the piezoelectric material (mechanical current) is limited by the temperature rise caused by heat generation. In applications, high-power piezoelectric devices always accompany with high vibration velocity and temperature rise. It should be noted that the effect creates a limiting factor of temperature for piezoelectric materials.

### 1.2.3 Power Limits of Piezoelectric Transformers

Nowadays, DC/DC converter trends are increasing demands on high power density, high efficiency, and miniaturization. PT based DC/DC converter was an attractive candidate due to several advantages such as high efficiency, low profile, no EMI radiation, high power density and easier for mass production. However, in practice it is



not easy to control PT in a converter. PT-based converter prefers operated in narrow bandwidth, fixed loading condition and high voltage / low current applications. In past years, the solution to operate at fixed frequency was proposed [14]-[19] and it improves the feasibility of the PT based converters, but the limitation of the output current (power) capacity of PT-based converter is still a problem. As to the power limit of piezoelectric transformer, temperature build-up effect, electromechanical limits and the circuit topology especially in the output rectifier are the predominant causes that should be taken into consideration [20]. Many researches made efforts to increase the output current of the converter by connecting different inductive circuits at the PT secondary terminal, such as step-down transformer and the current-doubler rectifier [21]-[22]. However, adding the inductive circuit sacrifices the inherent advantage of the PT, and the root cause of temperature build-up effect is still an unsolved problem as the physical limitation. This physical limitation is due to limit value of the vibration velocity of the PTs. Once the PT exceeds the vibration velocity threshold, the temperature rise of PT would increase dramatically and start temperature build-up, increase the internal losses and cause instability. Typically, the large output current is directly linked with high vibration velocity [23] , so the PT is difficult to apply in the high current applications.

To understand the relationship between the temperature rise and the internal loss of the PT, Uchino *et al.* divided the internal loss into three parts in the equivalent circuit of the piezoelectric transducers [12]. Wakatsuki *et al.* and Joo *et al.* calculated the internal losses by strain, stress, electrical displacement, and electric field distribution by finite element modeling [24]-[25]. Thomas *et al.* presented a method to determine the resulting temperature distribution which caused by internal losses in piezoelectric slabs [26]. Moreover, Albareda *et al.* verified the increment of the dissipation resistance and the temperature rise are both directly proportional to the square of the vibration velocity

near the mechanical resonance frequency of the PT [27]. This result can be used to establish a prediction phenomenological theoretical model. According to the previous results, we know that the maximum power of the PT is possible to be increased by means of preventing the overheating problem. There were several options to dissipate the heat efficiently. Insung *et al.* proposed a ring-dot-shape piezoelectric transformer with a central hole to obtain a better thermal radiation [28]. This design could achieve more uniform temperature distribution and decrease the maximum temperature of the PT structure; therefore the output current can be increased. Shao *et al.* adopted the contact heat transfer to dissipate the heat on the PT in order to improve the power density of PTs [29]. In our previous research, a novel cooling method which combined the heat transfer equipment and thermoelectric cooling module to dissipate the heat and can effectively enhance the output power of PT [30]. However, the cooling device cannot satisfy the low-profile requirements and the power consumption of the thermoelectric cooling module was too high to get high efficiency of the entire PT system. To overcome the problem, we added low-profile commercial thermal pads to the PT with an auxiliary piezoelectric fan to dissipate the heat and to improve the output power simultaneously [31].

### **1.3 Framework of the Dissertation**

This dissertation includes six chapters. The major content of each chapter is offered as follows:

**Chapter 1** makes the introduction of this dissertation.

**Chapter 2** presents the basic theory of the piezoelectric structure, introduces the different configurations of PT, derives the general equivalent circuit of piezoelectric

structure, and demonstrates the measurement method of the equipment circuit.

**Chapter 3** analyses the physical limitation of piezoelectric transformers and presents the thermal analysis of PT. To analyze the working characteristic of piezoelectric transformer at high vibration level, a nonlinear equivalent circuit which contains the temperature-dependent nonlinear resistance was used.

**Chapter 4** develops different mechanisms of heat transfer equipment to improve the output power (current) of PT. After utilizing the heat transfer equipment, the experiment result shows the mechanical current of the piezoelectric transformer can increase from 0.382A @ 2W to 0.972A @ 9W and the maximum output power of the piezoelectric transformers increase from 3.43W to 9.29 W at specific temperature. In this chapter, COMSOL Multiphysics version 3.5a was used to observe the heat generation and temperature distribution of the multi-layer PT to verify the experimental result.

**Chapter 5** implements the proposed PT with cooling system into a DC/DC converter. The vibration velocity, dimensional constraints, energy balance, quality factor correction and ZVS conditions are all considered to develop the complete design procedure. In the chapter, we also compare the output current capacity and the size of two different rectifying circuits, the full-wave bridge rectifier and current-doubler.

**Chapter 6** concludes the result of this dissertation, and give some suggestions for future research.

## **Chapter 2 Basic Theory of the Piezoelectric Transformer**

Piezoelectric transformers (PTs) made with piezoelectric materials have been extensively commercialized in recent years because of the unique electro-mechanical properties. Piezoelectric materials possess the ability to couple mechanical and electrical fields so that there are many different applications can be achieved with the piezoelectric layers such as sensors, resonators, actuators, dampers, harvester, and transformers. According to the characteristic of piezoelectric material and direct inverse piezoelectric effect, PTs have several inherent advantages such as better efficiency, low profile, no electromagnetic interference (EMI) radiation, high power density, and ease of mass production comparing to the conventional electromagnetic transformers.

However, PTs for power applications should take into consideration not only the material characteristic but the basic mechanical and electrical behaviors of the piezoelectric structure especially the vibration and the generated electrical energy of a piezoelectric structure. The objective of this chapter was to build up a theoretical model to connect the mechanical vibration and the electrical properties for PTs. Except for the theoretical analysis of different PTs vibration types, equivalent electrical circuit was utilized to analyze the relationship between piezoelectric structure dynamics and external shunt circuits. The analysis developed in this chapter describes the basic theory of the piezoelectric transformer, which is the basis of the following chapters. For high power application, a more important subject is to deal with the extensive internal losses of PTs at high vibration level. In this chapter, we also investigated the internal losses of PTs and presented a measurement method to quantify the losses. Therefore, PTs can be properly designed base on the theoretical analysis and method.

## 2.1 Fundamentals of Piezoelectricity

### 2.1.1 Piezoelectric Materials

The unique characteristic of piezoelectric materials, which is direct piezoelectric effect and inverse piezoelectric effect, was discovered by Jacques and Pierre Curie in 1880's. Piezoelectric effect can be seen as the reversible process, and there is a linear electromechanical interaction between the mechanical and the electrical state in crystalline materials with no inversion symmetry [32]. Direct piezoelectric effect and inverse piezoelectric effect can be described:

- Direct piezoelectric effect: when a mechanical force is applied, the internal generation of electrical charge can be produced but not exceeding their withstanding limitation. Piezoelectric actuators operate based on this effect.
- Inverse piezoelectric effect: when an electrical field is applied, the internal generation of mechanical strain can be produced but not exceeding their withstanding limitation. Piezoelectric transducers operate based on this effect.

As mentioned in section 1.2, piezoelectric materials can be broadly classified into three groups: single crystal, piezo-ceramic materials and piezo-polymer materials. In this dissertation, we utilize the lead zirconate titanate (PZT) material to build-up our power devices according to the good electromechanically coupling and easier automatic manufacturing process. PZT (chemical notation:  $\text{PbZr}_{1-x}\text{Ti}_x\text{O}_3$ ) is the most common piezo-ceramic, and its piezopolymer counterpart is Polyvinylidene Fluoride (PVDF). Lead Zirconate Titanate (PZT) possesses the abilities of high actuation authority and fast actuation response so that it is a suitable actuator. In contrast with PZT, PVDF can be used to manufacture sensor because of the flexible, low stiffness and high damping characteristics. Like most piezoelectric devices, piezoelectric transformers are often manufactured from PZT or barium titanate ( $\text{BaTiO}_3$ ) based ceramic compositions

owing to their high coupling coefficients, high Curie temperature and ease of poling [33]. From previous research [34], we can also find out the result that the mechanical quality factor  $Q$  and electrical properties can be seen as a function of Curie temperatures for piezoelectric materials. No matter what kind of ceramic compositions, temperature is biggest effect factor on PTs' performance. The reason is that the structure and properties of the materials must be partially or completely changed [13] when the temperature of PT operates under or above a special point, *i.e.* Curie point. In recent years, PTs have extended to high power applications and the performance of PTs limited by the internal power dissipation. The heat generation and build-up hysteretic effects lead to the result of thermal instability. Furthermore, high intensification of the temperature gradient may cause rapid crack or thermal shock fracture growth [7]. It should be noted that the fracture behaviors of piezoelectric materials are more complex than that in conventional materials owing to the complicated coupling relationship between mechanical and electric behaviors [8]. Except the fracture problem, thermal depolarization condition cannot be avoided when the component temperature exceeds one-half the Curie temperature [9]. The thermal problems in piezoelectric materials become as the physical limitation and need to be dealt with especially in the high power applications. For instance, excessive temperature rise will decrease the quality factor  $Q$  of piezoelectric component during the operational process. Simultaneously the vibration energy cannot be increased even if under higher excitation voltage [13]. The PZT is the proper material for PT's high power applications owing to the high Curie temperature ( $>300\text{ }^{\circ}\text{C}$ ) and high quality factor  $Q$  ( $>1400$ ).

### 2.1.2 Piezoelectric Actuation Mechanisms

Using piezoelectric transformers requires the understanding of mechanical and

electrical performance issues, characteristics of the piezoelectric material, and the deformation behavior and the electrical behavior of the structure. Understanding the basic concepts behind actuation mechanisms and elastic body may also be beneficial to designing and controlling PTs. The physical behaviors of piezoelectric elements can be described by the linear relationships such as elastic equations of motion, compatibility, and constitutive law. The elastic equations of motion can be seen as the relationship between the displacement, *i.e.* acceleration, and the stress. The compatibility is the relationship between the displacement and the strain related to the geometrical deformation of the structure. In addition, the constitutive law it describes the relationship between the stress and the strain, as determined by material characteristics. Since the material characteristics of piezoelectric ceramics are anisotropic, the physical constants of the constitutive law are generally given two subscript indices, *i.e.* tensor quantities, which refer to the direction of the two related quantities as shown in equation (2-1):

$$\begin{bmatrix} T_p \\ D_k \end{bmatrix} = \begin{bmatrix} c_{pq}^E & -e_{kp} \\ e_{kq} & \varepsilon_{ki}^S \end{bmatrix} \begin{bmatrix} S_q \\ E_i \end{bmatrix} \quad (2-1)$$

Where  $T_p$ ,  $S_q$ ,  $D_k$ , and  $E_i$  are the matrices of stress, strain, electric displacement, and electric field respectively;  $c_{pq}^E$ ,  $e_{kq}$ ,  $-e_{kp}$  and  $\varepsilon_{ki}^S$  are the matrices of elastic stiffness, piezoelectric stress/charge constant, piezoelectric stress/charge constant conjugation, and dielectric or permittivity constant respectively. The subscripts  $i, k = 1 \sim 3$  and  $p, q = 1 \sim 6$  represent the direction of each parameters and all the expression are based on the IEEE standard as shown in figure 2.1:

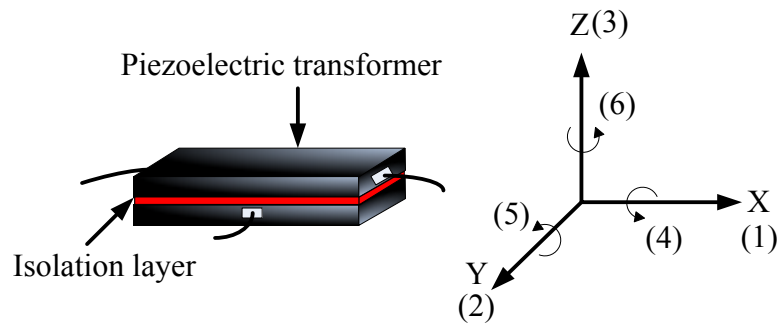


Figure 2-1. Designation of the direction and axes of PT actuation mechanisms

There are many different types of vibration behavior for the piezoelectric structures, and their corresponding dimensional conditions are complex owing to the fact that the vibration behavior is in three dimensional directions. As to the vibration behavior for the piezoelectric structures, it can be roughly divided into five types such as longitudinal mode, transverse mode, radial mode, thickness vibration mode, and shear mode.

- The longitudinal mode means that the electrical field (voltage) is applied along the poling direction (3-direction) to induce the vibration along the corresponding parallel direction (3-direction).
- The transverse mode means that the electrical field (voltage) is applied along the poling direction (3-direction) to induce the vibration along the corresponding perpendicular direction (1-direction).
- The radial mode is similar to the transverse mode. The applied voltage is perpendicular to the direction of the vibration, but the radial mode is a two dimensional vibration based on the symmetric characteristic.
- In shear mode, the electric field is orthogonal to the direction of polarization and a shear vibration is produced along the surface. The shear modes in plates can be divided into two categories, thickness-shear mode (15 mode) or thickness-twist mode [35]. It is depending on whether the shear displacement is parallel or



perpendicular to the wave propagation or mode variation direction.

## **2.2 Different Configurations of Piezoelectric Transformers**

### **2.2.1 Common Configurations of Piezoelectric Transformers**

Piezoelectric transformers possess the ability to transfer electrical energy from one circuit to another with structural vibration mechanism. No matter what kind of PT, it can be divided into two sections: which are the input section (primary side) and the output section (secondary side). The operating principle of PTs is: mechanical vibration in PT's input section can be excited by an input voltage source. Then, based on the electro-mechanical capacity, the output section of the PT receives the mechanical energy of the vibration and transforms into electric energy again. In practical application, a shunt circuit will connect to the secondary side of the PT to collect the electrical energy and to deliver it to the load. The primary side of the PT can be seen as a piezoelectric actuator that transforms the electrical energy to the mechanical energy. On the other hand, the output section converts the electrical energy transformed from the mechanical energy as a piezoelectric transducer. The categories of the piezoelectric transformers can be roughly divided into four types with different vibration modes and design considerations: Rosen, radial mode, thickness mode, and thickness-shear mode [36].

- **Rosen transformer (longitudinal vibration mode)**

The Rosen transformer's major concept is about a combination of ceramic piezoelectric material poled in opposite directions: a transverse mode piezoelectric actuator on the primary side and a longitudinal mode piezoelectric transducer on the secondary side [36]. Rosen-type transformers are suitable for step-up transformers since they provide high gain and high output impedance [37][38][39]. The frequency when

operating under longitudinal mode is around the order of 100k Hz. The single-layer Rosen-type transformer can provide a gain in the ratio of PT thickness to half length; therefore, multi-layer transformers have been developed to achieve higher voltage transforming ratios by introducing the number of layers. The typical uses of Rosen transformer were in CCFL backlighting [40]. In general, the typical Rosen transformer can generate an output power of 5-8 W, power density of 5-10W/cm<sup>3</sup>, and has a mass of around 2g [41].

- **Radial vibration mode PTs**

The representative of this vibrational mode is ‘Transoner’ PT, developed by Face Electronics in 1996 [41]. It mainly utilizes multiple stacked disc based piezoelectric material poled in the thickness direction [36]. By altering the amount of layers in the primary and secondary regions, the output can be controlled. The expected resonance frequency is around 50 to 250k Hz and it can provide a respectable power density of 40W/cm<sup>3</sup> [41]. The key in radial vibrational mode is the circular disc system, where the distance from the edges to the center would be equal, thus creating the best electromechanical effects [43]. Higher output power capacity can be achieved with the radial mode design comparing to an ordinary Rosen PT [45]. Transoners were utilized as step-up and step-down devices in fluorescent lamps ballasts.

- **Thickness vibration mode PTs**

The thickness vibrational mode works as the combination of two piezoelectric elements: a longitudinal mode piezoelectric actuator and a longitudinal mode piezoelectric transducer.. In the past, a major problem to this mode lies in the fundamental features of the material. PZT used in thickness mode PTs, has a high thickness mode

electromechanical coupling factor and a high transverse mode coupling factor. When the PT is vibrating, there may be make spurious vibrations, because the resonant frequencies for length and width modes are lower than that of the thickness mode. This causes undesirable losses and strain to the piezoelectric transformer [45]. Spurious vibrations from undesired modes increase the PT losses, increase the mechanical strain in the PT material, and attenuate the main vibration mode [46]. Those results lead to the lower efficiency, the lower effective coupling factor, and the reduction in maximum power density [46]. To overcome the problem, an evolution of the thickness mode PT was presented by Noliac in 2000 [46]. The Noliac design is ring shaped, has single or multilayer primary and secondary sections, typical power densities of  $\approx 50\text{W/cm}^3$ , and efficiencies exceeding 98%.

- **Thickness-shear vibration mode PTs**

The shear mode is different from the aforementioned mode because the major electric fields are applied orthogonally to the direction of the poles within the PT [47]. By exciting the primary section, shear strain is formed within the PT, thus generating a potential difference towards the secondary section. While this mode generates substantially greater amount of energy, its production method is slightly more difficult since it requires two distinct sets of electrodes for this mode to work properly [48].

Table 2-1. The comparison of design between different piezoelectric transformers [36].

<b>PT:</b>	<b>Rosen</b>	<b>Face Transoner</b>	<b>Noliac ring-type</b>	<b>Thickness-shear</b>
<b>Type of poling:</b>	thickness and length	unipolar: thickness	unipolar: thickness	unipolar: normal to E-field

<b>Vibration mode:</b>	longitudinal	radial	thickness	thickness-shear
<b>Transformation type:</b>	step-up	step-up/step-down	step-down	step-down
<b>Typical power density (W/cm<sup>3</sup>)</b>	5-10	40+	≈50	18 [47]
<b>Maximum power output (W)</b>	5-20	100+	50+	170 through 2 outputs
<b>Resonant frequency</b>	30-120kHz	50-250kHz	≈330kHz	≈260kHz

### 2.2.2 High Power Piezoelectric Transformers

The application of PTs has moved beyond the scope of mere CCFL backlighting. Researchers are putting effort in applying PTs in the area of power consumerism such as battery chargers, power supplies, converters, etc. The best way to improve the efficiency is to upgrade the whole system. Therefore, fields such as manufacturing, functionality and size are the main focus for development. The area that needs to be included in these applications includes step-down transformers with high power output, high efficiency power and output conversions, and low impedance. One of the frontrunners of this research is O.M. Stuetzer in 1966 [49]. He presented the basic idea of attaching piezoelectric disks on the opposite facets of a metal wall. Even though his idea was not viewed with great attention, it provided a jumping board for later research.

Thickness vibrational mode, i.e. Table 2-2 research (a), was brought into the spotlight by NEC in Japan in the 90s. The thickness model of 1 to 2 mm was considered in various works and the operating frequency were as high as 1 MHz [50][51][52]. The patents were are still held by the researchers of that time for the thickness vibrational mode models [53][54]. However, researchers in NEC soon realized that substantial

amount of power were lost by current circulation, thus a new designs were proposed, as seen in Table 2-2 research (a) and (c). Specifically, longitudinal vibration mode were used [54][56], but their level of efficiency still left a lot to be desired. In addition, Korea research groups [57] have refined the initial uni-poled PT developed by Berlincourt in late 60s and re-considered them for step-down applications, i.e. Table 2-2 research (d). An U.S. based company named Face Electronics invented the radial mode transformer in 1996, as seen in Table 2-2 research (f) [58]. The power density and toughness has proved to be much better than previous designs and it served as a transformer model for future use. In the early 2000, an innovative use inductor-less drivers has eliminated the requirement of magnetic components. The aforementioned model is commercially called Transoner, and it is capable of providing energy at a density of 40W/cm<sup>3</sup>. Other designs has also being developed, such as the contour-extensional design shown in Table 2-2 research (g) [59] and the ring-shaped thickness design as shown in Table 2-2 research (e)[59].

Table 2-2. Different types of power piezoelectric transformers [41].

Research	(a) Japan NEC,1992 [50]-[52]	(b) Japan, NEC,1995 [55][56]	(c) Japan, NEC,1995 [55][56]	(d) Korea [57]
Vibration Mode	Thickness	Longitudinal	Longitudinal	Contour
Polarization	Unipoled: Thickness	Unipoled: Longitudinal	Unipoled: Transversal (Thickness)	Thickness
Resonant Freq.	1MHz	50-150kHz	50-150kHz	50-150kHz
Research	(e) Europe, Noliac,	(f) USA, Face,	(g) Japan, NEC,	

	1998[59]	1996[58]	1997[59]
Vibration Mode	Thickness	Radial	Contour
Polarization	Unipoled: Thickness	Unipoled: Thickness	Unipoled: Thickness
Resonant Freq.	400kHz	50-250kHz	50-250kHz

## 2.3 The Equivalent Circuit of the Piezoelectric Transformer

The equivalent circuit often used to describe the piezoelectric elements since piezoelectric layers are usually connected to a circuit or even used as an electric component in a power system. Owing to the fact that piezoelectric transformer is the combination of two piezoelectric elements as the actuator and transducer, piezoelectric transformer can be derived by connecting two physics-based equivalent circuit models of piezoelectric elements. In this section, we can analyze the equivalent circuit model of the single piezoelectric element first. The modeling methodology is then extended to the piezoelectric transformer and used to analyze the working condition of PT.

The physics-based equivalent circuit model for the single piezoelectric element can be represented as shown in Figure 2-2.

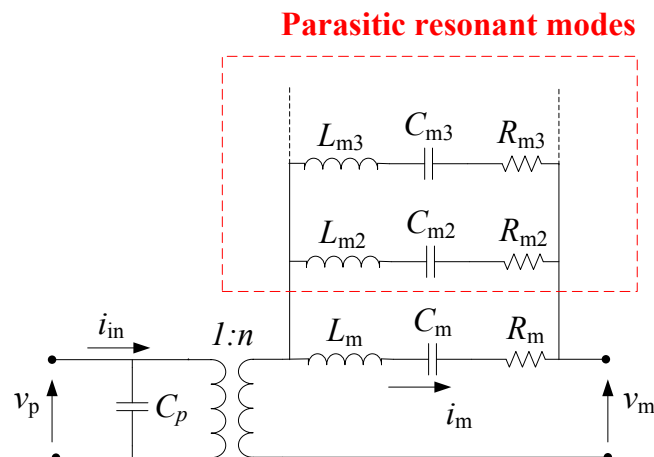


Figure 2-2. The equivalent circuit of the piezoelectric structure

The series inductor-capacitor-resistor resonant branch composed of mechanical inductor  $L_m$ , mechanical capacitor  $C_m$ , and mechanical resistor  $R_m$  can be used to emulate the mechanical resonance of the vibration. There are many other resonant branches in the equivalent circuit owing to the existence of infinite vibration mode in the piezoelectric structure, and they can be seen as the parasitic resonant modes in the piezoelectric structure. No matter which type of vibration mode, Figure 2-2 illustrates the equivalent circuit that describes the electro-mechanical behavior of the piezoelectric structure and the energy transformation between the mechanical energy and the electrical energy at the resonance [60].

In Figure 2-2, the mechanical current  $i_m$  and mechanical voltage  $v_m$  can be analog to the mechanical velocity and the mechanical force respectively. As to other equivalent parameters, they can be derived based on this physics-based equivalent circuit model [61]:

- $v_p$  is the applied or induced voltage on the electrode plates,
- $C_p$  is the capacitance between the electrode plates,
- $L_m$  is the equivalent mechanical mass analogy to electric inductor,
- $C_m$  is the equivalent mechanical compliance analogy to electric capacitor,
- $R_m$  is the equivalent mechanical resistance analogy to electric resistor,
- $v_m$  is the equivalent mechanical force analogy to electric field,
- $n$  is the equivalent mechanical force factor analogy to turns ratio.
- $L_{m2}$ ,  $C_{m2}$ ,  $R_{m2}$ ,  $L_{m3}$ ,  $C_{m3}$ , and  $R_{m3}$  are the equivalent parameters of the parasitic resonant modes

It should be noted that the parasitic resonant modes can be neglected owing to the

fact that the piezoelectric structure operates at a specific frequency in most cases. Therefore, the equivalent circuit of Figure 2-2 can be simplified to Figure 2-3.

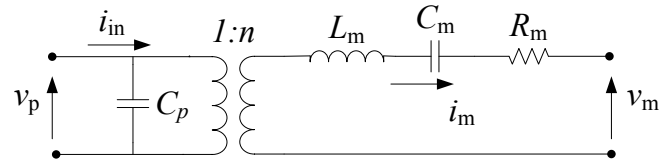


Figure 2-3. The simplified equivalent circuit of the piezoelectric layer.

Although the relationship between the dimensional parameters and the equivalent circuit components are different depending on the operating vibration modes and wavelengths even for the same vibration type, the first mode is the most often used vibration mode in practice. Therefore, based on the different vibration type of condition, the relationships between the dimensional parameters and the equivalent circuit components of the first mode equivalent circuit were arranged as shown in Table 2-3.

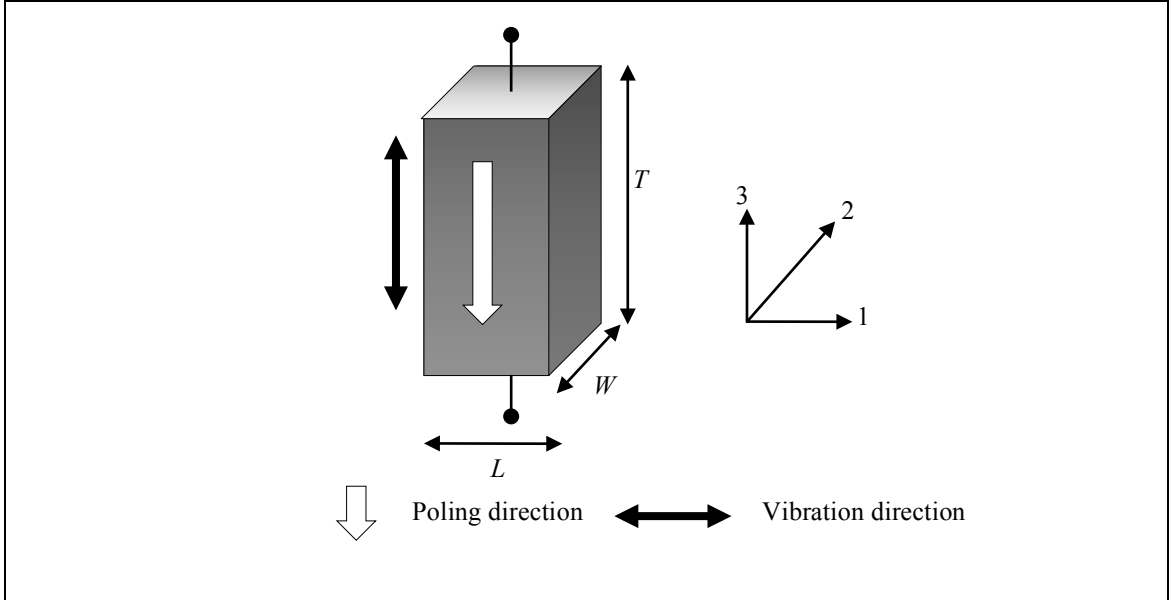
Table 2-3. Coefficients of different vibration type piezoelectric layer at first mode [60].

Types	$\omega_0$	$L_m$	$C_m$	$R_m$	$C_p$	$n$
31	1. $\frac{4z}{L}$	2. $\frac{\rho_m}{L}$	3. $\frac{1}{L^2}$	4. $\frac{1}{Q_m}$	5. $\epsilon_{33}^S$	6. $\frac{Wd_3^E}{s_{11}^E}$

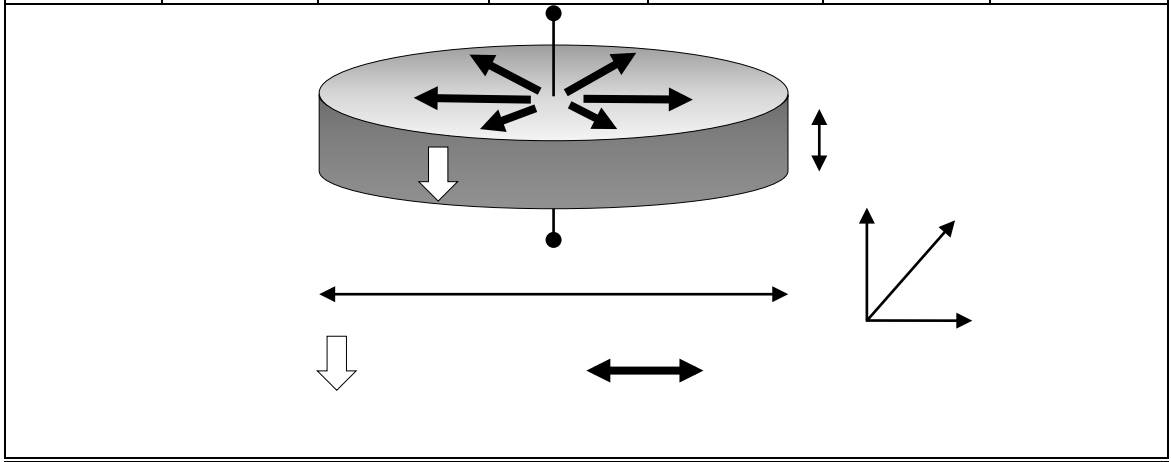
Poling direction      Vibration direction



7. 3 3	8. $\frac{4\lambda}{\rho_m}$	$\rho_m$	9. $\frac{1}{L_n}$	10. $\frac{1}{Q_m}$	11. $\epsilon_{33}^S$	12. $\frac{Wd_3}{s_{11}^E}$
-----------	------------------------------	----------	--------------------	---------------------	-----------------------	-----------------------------



13. R a d i a l	14. $\frac{\pi d}{t}$	15. $\frac{\rho_m}{t}$	16. $\frac{1}{L_n}$	17. $\frac{1}{Q_m}$	18. $\epsilon_{33}^S$	19. $\frac{2\pi}{s_{11}^E}$
--------------------------------	-----------------------	------------------------	---------------------	---------------------	-----------------------	-----------------------------



20.  $\omega_0$  is the natural frequency of the PT (rad/s).  
 $N_L, N_P$  are the frequency constants in the longitudinal vibration and the plane vibration respectively ( $\text{kHz}\cdot\text{mm}$ ).  
 $\rho_m$  is the density ( $\text{kg}/\text{m}^3$ ).  
 $\nu$  is the Poisson's ratio.  
 $Q_m$  is the mechanical quality.  
 $\epsilon_{33}^S$  is the permittivity at constant strain condition, i.e. constant  $S$  ( $\text{F}/\text{m}$ ).  
 $d_{31}, d_{33}$  are the piezoelectric constants ( $\text{m}/\text{V}$ ).  
 $s_{11}^E, s_{33}^E$  are the compliance constants under the constant electric field.  
 $L, W$  and  $T$  are the dimensional factors of the rectangular PT, which represent length, width and thickness respectively.  
 $R$  is the dimensional factors of the circular PT (i.e. Diameter of the circular PT= $2R$ ).

As mentioned before, piezoelectric transformer can be seen as the combination of two piezoelectric elements, i.e. actuator and transducer. The equivalent circuit model can be extended from the piezoelectric element to the piezoelectric transformer and well matched. Figure 2-4(a) illustrates the physics-based equivalent circuit model of a piezoelectric transformer composed of two piezoelectric elements, i.e. input section and output section. Each section can be seen as the single piezoelectric element but linked together to represent the electrical-to-mechanical energy transformation. According to the same simplifying method, this equivalent circuit is only valid when the PT is operating near its specific resonance frequency. In addition, the physics-based equivalent circuits in Figure 2-4(a) can be linked based on prior works [60], so that we can derive the whole physics-based equivalent circuit as shown in Figure 2-4(b).

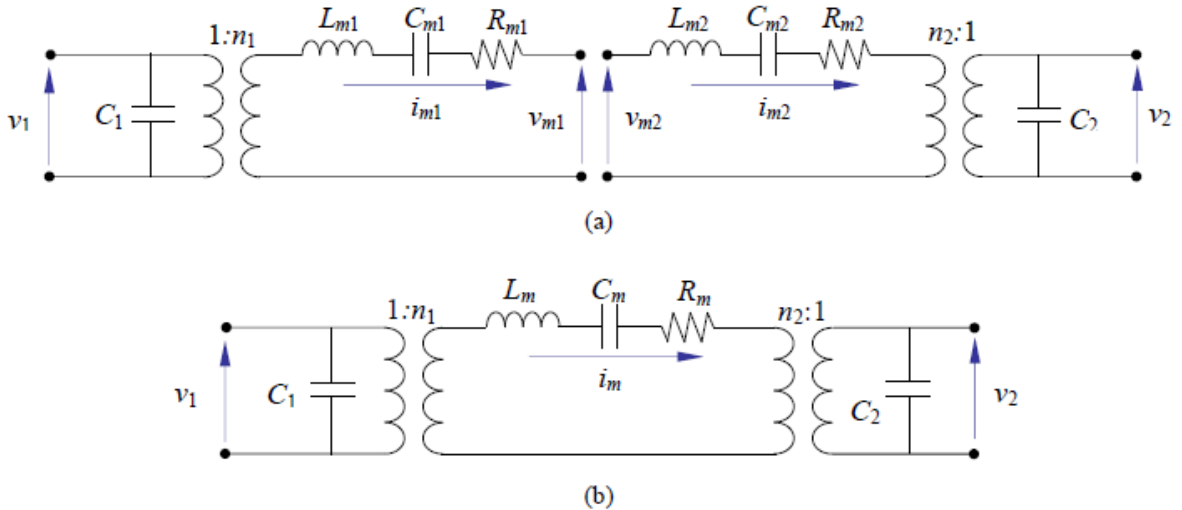


Figure 2-4. (a) Equivalent circuit of the PT by connecting two piezoelectric layers (b) simplified format of physics-based equivalent circuit model for PTs

In practice, we can further arrange the parameters in Figure 2-4(b) and derive the final format of physics-based equivalent circuit model for PTs as shown in Figure 2-5. It should be noted that  $v_1$  and  $v_2$  are linked directly to the values  $v_{in}$  and  $v_{out}$  respectively.

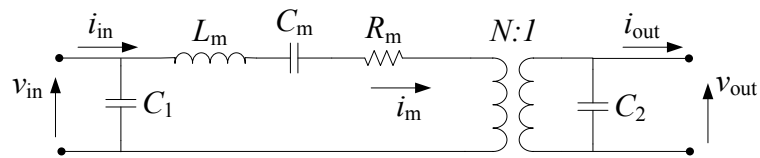
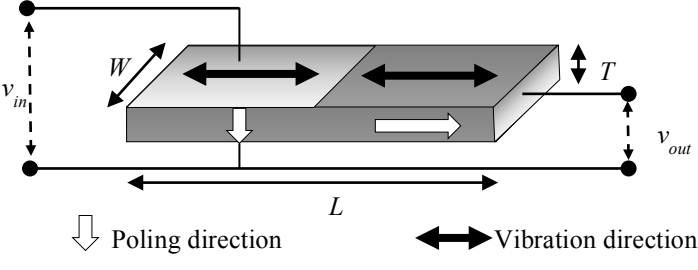
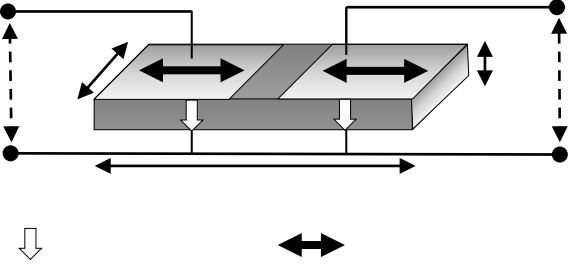
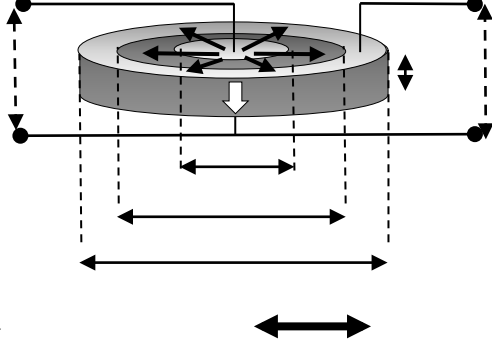


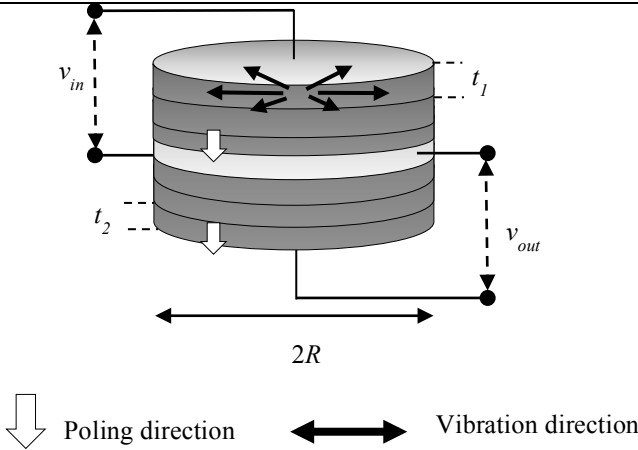
Figure 2-5. Final format of physics-based equivalent circuit model for PTs

Although there are many different type of piezoelectric transformers (e.g. 1.Rosen-type, 2.Uni-poled Longitudinal-type, 3.Concentric Disk-type, and 4.Stacked Disk-type), the equivalent circuit discussed above is conserved. From the previous research [60], the relationships between dimension factors and electric equivalent components for various kinds of PTs are listed in Table 2-4.

Table 2-4. Relationships between dimension factors and electric equivalent components for various kinds of PTs [60]

Type	$\omega_0$	$L_m$	$R_m$	$C_1$	$C_2$	$n_1$	$n_2$
1	$\frac{4\pi N_L}{L}$	$\frac{\rho_m LWT}{8}$	$\frac{1}{L_m \omega_0^2}$	$21. \frac{2\varepsilon_{33}^S WT}{L}$	$\frac{2\varepsilon_{33}^S WT}{L}$	$\frac{Wd_{31}}{s_{11}^E}$	$\frac{2WTd_{33}}{Ls_{33}^E}$

Rosen-type	 <p>22. <math>\Downarrow</math> Poling direction <math>\longleftrightarrow</math> Vibration direction</p>							
2	$\frac{4\pi N_L}{L}$	$\frac{\rho_m L W T}{8}$	$\frac{1}{L_m \omega_0^2}$	$\frac{1}{Q_m} \sqrt{\frac{L_m}{C_m}}$	$\frac{\epsilon_{33}^S W L}{2T}$	$\frac{\epsilon_{33}^S W L}{2T}$	$\frac{W d_{31}}{s_{11}^E}$	$\frac{W d_{31}}{s_{11}^E}$
Uni-poled Longitudinal-type	 <p><math>\Downarrow</math> <math>\longleftrightarrow</math></p>							
2	$\frac{\pi N_P}{T}$	$\frac{\rho_m \pi R_3^2 T}{1.4}$	$\frac{1}{L_m \omega_0^2}$	$\frac{1}{Q_m} \sqrt{\frac{L_m}{C_m}}$	$\frac{\epsilon_{33}^S \pi R_1^2}{T}$	$\frac{\epsilon_{33}^S \pi (R_3^2 - R_2^2)}{T}$	$\frac{2\pi R_1 d_{31}}{s_{11}^E (1-\nu^2)}$	$\frac{2\pi R_1 d_{31} \alpha}{s_{11}^E (1-\nu^2)}$
Concentric Disk-type	 <p><math>\Downarrow</math> <math>\longleftrightarrow</math></p> <p><math>\alpha = 1 - \frac{R_2 J_1(k_1 R_2)}{R_3 J_1(k_1 R_3)}</math> where <math>J_1</math> is the Bessel function[60].</p>							
2	$\frac{\pi N_P}{T}$	$\frac{\rho_m \pi R^2 \beta}{2}$	$\frac{1}{L_m \omega_0^2}$	$\frac{1}{Q_m} \sqrt{\frac{L_m}{C_m}}$	$\frac{m_1 \epsilon_{33}^S \pi R^2}{t_1}$	25. $\frac{m_2 \epsilon_{33}^S}{t_2}$	$\frac{2\sqrt{2}\pi R d_{31} m_1}{s_{11}^E (1-\nu^2)}$	$\frac{2\sqrt{2}\pi R d_{31} m_2}{s_{11}^E (1-\nu^2)}$

<p>Stacked Disk-type</p>	 <p style="text-align: center;"><math>\beta = m_1 t_1 - m_2 t_2</math> where <math>m_1</math> and <math>m_2</math> are the numbers of layers of the input section and the output section respectively.</p>
<p>26. <math>\omega_0</math> is the natural frequency of the PT (rad/s).  <math>N_L, N_p</math> are the frequency constants in the longitudinal vibration and the plane vibration respectively (<math>\text{kHz}\cdot\text{mm}</math>).  <math>\rho_m</math> is the density (<math>\text{kg}/\text{m}^3</math>).  <math>\nu</math> is the Poisson's ratio.  <math>Q_m</math> is the mechanical quality.  <math>\epsilon_{33}^S</math> is the permittivity at constant strain condition, i.e. constant <math>S</math> (F/m).  <math>d_{31}, d_{33}</math> are the piezoelectric constants (m/V).  <math>s_{11}^E, s_{33}^E</math> are the compliance constants under the constant electric field.  <math>L, W</math> and <math>T</math> are the dimensional factors of the rectangular PT, which represent length, width and thickness respectively.  <math>R, R_1, R_2</math> and <math>R_3</math> are the dimensional factors of the circular PT.</p>	

## 2.4 Equivalent Circuit Extraction for the Piezoelectric Transformers

In this section, a common method is implemented to extract the parameters in equivalent circuit of the PTs. However, it is a fact that those equivalent circuit parameters vary with the temperature rise of PT especially at high excitation voltage. Here, we define the equivalent circuit parameters as the low excitation parameters which are measured at room temperature ( $25^\circ\text{C}$ ). The nonlinear effect accompanied with heat generation has not yet taken into account, and we will discuss the nonlinear

effect caused by thermal issues in next chapter.

To obtain the parameters of the equivalent circuit, we could use the impedance analyzer (Agilent 4294A, Agilent Technologies Inc., Santa Clara, CA) and derive these parameters by connecting the input terminal and output terminal in short-circuit [40]. The equivalent circuit employed by 4294A impedance analyzer is shown in Figure 2-6:

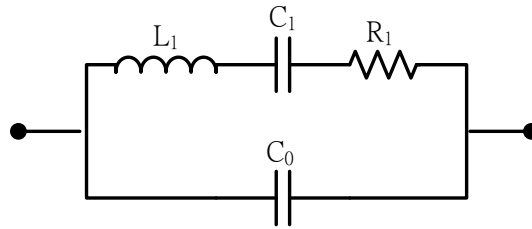


Figure 2-6. 4294A impedance analyzer and PT equivalent circuit model

Comparing Figure 2-5 with Figure 2-6, it may be seen that the equivalent circuit parameters in input section can be measured by the Agilent 4294A impedance analyzer by shorting the output terminal. Similarly, the equivalent circuit parameters in output section can be also measured by shorting the input terminal. The equivalent circuit model of the Agilent 4294A impedance analyzer is identical to the equivalent circuit model of the PT, but with one terminal shorted. The relationship can be found in Table 2-5:

Table 2-5. The relationship between 4294A and PT equivalent circuit model.

	$R_1$	$L_1$	$C_1$	$C_0$
Output terminal is short	$R_m$	$L_m$	$C_m$	$C_1$
Input terminal is short	$\frac{R_m}{n^2}$	$\frac{L_m}{n^2}$	$n^2 C_m$	$C_2$

Except for the measurement of equivalent circuit parameters, the resonant frequency and anti-resonant frequency corresponding to different vibration modes of the PT can be obtained by the impedance analyzer. Figure 2-7 shows the first mode

resonant frequency (marker 0) and anti-resonant frequency (marker 1) of the “Type A” piezoelectric transformer utilized in this dissertation.

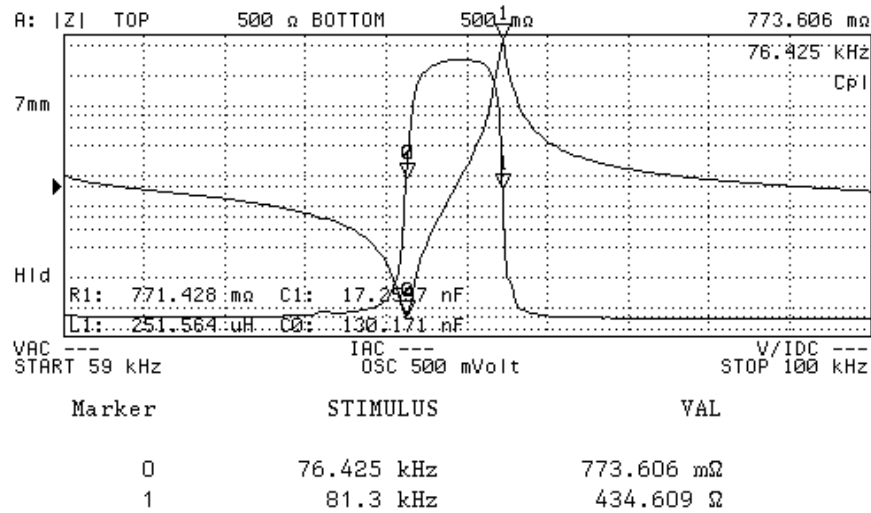


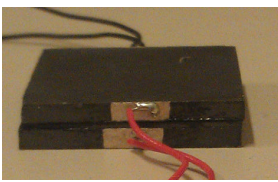


Figure 2-7. Input impedance of the “Type A” PT with resonant frequency (marker 0) and anti-resonant frequency (marker 1)

In addition, the method of shorting the output terminal can be used to derive the mechanical current passing through the mechanical resonant branch. The detail measurement method will present in next chapter. In this dissertation, there are three different types of PT provided by Eleceram Technology Co. Ltd., Taiwan such as Type A, Type B, and Type C. All the PTs are multi-layer rectangular transformer with internal circular electrodes connected in parallel and thickness polarization. Different size and number of layers for PTs are provided according to the request of our experimental requirement as shown in Table 2-6.

Table 2-6 Size and structure of PTs in this dissertation

Type A	Input section	Output section	Isolation	
PT size:	No. of layers 4	No. of layers 4	No. of layers 1	
25mm*25mm*2.1mm	Thickness per	Thickness per	Thickness per	

	layer 0.2mm (0.2*4=0.8mm)	layer 0.2mm (0.2*4=0.8mm)	layer 0.5mm (0.5*1=0.5mm)	
<b>Type B</b>  PT size: 25mm*25mm*3.7mm	Input section No. of layers 8 Thickness per layer 0.2mm (0.2*8=1.6mm)	Output section No. of layers 8 Thickness per layer 0.2mm (0.2*8=1.6mm)	Isolation No. of layers 1 Thickness per layer 0.5mm (0.5*1=0.5mm)	
<b>Type C</b>  PT size: 22mm*22mm*4.5mm	Input section No. of layers 4 Thickness per layer 0.5mm (0.5*4=2mm)	Output section No. of layers 4 Thickness per layer 0.5mm (0.5*4=2mm)	Isolation No. of layers 1 Thickness per layer 0.5mm (0.5*1=0.5mm)	

The key parameters of the piezoelectric material are summarized in Table 2-7.

Table 2-7. Properties and key parameters of the piezoelectric material.

<p><b>Material properties (PZT-QA, ELECERAM TECHNOLOGY Co., Ltd., Taiwan):</b></p> <p><math>K_p = 0.58</math> is the electromechanical coupling coefficient</p> <p><math>d_{33} = 320 \times 10^{-12}</math> is the piezoelectric constants (<math>\text{m V}^{-1}</math>)</p> <p><math>Y_{33} = 320 \times 10^{-12}</math> is the elastic constants (<math>\text{N m}^{-2}</math>)</p> <p><math>\rho_m = 7.9</math> is the density (<math>\text{g cm}^{-3}</math>)</p> <p><math>N_p = 2200</math> is the frequency constants of the plane vibration (<math>\text{kHz mm}</math>)</p> <p><math>s_{11}^E = 1.14 \times 10^{-11}</math> is the compliance constant under the constant electric field, i.e. constant <math>E</math></p> <p><math>Q_m = 1800</math> is the mechanical quality factor</p> <p><math>d_{31} = -140 \times 10^{-12}</math> is the piezoelectric constants (<math>\text{m V}^{-1}</math>)</p> <p><math>Y_{31} = -140 \times 10^{-12}</math> is the elastic constants (<math>\text{N m}^{-2}</math>)</p> <p><math>\nu = 0.16</math> is Poisson's ratio</p> <p><math>\epsilon_{33}^S = 1420 \times 8.854 \times 10^{-12}</math> is the permittivity at constant strain condition, i.e. constant</p>
--



$S$ (F m <sup>-1</sup> )
Unstable temperature of PT: 55 °C
Operating frequency: 1 kHz higher than $f_r$

To obtain the parameters of the equivalent circuit, we could derive these parameters by connecting the input terminal and output terminal in short-circuit respectively. The experimental results measured by the impedance analyzer are listed in Table 2-8. It should be noted that  $R_0$  was measured at room temperature (25°C).

Table 2-8. The experimental result obtained by impedance analyzer

Parameters of the equivalent circuit of Type A piezoelectric transformer								
$f_r$ (KHz)	$f_a$ (kHz)	$R_0$ (Ω)	$L_m$ (mH)	$C_m$ (nF)	$C_1$ (nF)	$C_2$ (nF)	$N$ (-)	$T$ °C
76.4	81.3	0.771	0.251	17.25	130.171	129.8	1	25
Parameters of the equivalent circuit of Type B piezoelectric transformer								
$f_r$ (KHz)	$f_a$ (kHz)	$R_0$ (Ω)	$L_m$ (mH)	$C_m$ (nF)	$C_1$ (nF)	$C_2$ (nF)	$N$ (-)	$T$ °C
74.99	80.9	0.655	0.1	44.01	271.343	272.01	1	25
Parameters of the equivalent circuit of Type C piezoelectric transformer								
$f_r$ (KHz)	$f_a$ (kHz)	$R_0$ (Ω)	$L_m$ (mH)	$C_m$ (nF)	$C_1$ (nF)	$C_2$ (nF)	$N$ (-)	$T$ °C
93.78	98.3	1.37	0.837	3.799	36.28	37.05	1	25

## 2.5 Losses in Piezoelectric Transformers

In practice, understanding the working limitations of PTs is the first step in the design process. As mentioned in previous sections 1.2, the temperature build-up problem arising from excessive internal losses is the predominant limitation of PT in high-passing-current applications [1]-[3]. Owing to the fact that internal losses often convert into thermal energy, the piezoelectric transformer easily becomes unstable or even crack with temperature rise because of the excessive internal losses. The output current (power) of PT is also limited by temperature build-up effect generated by

mechanical and electrical losses, especially when driving at high vibration velocity. Generally, there are three types of losses in PT: dielectric, piezoelectric, and mechanical losses [12]. According to the constitutive equation 2.1, dielectric loss is caused by the hysteresis between the electric field  $E$  and electric displacement  $D$ ; piezoelectric loss is the electromechanical hysteresis between the strain  $S$  and electric field  $E$ ; mechanical loss includes the internal elastic loss in piezoelectric material hysteresis between the stress  $T$ , strain  $S$  and mechanical vibrations from PT body to the ambient environment. From the point of view for the constitutive equation, the dielectric losses density  $P_{D-Loss}$  (W/m<sup>3</sup>) can be determined by equation (2-2), where:

$\omega$  is the angular excitation frequency

$E$  is the electric field amplitude vector

$\varepsilon$  is the Relative permittivity vector

$\eta_e$  is the dielectric loss factor

$$P_{D-Loss} = 0.5\omega E^2 \varepsilon \eta_e \quad (2-2)$$

In the other hand, the mechanical losses density  $P_{M-Loss}$  (W/m<sup>3</sup>) is given by (2-3),

where:

$\eta_m$  is the mechanical loss factor

$D$  is the Elasticity matrix

$S$  is the Strain vector

Re is the real part label

*Conj* is the conjugate label

$$P_{M-Loss} = 0.5\omega \eta_m \text{Re}\{S[\text{Conj}(DS)]\} \quad (2-3)$$

However, the relationship as above is not intuitive for users to analyze and predict the losses of the PTs. In this dissertation, internal losses of the PT are modeled by an equivalent circuit as an analytical approach. From previous research [62], the

electrostatic capacitor is considered to be the influencing factor of the dielectric losses. Whenever the polarity of current flowing through the capacitor changes, a part of energy losses which is caused by the effect of dielectric losses. Due to the consideration of dielectric losses, the equivalent circuit of the electrostatic capacitor is composed of an ideal capacitor and a resistor which are in parallel with each other as shown in Figure 2-8. In Figure 2-8, the equivalent circuit is assumed under the output terminal open condition.

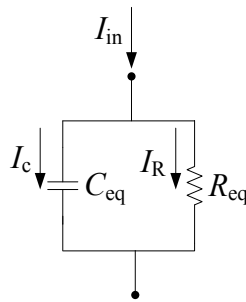


Figure 2-8. Equivalent circuit of the electrostatic capacitor

The current flowing through  $R_{eq}$ ,  $I_R$ , represents the energy losses in the capacitor. The angle between  $I_c$  and  $I_R$ ,  $\delta$ , is called the dielectric loss angle as shown in Figure 2-9.

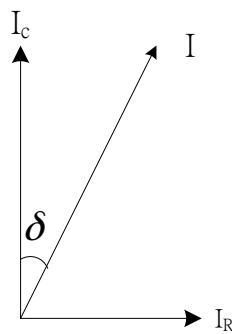


Figure 2-9. Current in the equivalent circuit of capacitor

From Figure 2-9,  $\tan \delta$  can be derived, as shown in equation (2-4).

$$\tan \delta = \frac{I_R}{I_C} = \frac{X_c}{R_{eq}} = \frac{1/\omega C_{eq}}{R_{eq}} = \frac{1}{\omega R_{eq} C_{eq}} \quad (2-4)$$

If the input voltage  $V=V_0\sin \omega t$ , the power loss due to the resistor  $R_{eq}$  is

$$P_{D-loss} = \frac{V^2}{R_{eq}} \quad (2-5)$$

The energy which can be stored in the electrostatic capacitor is  $P_{store}$ , thus

$$P_{store} = \frac{1}{2} C_{eq} V_{max}^2, \quad (2-6)$$

where  $V_{max} = V_0.$  (2-7)

Then the loss factor, *i.e.* dielectric dissipation factor, can be defined as shown in equation (2-8).

$$\text{Loss Factor} = \frac{P_{D-loss}T}{2\pi P_{store}} = \frac{I}{\omega R_{eq} C_{eq}} = \tan \delta \quad (2-8)$$

Moreover, in consideration of the dielectric losses of piezoelectric material, two resistors  $R_{d1}$  and  $R_{d2}$  were added in the equivalent circuit of PT. To measure the dielectric losses, the output terminal was opened as shown in Figure 2-10.

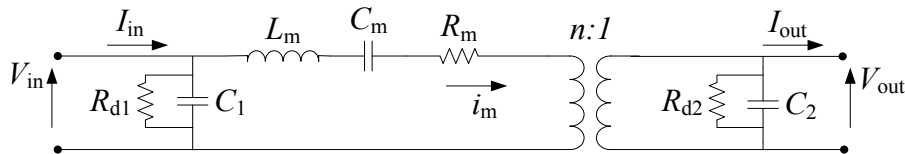


Figure 2-10. Equivalent circuit with dielectric losses

It is the fact that the two resistors  $R_{d1}$  and  $R_{d2}$  are much larger than  $R_m$  can be found. Based on the conditions that the operation frequency is around the resonant frequency and the output terminal is under open condition, the relation between  $V_{in}$  and  $V_{out}$  can be assumed as shown in equation (2-9).

$$V_{in} = V_{RLC} + nV_{out} \sim nV_{out} \quad (2-9)$$

By neglecting  $L_m$ ,  $C_m$  and  $R_m$ , the equivalent circuit can be simplified further as shown in Figure 2-11.

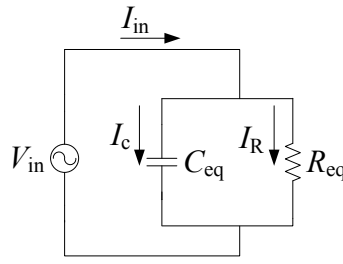


Figure 2-11. Simplified equivalent circuit.

Where 
$$C_{eq} = C_1 + \frac{I}{n^2} C_2 \quad (2-10)$$

and 
$$R_{eq} = \frac{n^2 R_{d1} R_{d2}}{R_{d1} + n^2 R_{d2}} \quad (2-11)$$

Assume 
$$V_{in} = V_0 \sin \omega t, \quad (2-12)$$

Then the current flowing through the capacitor  $I_c$  is

$$I_c = C_{eq} \frac{dV_{in}}{dt} = \omega C_{eq} V_0 \cos \omega t \quad (2-13)$$

Current flowing through the resistor  $I_R$  is

$$I_R = \frac{I}{R_{eq}} V_0 \sin \omega t \quad (2-14)$$

According to Kirchoff's current law,

$$\begin{aligned} I_{in} &= I_c + I_R = \omega C_{eq} V_0 \cos \omega t + \frac{I}{R_{eq}} V_0 \sin \omega t \\ &= V_0 \sqrt{\omega^2 C_{eq}^2 + \frac{I^2}{R_{eq}^2}} \left( \frac{\omega C_{eq}}{\sqrt{\omega^2 C_{eq}^2 + \frac{I^2}{R_{eq}^2}}} \cos \omega t + \frac{I}{R_{eq} \sqrt{\omega^2 C_{eq}^2 + \frac{I^2}{R_{eq}^2}}} \sin \omega t \right) \end{aligned} \quad (2-15)$$

where 
$$\sin \delta = \frac{I}{R_{eq} \sqrt{\omega^2 C_{eq}^2 + \frac{I^2}{R_{eq}^2}}} \quad (2-16)$$

and

$$\cos \delta = \frac{\omega C_{eq}}{\sqrt{\omega^2 C_{eq}^2 + \frac{1}{R_{eq}^2}}} \quad (2-17)$$

Thus,

$$I_{in} = V_0 \sqrt{\omega^2 C_{eq}^2 + \frac{1}{R_{eq}^2}} \cos(\omega t - \delta) \quad (2-18)$$

where

$$\tan \delta = \frac{1}{\omega R_{eq} C_{eq}} \quad (2-19)$$

Equation (2-19) is corresponding to equation (2-8). Thus, by measuring the input voltage  $V_{in}$  and input current  $I_{in}$ , while the output terminal is opened, the loss factor  $\tan \delta$  can be obtained.

As to the mechanical losses  $P_{m-loss}$ , it should be noted that the mechanical losses can be seen as the major losses in the material when the operating frequency is set near the PT's resonant frequency, i.e. high vibration level. The mechanical losses result from the friction of the crystalline structure when PT vibrates. Because the vibration velocity is directly proportional to the friction, the larger vibration velocity leads to the larger mechanical losses. In the equivalent circuit, the vibration velocity can be analog to the mechanical current  $i_m$  and the mechanical losses are equal to  $i_m^2 R_m$  where  $R_m$  is the mechanical resistance in the mechanical resonant branch  $L_m-C_m-R_m$ . Both of the mechanical current and mechanical resistance can be seen as the key factors related to the mechanical losses.

For a given material, the maximum mechanical current value exists as the threshold vibration velocity. This value is usually within 0.3~1A (i.e. 0.3m/s~1m/s). On the other hand, the mechanical resistance is a temperature dependent factor which is proportional to the temperature rise of the PT. To clearly describe the relationships between the main physical parameters, the tendency between them has been described

in section 3.5. In this dissertation the operating frequency is set near the resonant frequency, so the effect of the dielectric losses and piezoelectric losses are small and can be neglected. We assumed that heat is only generated from mechanical loss,  $P_{m-loss}$ , since mechanical loss is the dominant internal loss in the PT.

## 2.6 Characteristics of the Piezoelectric Transformers Connected with a Linear Load

To realize the characteristics of the piezoelectric transformers connected with a linear load, we can divide the inquiry into three parts such as voltage transfer coefficient (voltage gain), output power, and efficiency. All the parameters vary with the load value because of being a resonant device those parameter of PT is strongly dependent on load [13][63]. In practice, we can analyze the relationships above by using an equivalent circuit of PT with resistive load. Figure 2-12 shows the PT equivalent circuit connected to a load that is adopted to analyze the characteristics of the PT.

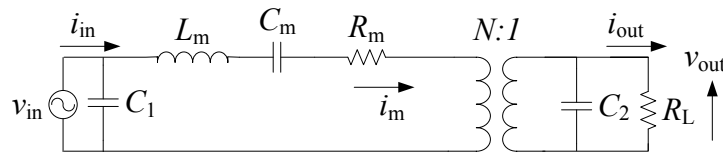


Figure 2-12. Equivalent circuit of PT connected to a load

To derive the output to input voltage ratio, Figure 2-12 can be simplified by reflecting the output capacitance  $C_2$  and load  $R_L$  from secondary side to primary side as shown in the Figure 2-13 (a). Furthermore, parameters in the primary side can be also reflected to secondary side with the same method as shown in the Figure 2-13 (b) [63].

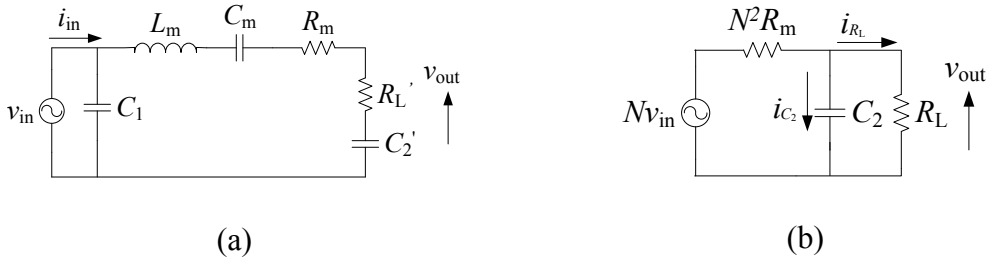


Figure 2-13. (a) Reflecting the output capacitance  $C_2$  and load  $R_L$  from secondary side to primary side (b) reflecting the parameters from primary side to secondary side

In Figure 2-13 (a), the equivalent circuit composed of series resistance  $R_L'$  and series capacitance  $C_2'$  can be regarded as a series parallel resonant tank [63].  $R_L'$  and  $C_2'$  are defined as shown in following equations:

$$R_L' = \frac{R_L}{N^2 [1 + (\omega_s R_L C_2)^2]} \quad (2-20)$$

$$C_2' = N^2 C_2 \frac{1 + (\omega_s R_L C_2)^2}{(\omega_s R_L C_2)^2} \quad (2-21)$$

where 
$$\omega_s = \frac{1}{\sqrt{L_m C_m}} \quad (2-22)$$

It should be noted that the input capacitance  $C_1$  does not affect the capability of transferring power to the load of PT. In Figure 2-13 (b), the currents  $i_{R_L}$  and  $i_{C_2}$  pass through the capacitance  $C_2$  and resistance  $R_L$  can be represented below:

$$i_{C_2} = j\omega_s C_2 v_{out} \quad (2-23)$$

$$i_{R_L} = \frac{v_{out}}{R_L} \quad (2-24)$$

According to Kirchhoff's voltage law, the relationship between output and input voltage can be obtained as shown in equation (2-25):



$$Nv_{in}=N^2R_m(i_{C_2} + i_{R_L})+v_{out}. \quad (2-25)$$

The voltage gain of the PT can then be obtained with the equations (2-23), (2-24), and (2-25):

$$G_v = \frac{v_{out}}{v_{in}} = \frac{N}{(1 + \frac{N^2 \cdot R_m}{R_L}) + jN^2 \omega_s R_m C_2} \quad (2-26)$$

and

$$|G_v| = \frac{N}{\sqrt{(1 + \frac{N^2 \cdot R_m}{R_L})^2 + (N^2 \omega_s R_m C_2)^2}} \quad (2-27)$$

We can obtain the maximum voltage gain when the load resistance  $R_L \rightarrow \infty$

Where

$$|G_v|_{\max} = \frac{N}{\sqrt{1 + (N^2 \omega_s R_m C_2)^2}} \quad (2-28)$$

In addition, the output power of the piezoelectric transformer can be defined as shown in the equation below:

$$P_{out} = \frac{|v_{out}|^2}{R_L} = \frac{N^2 |v_{in}|^2}{R_L \left[ (1 + \frac{N^2 \cdot R_m}{R_L})^2 + (N^2 \omega_s R_m C_2)^2 \right]} \quad (2-29)$$

From the previous research [63], maximum power can be delivered to the load when  $R_L = R_m$ . It should be noted that since  $R_L$  is convex, two  $R_L$  satisfy the maximum power condition and that hence two the load resistance  $R_L$  can be delivered at maximum power condition.

$$(P_{out})_{\max} = \frac{|v_{in}|^2}{4R_L} \quad (2-30)$$

Where

$$R_L = N^2 R_m \quad (2-31)$$

and 
$$R_L = \frac{1}{\omega_s^2 R_m (N^2 C_2 + C_m)} \quad (2-32)$$

As to the efficiency of PT, it can be delivered with the relationships between input and output power below:

$$P_{in} = N^2 R_m |i_{C_2} + i_{R_L}|^2 + P_{out} = N^2 R_m |j\omega_s C_2 v_{out} + \frac{v_{out}}{R_L}|^2 + \frac{|v_{out}|^2}{R_L} \quad (2-33)$$

and 
$$P_{out} = \frac{|v_{out}|^2}{R_L} \quad (2-34)$$

$$\eta = \frac{\frac{|v_{out}|^2}{R_L}}{N^2 R_m |j\omega_s C_2 v_{out} + \frac{v_{out}}{R_L}|^2 + \frac{|v_{out}|^2}{R_L}} \quad (2-35)$$

Thus,

$$= \frac{1}{1 + \frac{N^2 R_m}{R_L} + N^2 R_m R_L (\omega_s C_2)^2}$$

According to the relationship above, the maximum efficiency can be delivered at the optimal load condition:

Where 
$$R_L = \frac{1}{\omega_s C_2} \quad (2-36)$$

Thus, 
$$\eta_{max} = \frac{1}{1 + 2N^2 \cdot R_m \omega_s C_2} \quad (2-37)$$

According to the above analysis results, the generic operational characteristics of piezoelectric transformers can be depicted as shown in Figure 2-14:

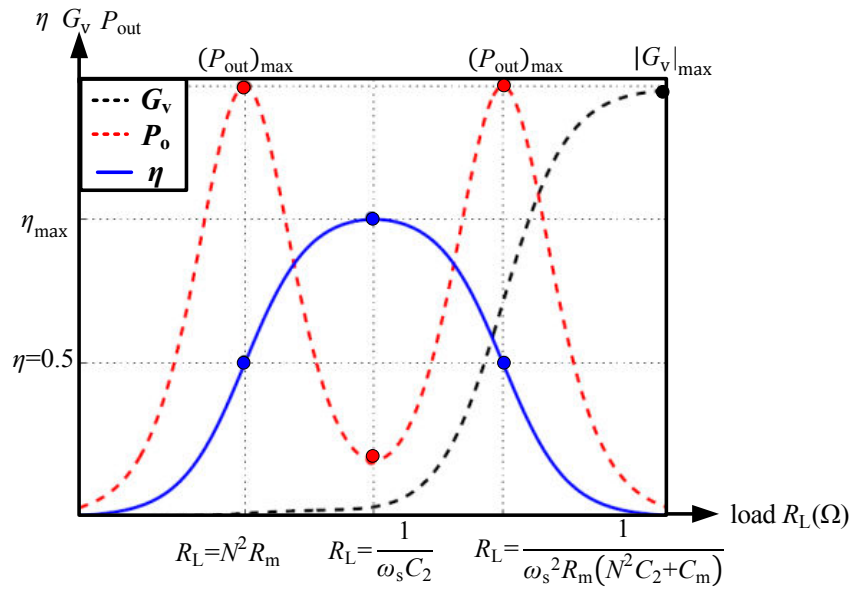


Figure 2-14. Generic operational characteristics of piezoelectric transformers [63]

## 2.7 Summary

In this chapter, the basic theory and characteristic of piezoelectric transformers were introduced. Although the piezoelectric structure has the infinite vibration modes, but only the specific resonant mode will be adopted or considered in general use. All types of the vibration can be concluded to the equivalent circuit to aid the design in the following chapter. Therefore, the equivalent circuit was derived based on the electro-mechanical coupled equations. A piezoelectric layer with a shunt circuit, and the virtual feedback controller was introduced to express the contribution of the shunt circuit. The equivalent circuit and the electro-mechanical coupled equations are two useful concepts for the designer of the piezoelectric device. These two concepts will be repeated to use in our design in the following chapters. Furthermore, the internal losses of PTs are also discussed in this chapter, and the relationship between internal losses and heat generation of PTs will be detailed in next chapter.

# **Chapter 3 Thermal Analysis of Multi-Layer Piezoelectric Transformer**

## **3.1 Introduction**

In this section, we design a multi-layer PT which possesses high passing current capacity with low profile. A theoretical-phenomenological model is proposed to explain the relationship between the vibration velocity and the temperature rise on the PT. Furthermore, we use flexible graphite tapes and thin aluminum pad on the PT to dissipate the heat generated from internal energy losses. Comparing to the previous research, graphite tapes and the thin copper layers can be directly stick on the PT and can efficiently decrease the temperature rise of the PT without extra power consumption. Our experimental result will confirm that it could satisfy the low profile requirement, while improving the PT output current capacity at the same time. The maximum output current capacity can increase 20% when the condition of PT temperature is kept below 55°C. Moreover, both of the output current and output power of the PT are improved by using the thermal dissipation layers. On the other hand, according to previous research [65], expanding the number of layers of multilayer PT, i.e. input and output section, can increase the capacity of passing current, and thus the mechanical current and output current. We also design two types of PTs with the same length and width but different number of layers (thickness) to compare the threshold vibration velocity and thermal characteristic. The methods to increase the output current and output power of the PT by using the thermal layers or enlarging the number of PT's layers have been analyzed and assessed simultaneously.

## **3.2 Analysis of Heat Generation and Temperature Rise for**

## Multi-layer Piezoelectric Transformers

PT may enter into unstable state with temperature rises because of the excessive internal losses under high-power conditions [64]. In other words, the temperature rise is a physical limitation for the high power applications of PTs. The excessive temperature rises are typically occurred when carrying high output current especially when output current is larger than around 1 A [14]. This fact implies that the PT is only suitable in the case of low output current. To overcome the low-current limitation, the analysis of the heat generation from internal losses and vibration of PT is required. As mentioned before, there are three types of losses in PT: dielectric loss  $q_{D-Loss}$ , piezoelectric loss  $q_{p-Loss}$  and mechanical loss  $q_{M-Loss}$  [12]. Usually the piezoelectric loss is ignored because it is relatively small [26]. Therefore the total losses can be expressed as:

$$q_{T-Loss} = q_{D-Loss} + q_{M-Loss} \quad (3-1)$$

When the PT is working, the heat generated by the losses in equation (3-1) can be dissipated to the ambient environment by heat transfer or can be stored inside the PT.

$$q_{T-Loss} = q_{E-Loss} + q_{S-Loss} \quad (3-2)$$

Where  $q_{E-loss}$  is the heat flux dissipated to the ambient environment, it is composed of conduction, radiation and convection effects [1], and  $q_{S-loss}$  is the heat flux stored in the PT. It is related to the density  $\rho$ , specific heat  $c_p$  and total volume  $V_T$  of the PT:

$$q_{S-Loss} = \rho c_p V_T \frac{dT}{dt} \quad (3-3)$$

Although the PT possesses the heat dissipation capacity  $q_{S-Loss}$ , the excessive heat generation from internal losses leads to the obviously temperature rise. The maximum storage heat capacity  $(q_{S-Loss})_{Max}$  of the PT is limited by the piezoelectric material characteristic. Therefore, with the same piezoelectric material, the heat dissipation ability limits the PT power density.

For simplicity, we can use the thermal conductance to model the thermal balance [29].

The relationship between stable temperature rise ( $T_s - T_0$ ) and total power dissipated in the PT is shown in equation (4):

$$q_{T-Loss} = Y_{PT}(T_s - T_0) \quad (3-4)$$

Where  $Y_{PT}$  represents the thermal conductance of heat dissipation ability,  $T_s$  represents the stable temperature of PT while the energy losses and the generated heat ( $q_{T-loss}$ ) achieve a balance with the heat dissipation ( $q_{E-Loss}$ ) to the ambient environment, and  $T_0$  is the ambient temperature. When the PT operates in the low-power transmission, the temperature rise and the heat generation of the PT are limited due to the PT's thermal conductance of heat dissipation ability. On the contrary, both of the PT's working temperature and heat generation increase rapidly in high-power transmission owing to the excessive heat generation. Once the overbalance of heat exceeds the maximum storage heat capacity  $(q_{S-Loss})_{Max}$  of the PT, it will decrease the quality factor of the piezoelectric material significantly. Accordingly, the overgreat temperature rise of PT should be regarded as a thermal limitation to prevent PT's susceptibility to crack or depoling. It is the reason why many researchers analyzed or experimentally determined thermally limited maximum power density by restricting the rise in PT temperature above its surroundings to 20°C [36][39]. In this dissertation we measure the maximum mechanical current and output power under the temperature rise constraints 30°C of PT comparing to the ambient temperature, and the 55 °C temperature limitation of PT is determined as the PT's maximum storage heat capacity.

### **3.3 Analysis of Temperature-Dependent Nonlinear Resistance in PT Equivalent Circuit**

Equation (3-4) shows the balance of the heat flux of the PT. However, it does not mention design parameters of the PT such as the current and the voltage. To link these

parameters with heat characteristics of the PT with high vibration level easily, a single-mode non-linear equivalent circuit [27] was adopted as shown in Figure 3-1.

There are two basic assumptions of this equivalent circuit:

- 1. The operating frequency is set near the resonant frequency. It should be noted that the resonance frequency is shifted with temperature rise [64], thus we assume that operating frequency don't varies in our model.
- 2. The piezoelectric losses and the dielectric losses were both neglected since the mechanical losses is the dominated internal loss in the PT. In other words, we assume that the heat is only generated from the mechanical loss, *i.e.*

$$P_{m\text{-Loss}} = R_m i_m^2$$

The typical equivalent circuit of the PT is composed of mechanical resonant branch  $L_m$ - $C_m$ - $R_m$ , two clamped capacitors  $C_1$ ,  $C_2$  and electromechanical transformation ratio  $N$ . These parameters are fixed at constant temperature.

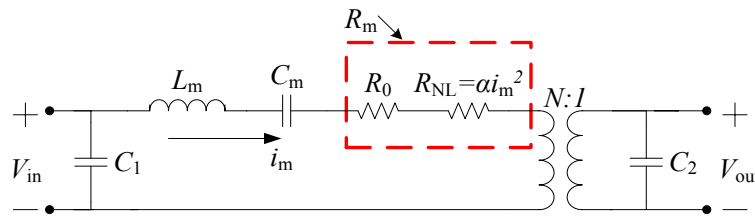


Figure 3-1. Nonlinear equivalent circuit of piezoelectric transformer.

To take into accounts the temperature effect, a non-linear thermal resistance  $R_{NL}$  is introduced in the equivalent circuit of Figure 3-1. This nonlinear resistance is introduced to take into account the effect of the large vibration amplitude and heat on the quality factor of the piezoelectric material. Thus, the mechanical resistance  $R_m$  includes two terms: a low excitation resistance  $R_0$  and a non-linear resistance  $R_{NL}$ .

$$R_m = R_0 + R_{NL} \quad (3-5)$$

According to Albareda's non-linear model of piezoelectric transducers [27], the nonlinear resistance  $R_{NL}$  is a function of mechanical current square, such as:

$$R_{NL} = \alpha i_m^2 \quad (3-6)$$

Where mechanical current  $i_m$  can be considered to be equivalent to the vibration velocity passes through the mechanical branch and  $\alpha$  characterizes the temperature-dependence of the resistance, *i.e.*  $\alpha(T^\circ\text{C})$ .

In our experimental results, both of the coefficient  $\alpha$  and the mechanical resistance  $R_m$  were increased with temperature rise. In addition, combining the assumption 2 and equations (3-4)-(3-6), the relationship between mechanical current and temperature rise was shown in equation (7):

$$i_m^2 (R_0 + \alpha i_m^2) = Y_{PT} (T_S - T_0) \quad (3-7)$$

In equation (3-7),  $R_0$  and coefficient  $\alpha$  are based on the piezoelectric material properties and piezoelectric structure configuration. Therefore, considering the same PT, the mechanical current is determined by the thermal conductance and acceptable temperature rise. On the other hand, based on circuit analysis, the output current  $i_{out}$  of the piezoelectric transformer is positive related to the mechanical current as shown in equation (3-8):

$$i_{out} = N i_m + i_{C2} \quad (3-8)$$

This is the underlying reason that the PT output current is typically limited by the temperature rise. Fortunately, equation (3-7) also implies that the maximum output current of the PT can be increased by improving the heat transfer characteristic of the PT. In Figure 3-1, except for  $R_{NL}$ , other parameters of the equivalent circuit of PT can be measured by an impedance analyzer Agilent 4294A. To obtain the parameters of the equivalent circuit, we could derive these parameters by connecting the input terminal



and output terminal in short-circuit respectively as mentioned in section 2.4. To derive the nonlinear resistance  $R_{NL}$  as shown in equation (3-5), we can measure the temperature-independent resistance ( $R_0$ ) and parameter  $N$  by the impedance analyzer first. Then, we obtain the temperature-dependent resistance ( $R_{NL}$ ) by measuring the output short-circuited current  $i_{out}$  as shown in Figure 3-2.

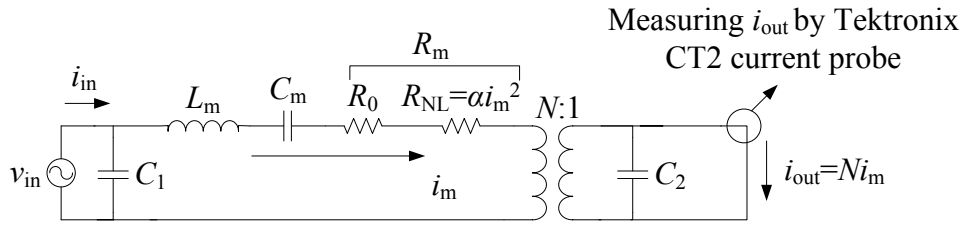


Figure 4

Figure 3-2. The method of shortening the output terminal to measure the mechanical current and nonlinear resistance

According to the equivalent circuit shown in Figure 3-2, we know that:

$$i_{out} = Ni_m \quad (3-9)$$

and

$$P_{in} = i_m^2 R_m \quad (3-10)$$

Combining equations (3-9) and (3-10), the following equation can be derived:

$$R_{NL} = P_{in} / (i_{out}/N)^2 - R_0 \quad (3-11)$$

In this work to observe the nonlinear resistance  $R_{NL}$  in different vibration levels, the output short-circuit current  $i_{out}$  and input power  $P_{in}$  were measured with increasing input voltage  $V_{in}$ . The experimental values and simulation values of  $R_{NL}$  are shown in section 3.6.

### 3.4 Heat Flowchart of the PT and PT's Control Loop of the Energy Losses

The energy losses of the PT are usually transferred into thermal energy, which leads to the temperature rise. Then this temperature rise leads to change of material

parameters and to increase the mechanical resistance  $R_m$ ,  $\alpha(T^\circ\text{C})$  value and thus the mechanical losses. Finally, the excessive heat generation becomes the major problem of PT's output capacity. Fortunately, we can overcome the problem if the accumulated heat in the PTs can be easily dissipated by using a heat transfer method. In this section, thermal layers consisted of aluminum pad and graphite tape as the heat dissipation device are applied to dissipate the heat of PT as shown in Figure 3-3.

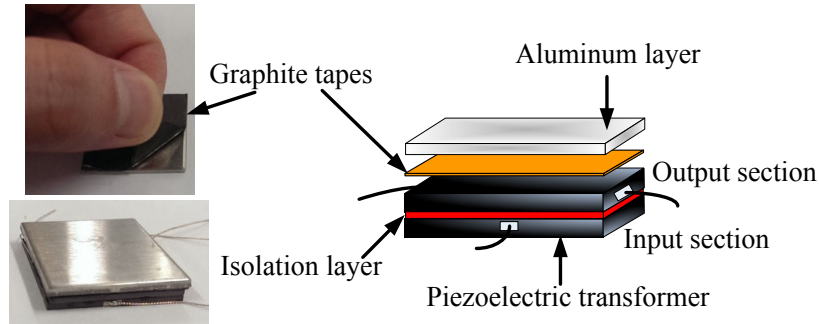


Figure 3-3. Structure of PT and thermal layers

Based on Figure 3-3, the additional thermal conductance heat dissipation abilities  $Y_{\text{Aluminum-Pad}}$  and  $Y_{\text{Graphite-Tape}}$  are contributed from aluminum pad and graphite tape as shown in equation (3-12).

$$P_{\text{m-Loss}} = (Y_{\text{Total}})(T_S - T_0) = (Y_{\text{PT}} + Y_{\text{Aluminum-Pad}} + Y_{\text{Graphite-Tape}})(T_S - T_0) \quad (3-12)$$

In equation (3-12), the increased total thermal conductance  $Y_{\text{Total}}$  efficiently limited the temperature rise  $(T_S - T_0)$  of the PT with constant mechanical loss  $P_{\text{m-loss}}$ . According to the results,  $\alpha(T^\circ\text{C})$  value and temperature-dependent resistance  $R_{\text{NL}}(T^\circ\text{C})$  can both be reduced in the same mechanical current condition. To understand how the cooling system increases the PT output current capacity, the heat flowchart of the PT associated with or without the heat dissipation device is shown in Figure 3-4.

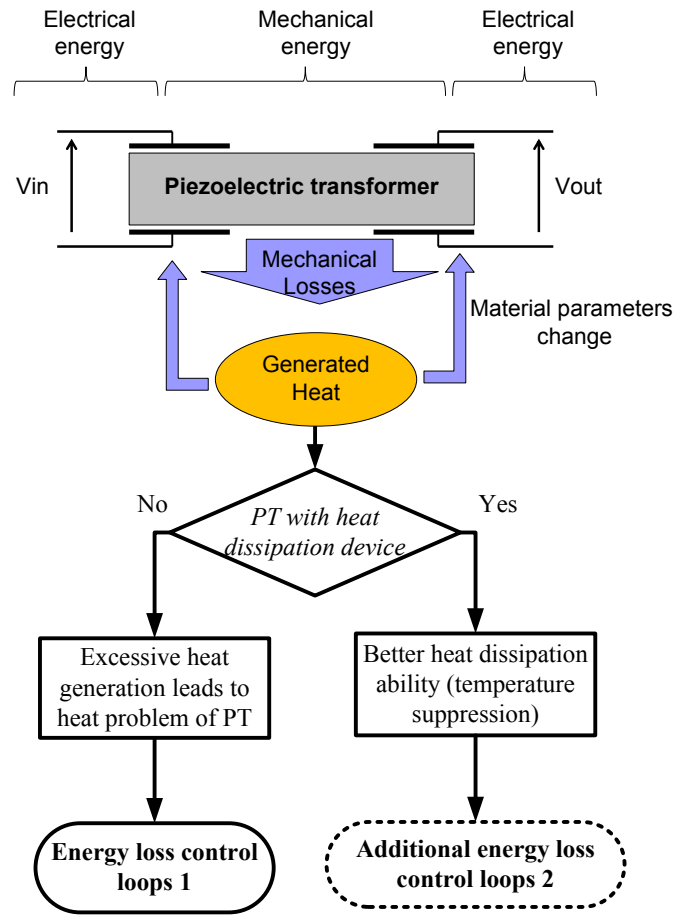
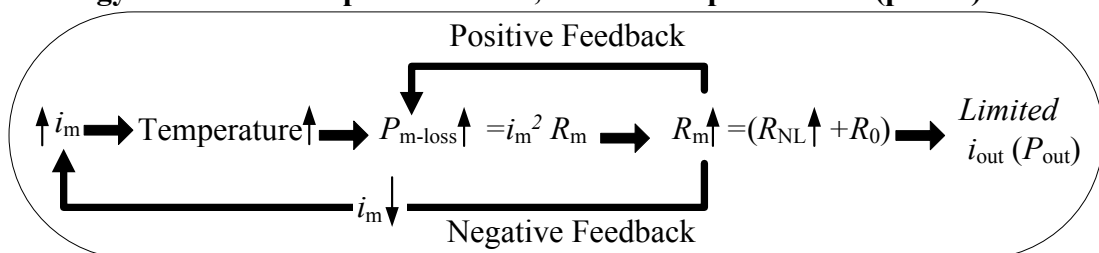


Figure 3-4. Heat flowchart of the PT associated with or without the heat dissipation device

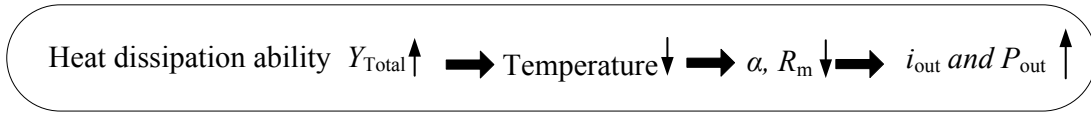
According to the Figure 3-4, the losses of the PT are mostly transferred into thermal energy and that leads to the PT temperature rise. Then this temperature rise leads to changes of material parameters and increases the mechanical resistance  $R_m$ ,  $\alpha(T^{\circ}\text{C})$  value and thus the mechanical losses. In addition, the different results of the energy loss loops associated with or without the heat dissipation device are divided into energy loss loop 1 and 2 respectively as shown in Figure 3-5(a) and Figure 3-5(b).

**Energy loss control loops 1: unstable, limited output current (power) of PT**



(a)

**Energy loss control loops 2: increasing the output current (power) capacity of PT**



(b)

Figure 3-5. (a) PT thermal feedback loop and (b) PT with cooling system thermal feedback loop.

As we can see from the Figure 3-5(a), considering the case without the heat dissipation device, the temperature rise leads to a thermal positive feedback. In the same time, there is a negative feedback loop when the PT input voltage is a constant. It is the fact that the positive feedback loop limits the output current. In addition, the negative feedback loop is as the limitation of the passing current capacity of PT. On the contrary, the PT thermal loop with cooling system is shown in Figure 3-5(b). The function of the heat dissipation device is to reduce the temperature-dependent resistance  $R_{\text{NL}}(T^{\circ}\text{C})$  and coefficient  $\alpha(T^{\circ}\text{C})$ . Therefore, according to equation (3-12) and assumption 2 in section 3.3, the mechanical resistance and the mechanical losses are both decreased. Considering the PT input voltage is constant, the PT passing current capacity is increased at the same time and it would lead to the increases of the output current (power) of the PT. It should be noted that smaller the coefficient  $\alpha$  is, the lower the mechanical losses will be produced at a constant stable operating temperature of the PT.

Except for the heat dissipation method, as mentioned before we also design two types of PTs with the same length and width but different number of layers (thickness) to increase the output current (power) of the PT based on the structural design point of view. We follow the design guideline that Prieto *et al* presented to discuss the output power capacity of PT with different thickness of the secondary bulk zone, size, and number of layers in multi-layer PT [65]. Therefore, we design the multi-layer PT with

different number of layers to compare the maximum storage heat capacity  $(q_{S-Loss})_{Max}$ . Furthermore, It can be used to compare the thermal conductance, threshold vibration velocity, and other thermal characteristics with heat dissipation method.

### 3.5 Experimental setup

Experimental setup is shown in Figure 3-6. We incorporated the function generator (Instek SFG-2004) and power amplifier (nF HSA4052) to control the switching frequency and to drive the PT. A contact temperature sensor was used to monitoring the PT temperature in different driving conditions. The contacted aluminum pad and graphite tape were used as the thermal layers to increase the performance of the PT. Furthermore, we also design two types of PTs with the same length and width but different number of layers (thickness) to compare the threshold vibration velocity and thermal characteristic.

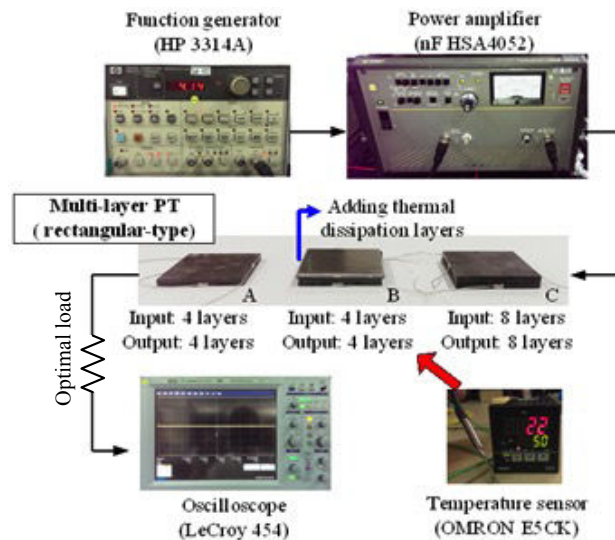


Figure 3-6. Experimental setup.

Expanding the number of layers of multilayer PT, *i.e.* input and output section, can increase the capacity of passing current, and thus the mechanical current and output current. However, once the effect of temperature build-up becomes heavy in high

vibration condition, mechanical current cannot be increased even if under higher excitation voltage. To improve the output current (that mean power) of PT, the accumulated heat must be released rather than the increment of layers or size only. To verify the statements, we present three different experimental cases to analyze the relationships between the input voltage, vibration velocity (mechanical current  $i_m$ ), non-linear resistance  $R_{NL}$ , ability of thermal conductance  $Y$ , and generated heat of the PT as shown in Table 3-1.

Table 3-1. Size and structure of experimental cases

<p><b>Case A</b></p> <p>Utilizing “type A” PT</p> <p>size:</p> <p>25mm*25mm*2.1mm</p>	<p>Input section</p> <p>No. of layers 4</p> <p>Thickness</p> <p>0.2mm</p> <p>(0.2*4=0.8mm)</p>	<p>Output section</p> <p>No. of layers 4</p> <p>Thickness 0.2mm</p> <p>(0.2*4=0.8mm)</p>	<p>Isolation</p> <p>No. of layers 1</p> <p>Thickness</p> <p>0.5mm</p> <p>(0.5*1=0.5mm)</p>	<p>Without thermal</p> <p>dissipation layers</p>
<p><b>Case B</b></p> <p>Utilizing “type A” PT</p> <p>and thermal layers</p> <p>size:</p> <p>25mm*25mm*3.7mm</p>	<p>Input section</p> <p>No. of layers 4</p> <p>Thickness</p> <p>0.2mm</p> <p>(0.2*4=0.8mm)</p>	<p>Output section</p> <p>No. of layers 4</p> <p>Thickness 0.2mm</p> <p>(0.2*4=0.8mm)</p>	<p>Isolation</p> <p>No. of layers 1</p> <p>Thickness</p> <p>0.5mm</p> <p>(0.5*1=0.5mm)</p>	<p>*Aluminum pad</p> <p>Thickness 1.3mm</p> <p>*Graphite tape</p> <p>Thickness 0.3mm</p> <p>(1.3+0.3=1.6mm)</p>
<p><b>Case C</b></p> <p>Utilizing “type B” PT</p> <p>size:</p> <p>25mm*25mm*3.7mm</p>	<p>Input section</p> <p>No. of layers 8</p> <p>Thickness</p> <p>0.2mm</p> <p>(0.2*8=1.6mm)</p>	<p>Output section</p> <p>No. of layers 8</p> <p>Thickness 0.2mm</p> <p>(0.2*8=1.6mm)</p>	<p>Isolation</p> <p>No. of layers 1</p> <p>Thickness</p> <p>0.5mm</p> <p>(0.5*1=0.5mm)</p>	<p>Without thermal</p> <p>dissipation layers</p>

The properties of the PTs specimen and the model parameters measured by the impedance analyzer are given in Table 3-2.

Table 3-2. Properties of the PTs

Material properties (PZT-QA, ELECERAM TECHNOLOGY Co., Ltd., Taiwan):

$K_p = 0.58$  is the electromechanical coupling coefficient

$Q_m = 1800$  is the mechanical quality factor

$d_{33} = 320 \times 10^{-12}$  is the piezoelectric constants ( $\text{m V}^{-1}$ )

$Y_{33} = 320 \times 10^{-12}$  is the elastic constants ( $\text{N m}^{-2}$ )

$\rho_m = 7.9$  is the density ( $\text{g cm}^{-3}$ )

$N_p = 2200$  is the frequency constants of the plane vibration ( $\text{kHz mm}$ )

$s_{11}^E = 1.14 \times 10^{-11}$  is the compliance constant under the constant electric field, i.e. constant  $E$

$d_{31} = -140 \times 10^{-12}$  is the piezoelectric constants ( $\text{m V}^{-1}$ )

$Y_{31} = -140 \times 10^{-12}$  is the elastic constants ( $\text{N m}^{-2}$ )

$\nu = 0.16$  is Poisson's ratio

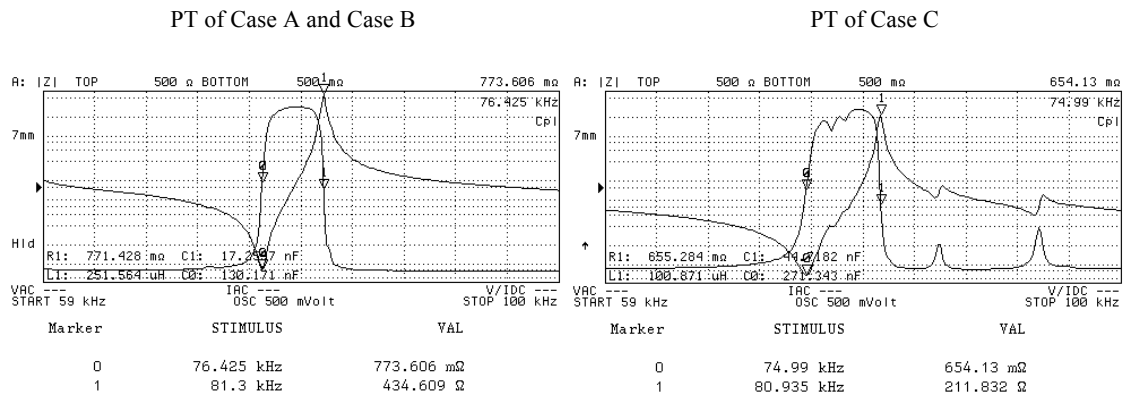
$\epsilon_{33}^S = 1420 \times 8.854 \times 10^{-12}$  is the permittivity at constant strain condition, i.e. constant  $S$  ( $\text{F m}^{-1}$ )

Unstable temperature of PT:  $55^\circ\text{C}$

Operating frequency:  $1\text{kHz}$  higher than  $f_r$

Optimal load ( $1/\omega C_2$ ): Case A and B =  $5\ \Omega$ ; Case C =  $10\ \Omega$

The experimental result obtained by impedance analyzer:



PT of Case A and Case B:

$f_r$	$f_a$	$R_0$	$L_m$	$C_m$	$C_1$	$C_2$	$N$	$T$
(KHz)	(kHz)	(Ω)	(mH)	(nF)	(nF)	(nF)	(-)	$^\circ\text{C}$
76.425	81.3	0.771	0.251	17.25	130.171	129.8	1	25

PT of Case C:

$f_r$	$f_a$	$R_0$	$L_m$	$C_m$	$C_1$	$C_2$	$N$	$T$
(KHz)	(kHz)	(Ω)	(mH)	(nF)	(nF)	(nF)	(-)	$^\circ\text{C}$
74.99	80.935	0.655	0.1	44.01	271.343	272.01	1	25

It is utilized the same PT in case A and case B, but the difference is with or without the thermal dissipation layers. In case C, we expand the number of layers of the multilayer PT without the thermal dissipation layers to compare with other cases. PTs in case A, B, and C are multi-layer rectangular transformer with internal circular

electrodes connected in parallel and thickness polarization. Graphite tape (MS-GTC-025-0.03T) was provided by Miézo Inc. Taiwan. In previous research [66], polypropylene membrane is applied to decrease contact wear of PT. It should be noted that graphite tape possesses high thermal conductivity, *i.e.* 450 W/m.K(X,Y direction) and 15 W/m.K(Z direction), to transfer the heat to the heat transfer equipment. Considering the heat transfer capacity, we use the graphite tape to replace the polypropylene membrane as the buffer layer.

### **3.6 Experimental results of PT with thermal dissipation layers**

The relationship between the temperature rise ( $T_s - T_0$ ), total power dissipated in the PT ( $P_{m-loss}$ ) and thermal conductance heat dissipation ability ( $Y$ ) is shown in equation (3-4) and (3-12). In this work we measure the mechanical losses and temperature rise to quantify the  $Y$  value (thermal conductance heat dissipation ability) [31]. In Figure 3-7 below, it is obviously that the  $Y$  value can be increased by using the thermal dissipation layers and expanding the layers of PT. Comparing to the case B and case C, the method to improve the  $Y$  value by adding thermal layers is more useful than the expansion of PT's layers with the same thickness.



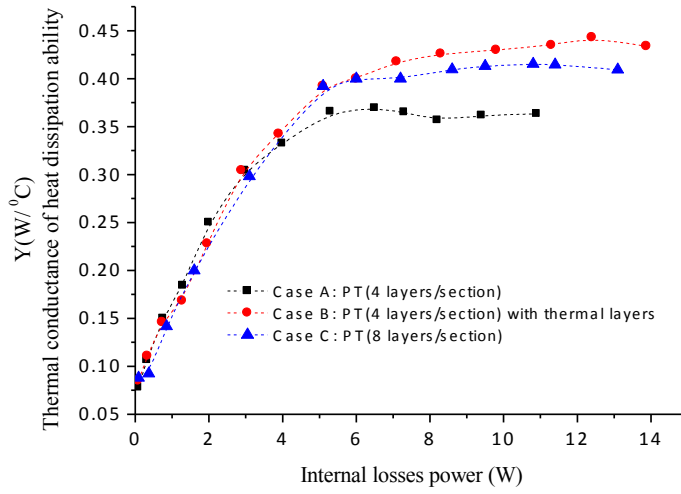


Figure 3-7. Characteristics between  $Y$  (thermal conductance) and temperature rise

According to the Figure 3-7 and equation (3-12), the increased thermal conductance ( $Y$  value) can efficiently limit the temperature rise ( $T_s - T_0$ ) of the PT owing to the improvement of heat dissipation ability. At the same mechanical current level, the suppression of the temperature rise can be directly decreased the temperature-dependent nonlinear resistance  $R_{NL}$  in PT and thus the mechanical resistance  $R_m$  as shown in Figure 3-8.

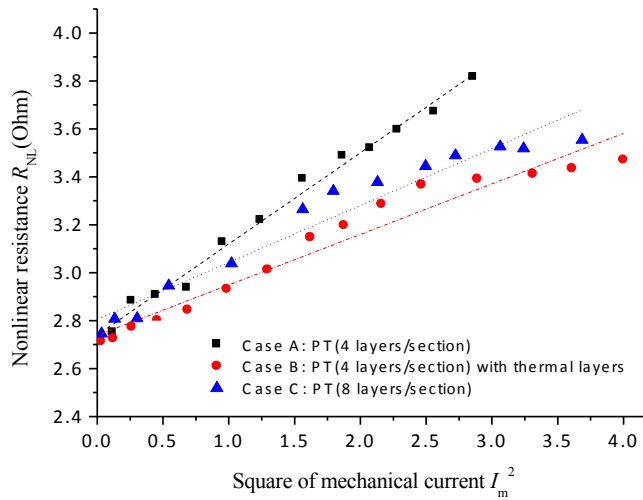


Figure 3-8. Relationship between the square of mechanical current and the  $R_{NL}$  at

different temperatures

From the assumption 2 in section 3.3, *i.e.*  $P_{m-Loss}=R_m i_m^2$ , it is revealed that the mechanical losses  $P_{m-loss}$  are also decreased at the same mechanical current level. In addition, Figure 3-8 verifies the increment of the mechanical resistance is a function of the square mechanical current  $i_m^2$ . As say before, in our work we determine thermally limited threshold vibration velocity as well as mechanical current by restricting the rise in PT temperature above its surroundings to 30 °C. The 55 °C temperature limitation of PT is determined as the PT's maximum storage heat capacity. The variation of mechanical current and the PT temperature are obtained by applying different input voltages as shown in Figure 3-9 and Figure 3-10. According to the experimental results, we know that it is possible to increase the maximum vibration energy of the PT under higher excitation voltage by preventing the overheating problem. The maximum mechanical current as the threshold vibration velocity can be increased from 1.69 A to 2 A at a specific temperature in case B. Comparing the case B and case C in Figure 3-10, the method utilized the thermal layers (case B) possesses better capacity than case C to improve the mechanical current at each input voltage level. Furthermore, the increment of the threshold vibration velocity in Case B is more obvious than other cases, and the growth is nearly 20%.

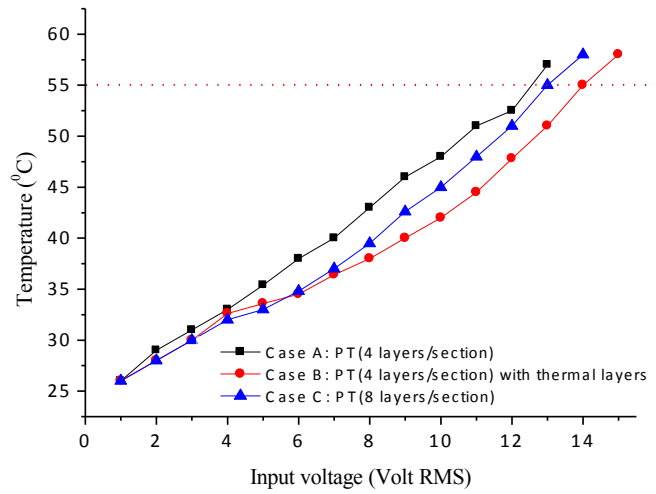


Figure 3-9. Relationships between temperature and input voltage.

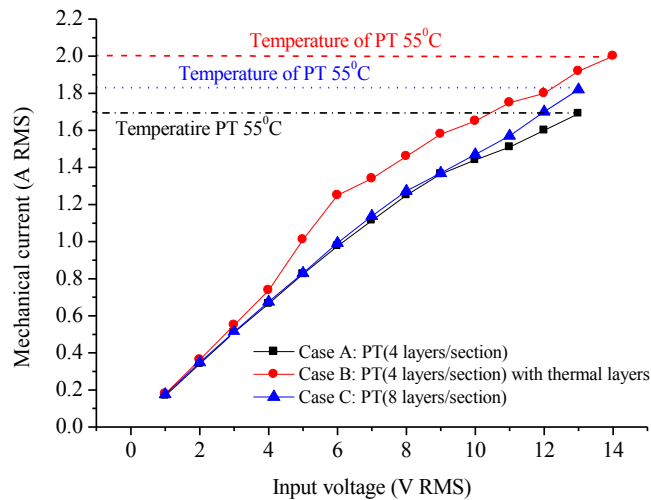


Figure 3-10. Relationships between mechanical current and input voltage.

According to the relationship between output current and mechanical current as shown in equation (3-8), the maximum output current under optimal load condition can be improved and thus the output power as shown in Figure 3-11. The measured results show that the highest output power of thermal dissipation layers used for PT can move from 10.9 W to 13.8 W at the temperature of 55°C under optimal load condition (an increase of 26%). Furthermore, all specimens kept a good efficiency (>70%) at the PT temperature limit of 55°C.

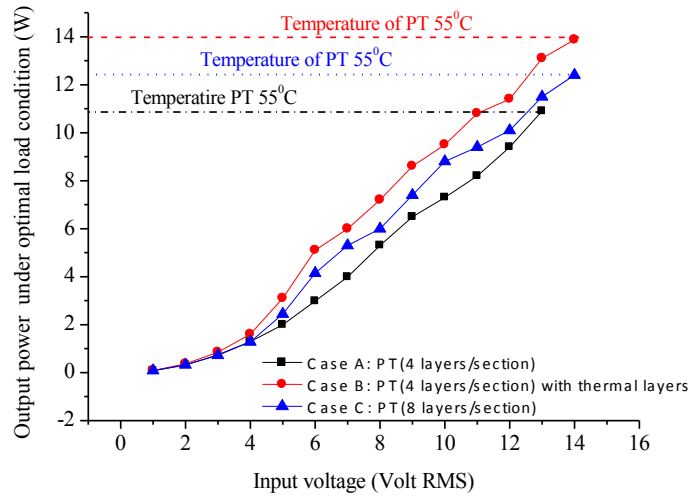


Figure 3-11. Output power enhancement in different methods.

### 3.7 Summary

In this section, the thermal layers consisted of graphite tape and aluminum pad were used to enhance the output power of a PT. It should be noted that the graphite tape is a perfect layer to decrease contact wear and transfer the heat. According to the experimental results, all specimens retained a satisfactory efficiency even at a temperature of 55°C. Due mainly to the improved ability to dissipate heat by using thermal dissipation layers, the PT passing current can be substantially increased under optimal load conditions instead of just expanding the PT's number of layers. The threshold vibration velocity, as well as the mechanical current, can be improved almost 20% when the condition of PT temperature is kept below 55°C, and thus the highest output power (an increase of 26%).

Moreover, we present a theoretical-phenomenological model. The model clearly indicates that it is possible to enhance the performance of the PT by decreasing the temperature-dependent nonlinear resistance  $R_{NL}$  value and by increasing the thermal

conductance  $Y$  value. This work investigates the temperature build-up problem of PT and presents a useful method allowed the piezoelectric transformer to be used in low-voltage, high-current applications.

# Chapter 4 Power Enhancement of PT by Using Heat Transfer Equipment

## 4.1 Introduction

In this section, we propose to design a PT suited for low-profile DC/DC converter applications, which the output power is increased by using heat transfer equipment. We examined several parameters, which allow us to produce a PT with optimal efficiency. We consider the influence of the temperature rise on losses as explain before. By maintaining the vibration mode and limiting the heat produced by the PT, this design can enhance the power capacities of the PT and thus increase the output power of the DC/DC converter. Based on the theoretical-phenomenological model developed in chapter 3 the design constraints and variables, such as the maximum mechanical current, the temperature distribution, the PT geometrical configuration and the energy balance, was used to determine the optimal PT configuration. In our final design, the PT power capacity is increased 3 times (i.e. from 4.54 W to 13.29 W) at specific temperature and the effects of the different cooling methods of the system were verified.

## 4.2 Different Mechanisms of Heat Transfer Equipment

The previous discussions show that to increase the output power of the PT, the coefficient  $\alpha$  must be reduced. In this work a cooling system that includes thermal pad, radiator, piezoelectric fan and thermoelectric cooling module are used to decrease the temperature and thus the coefficient  $\alpha$ . Once  $\alpha$  is reduced by the cooling system, both temperature-dependent resistance  $R_{NL}$  and mechanical losses resistance  $R_{m-loss}$  can be reduced in the same mechanical current condition. Specifically, a smaller  $\alpha$  value leads

to a smaller mechanical loss at a constant stable operating temperature of the PT. Figure 4-1 shows all different cooling structures, which includes:

- (a) Air cooling without any cooling device,
- (b) Contacted planar heat transfer equipment (HTE),
- (c) HTE with piezoelectric fan, and
- (d) HTE with thermoelectric cooling module.

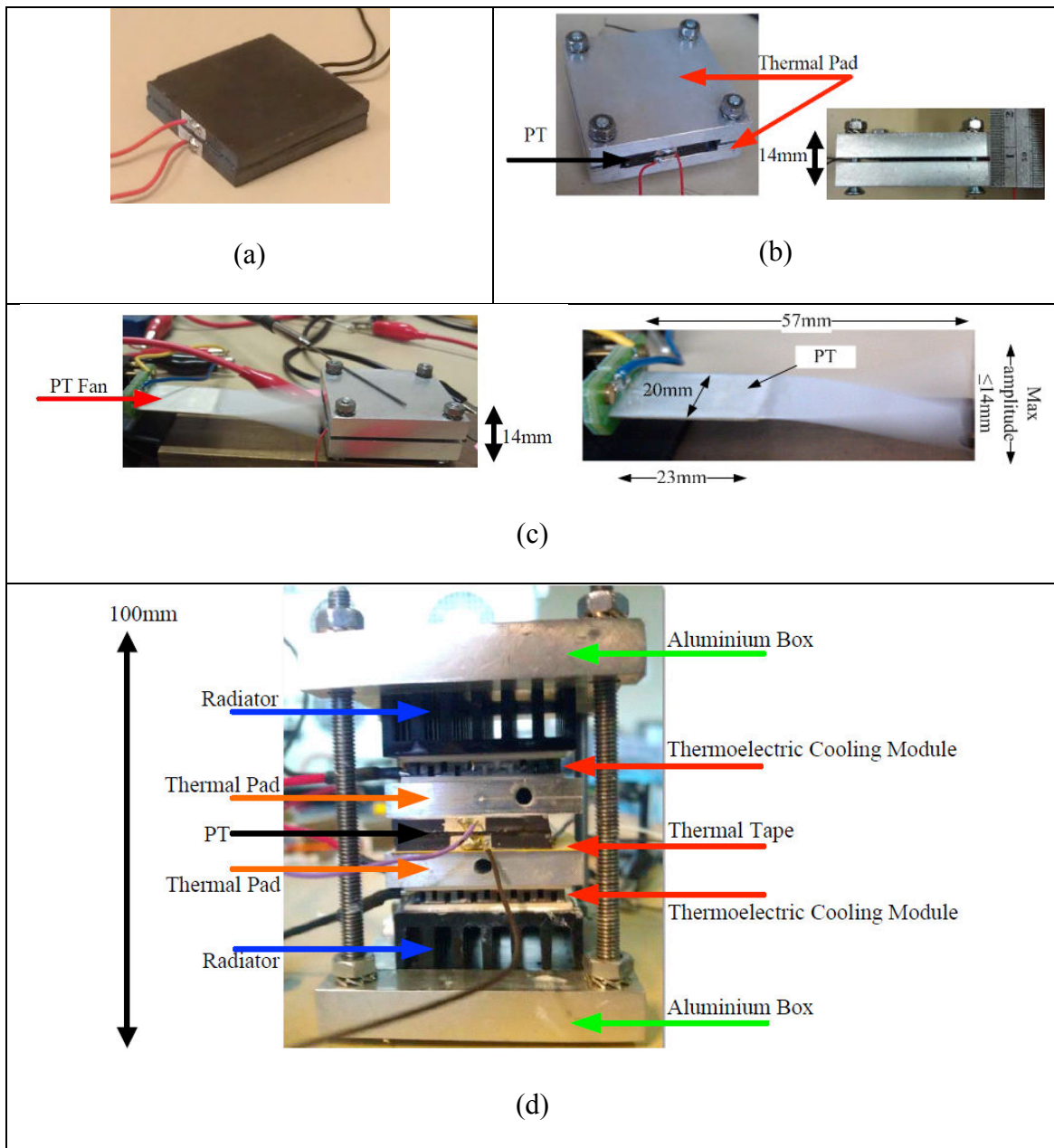


Figure 4-1. (a) Air cooling without any cooling device (b) Heat transfer equipment (HTE) (c) HTE and planar piezoelectric fan (d) HTE and thermoelectric cooling module

The HTE as shown in Figure 4-1(b) is an aluminum box was mounted onto a radiator, which served as a heat sink and provided an additional surface area of 16 cm<sup>2</sup> for cooling. To dissipate the heat of PT more efficiently and reach the miniaturization purpose, an auxiliary piezoelectric fan was applied as shown in Figure 4-1(c). In this dissertation, we also compare the performance between the HTE and another type of cooling structure, *i.e.* a pair of thermoelectric cooling modules mounted onto the thermal pad and radiator as shown in Figure 4-1(d).

As mentioned in chapter 3, the nonlinear resistance  $R_{NL}$  can be seen as the key parameter for estimating the heat dissipation capacity. In Figure 4-2, it is clear that the resistance  $R_{NL}$  is efficiently decreased by applying the cooling system for the same mechanical current. In addition, as the mechanical losses  $P_{m-loss}$  are a function of mechanical resistance  $R_m$ , the mechanical losses  $P_{m-loss}$  are also decreased by applying the cooling system. Obviously, the cooling methods applied by HTE with PT fan and thermoelectric cooling modules were regarded as the better ways to reduce the nonlinear resistance  $R_{NL}$  and to be adopted.

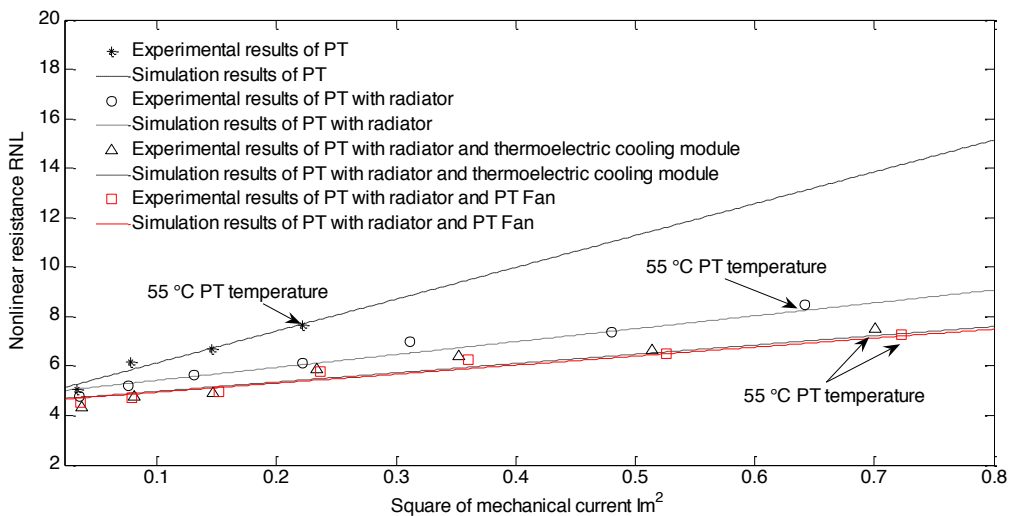


Figure 4-2. Nonlinear resistance  $R_{NL}$  as a function of the square of mechanical current and at different temperatures



It's a well-known fact that lowering the temperature of PT can cause the result that higher the mechanical quality factor  $Q_m$  for conventional hard PZT's. Although the temperature build-up effect is reduced by using the HTE, clamping the PT by aluminum pads may add significant damping which will eventually lower the  $Q_m$  (of the overall system). Aiming at this issue, the influence of thermal block's mass and clamping on the vibration had be explained and verified in the previous researches[29][67]. It is revealed that although temperature rise is considered the most critical problem for increasing PTs' potential power density, the solutions are mostly focused on trying new vibration modes or using other materials to improve the properties of PTs, such as their electromechanical coupling coefficients ( $k$ ) and mechanical quality factors. The improvement of these designs is not outstanding and the results still cannot satisfy the high power transfer requirement. In fact, researchers barely considered a complete study on the influence of ambient environment on the heat dissipation characteristics of PTs, or tried to conquer the heating problem with auxiliary designs like traditional electronic components. In their prevailing opinion, additional structures appear to bring even more severe problems for the vibrating PTs. However, a deliberate auxiliary cooling design can improve the available maximum power density of PTs by simultaneously maintaining their vibration mode and decreasing additional energy losses. We can explain the quality factor of PT with or without the aluminum pad as shown in the figure below:

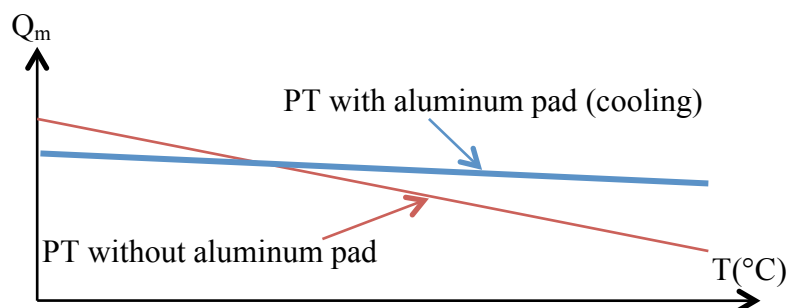


Figure 4-3. A comparison of the mechanical quality factor varied with temperature rise of PT between: PT with aluminum pad and PT without the aluminum pad

In the case of PT without aluminum pad, the  $Q_m$  value decreases rapidly with the temperature rise. On the contrary,  $Q_m$  value is maintained as a constant in the case of PT with aluminum pad.

### 4.3 Experimental setup

As to the experimental setup, we incorporated an IR2104 and IRF7431 for the gate driver and the MOSFET switches respectively. A function generator controls the switching frequency of the half-bridge. The series inductance  $L_s$  was set at 51  $\mu\text{H}$  with the switching frequency 94.3 kHz to achieve soft switching conditions, *i.e.* zero voltage switching (ZVS), as shown in Figure 4-4.

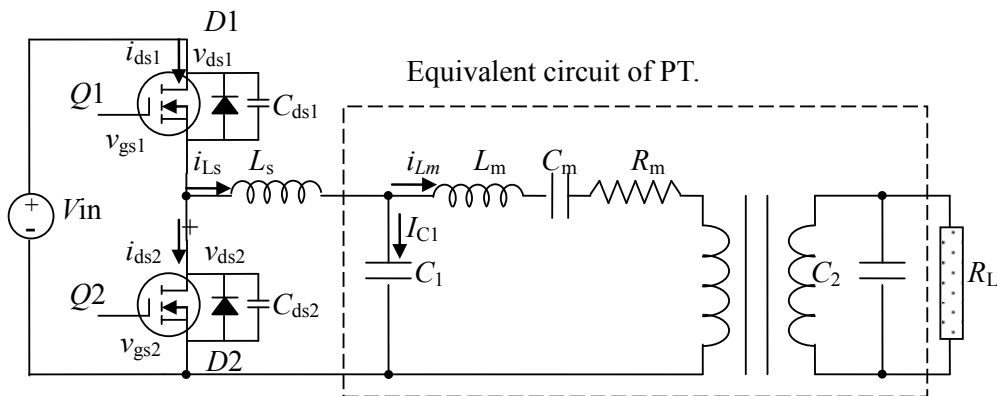


Figure 4-4. The half-bridge driving circuits with a piezoelectric transformer

In practice, one important requirement of the switching driving circuit is the ZVS condition. In switching power circuits, MOSFETs are usually used as switching components. MOSFETs have a drain to source parasitic capacitance  $C_{ds}$ . When the switch is at the “OFF” state, the parasitic capacitor is charged. At the instant of switching from “OFF” state to “ON” state, the voltage on the parasitic capacitor  $v_{ds}$  varies rapidly and thus a spike current  $i_{spike}$  is generated, *i.e.*  $i_{spike} = C_{ds}(dv_{ds}/dt)$ . The spike

current induces switching losses and becomes a source of EMI (ElectroMagnetic Interferences).

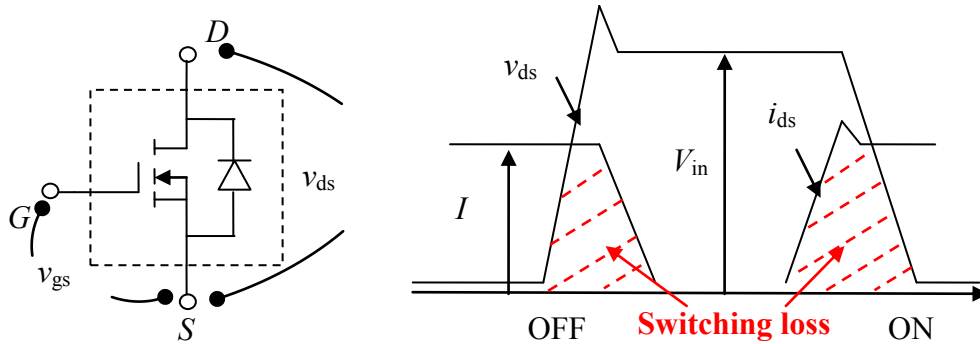


Figure 4-5. The production of switching loss in the power MOSFET

To solve these problems, the ZVS technique was proposed [68]. The ZVS means the switch turns “ON” after the parasitic capacitor of the switch has been already discharged to zero voltage. Since voltage on the parasitic capacitor is fully discharged to zero, there is no voltage variation ( $dv_{ds}/dt = 0$ ) during the switching instant and thus the spike current cannot be generated. The corresponding waveforms of the ZVS-mode half-bridge circuit is depicted in Figure 4-6:

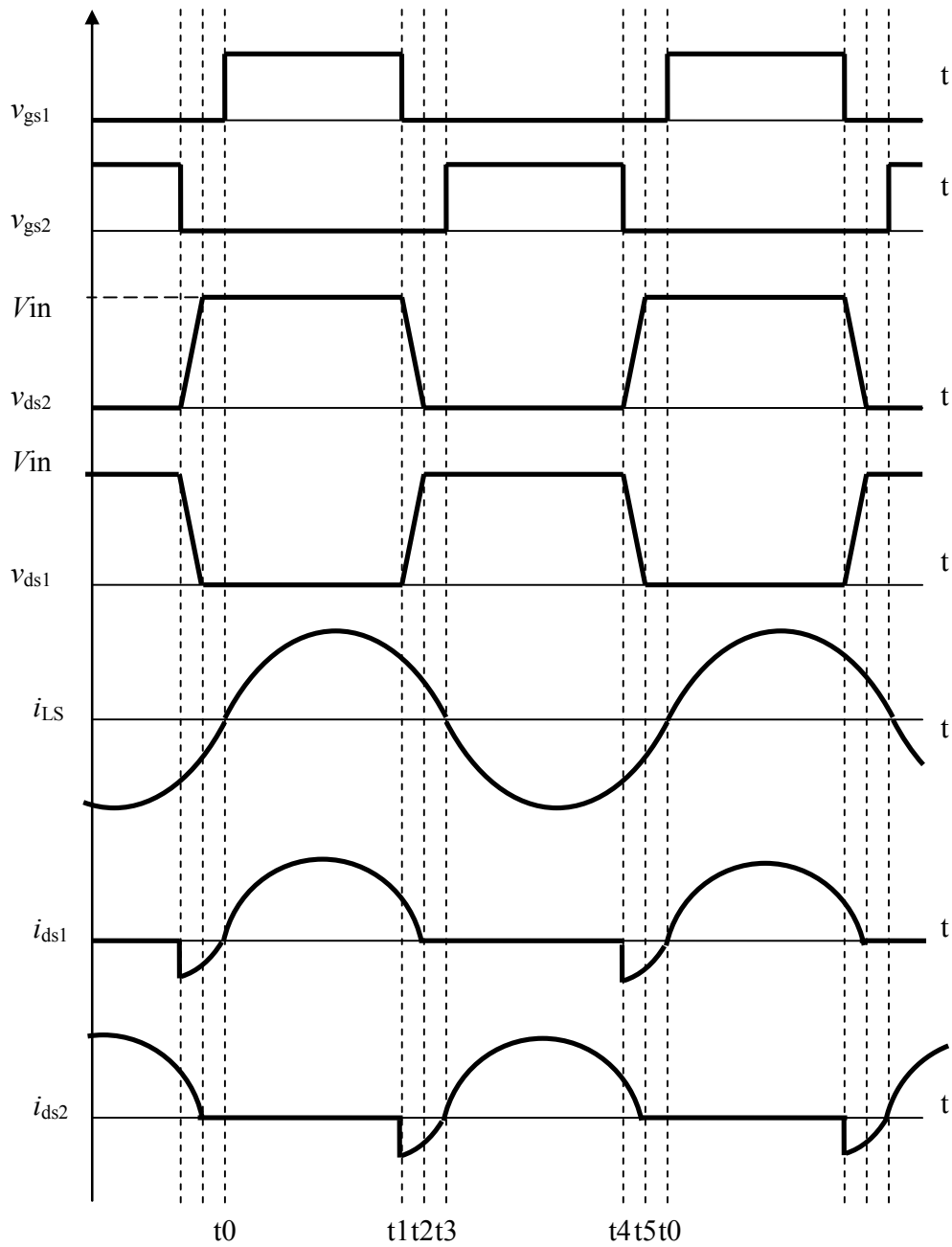


Figure 4-6. The corresponding waveforms of the ZVS-mode half-bridge circuit

Furthermore, the operation of the ZVS-mode half-bridge circuit with a PT is detailed as follows:

**Step 1.  $[t_0-t_1]$**

In this period, switch  $Q_1$  is “ON” and switch  $Q_2$  is “OFF”, thus  $v_{ds2}$  is equal to  $V_{in}$ . This state is over until switch  $Q_1$  is turned OFF.

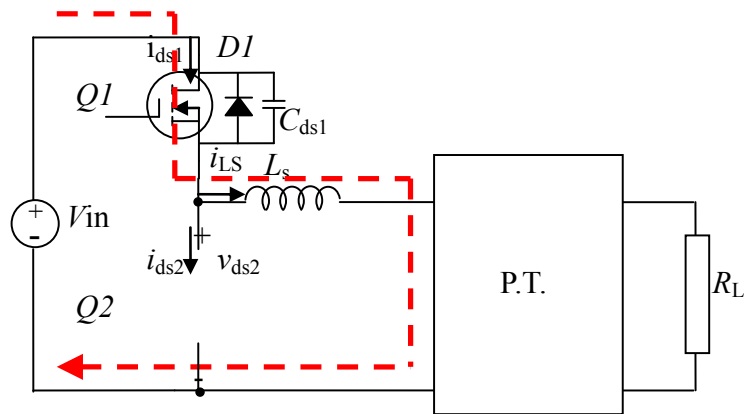


Figure 4-7. The operation of the ZVS-mode half-bridge circuit with a PT during mode 1

**Step 2.  $[t_1-t_2]$**

In this period, the switches  $Q_1$  and  $Q_2$  are both “OFF”, so this period corresponds to “dead time”. To achieve the ZVS condition, the input current  $i_{L_s}$  should flow in the positive direction (from the half-bridge circuit to the PT). According to the current flowing direction, the capacitor  $C_{ds1}$  is charged and the capacitor  $C_{ds2}$  is discharged. Therefore, the voltage of the high-side MOSFET  $v_{ds1}$  increases until reaching  $V_{DC}$ , and the voltage of the low-side MOSFET  $v_{ds2}$  decreases until reaching zero voltage. This period is the key of the ZVS condition. If the dead time is not large enough, voltage  $v_{ds2}$  cannot be fully discharged to zero and the low-side switch cannot be turned “ON” at zero voltage in the following stage. Therefore, increasing the dead time or the input current can help capacitor  $C_{ds2}$  to fully discharge.

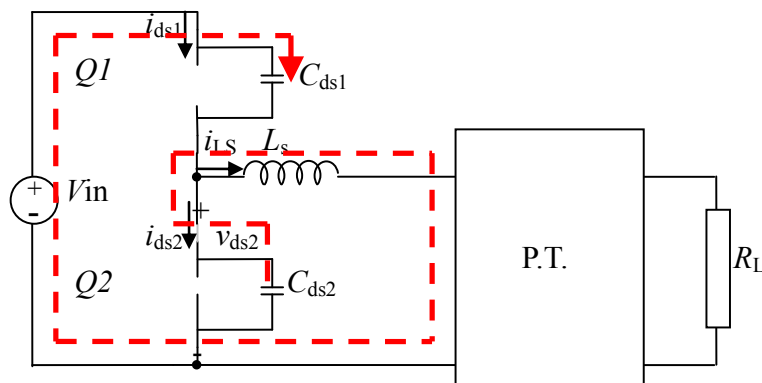


Figure 4-8. The operation of the ZVS-mode half-bridge circuit with a PT during mode 2

**Step 3 [ $t_2$ - $t_3$ ]**

In this period, switches  $Q_1$  and  $Q_2$  are both still “OFF”. Since voltage  $v_{ds2}$  has been discharged to zero, the body diode in the low-side MOSFET is forward bias. This period is over when switch  $Q_2$  is turned ON.

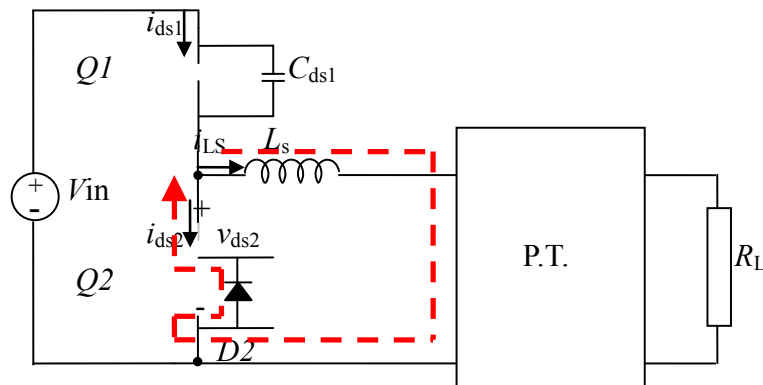


Figure 4-9. The operation of the ZVS-mode half-bridge circuit with a PT during mode 3

**Step 4 [ $t_3$ - $t_4$ ]**

In this period, switch  $Q_1$  is “OFF” and switch  $Q_2$  is “ON”. Since the voltage of the low-side switch has reached zero in the last period, switch  $Q_2$  is turned ON at the zero voltage condition, at instant  $t_3$ . In addition, the input inductor  $L_s$  and the PT input capacitor  $C_1$  achieve the resonance in this period. To ensure switch  $Q_1$  can switch at zero voltage condition in the following period, this resonance has to make the flowing direction of input current  $i_{L_s}$  reverse at instant  $t_4$ .

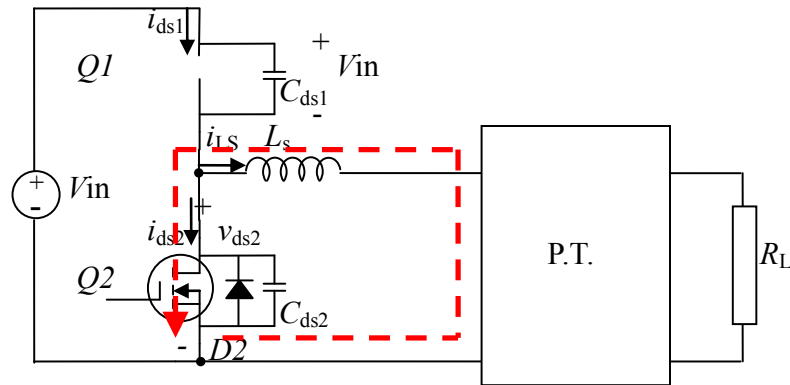


Figure 4-10. The operation of the ZVS-mode half-bridge circuit with a PT during mode

4

**Step 5 [ $t_4-t_5$ ] :**

In this period, switches  $Q_1$  and  $Q_2$  are both “OFF”. The input current  $i_1$  should flow in the negative direction (from PT to the half-bridge circuit) and capacitor  $C_{ds1}$  is discharged and capacitor  $C_{ds2}$  is charged. Therefore, the voltage of the high-side MOSFET  $v_{ds1}$  decreases until reaching zero, and the voltage of the low-side MOSFET  $v_{ds2}$  increases until reaching  $V_{DC}$ . Actually, this period is similar to *Step 2*, but the input current  $i_1$  is in a different direction.

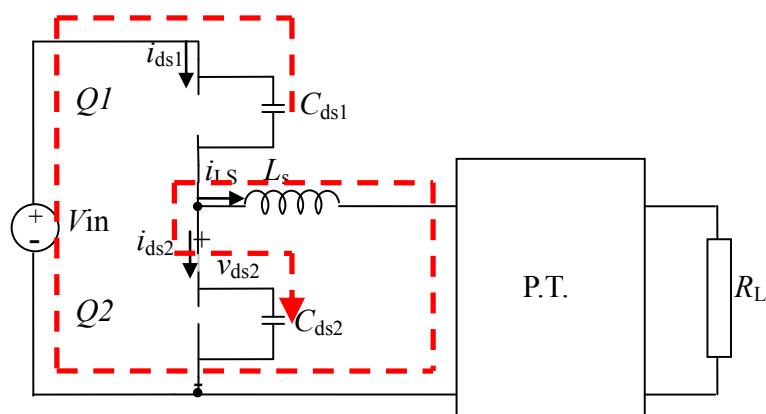


Figure 4-11. The operation of the ZVS-mode half-bridge circuit with a PT during mode

5

**Step 6 [ $t_6-t_0$ ] :**

In this period, switches  $Q_1$  and  $Q_2$  are both still “OFF”. Since the voltage  $v_{ds1}$  has been discharged to zero, the body diode in the high-side MOSFET is forward bias. This period is over when switch  $Q_2$  is turned ON.

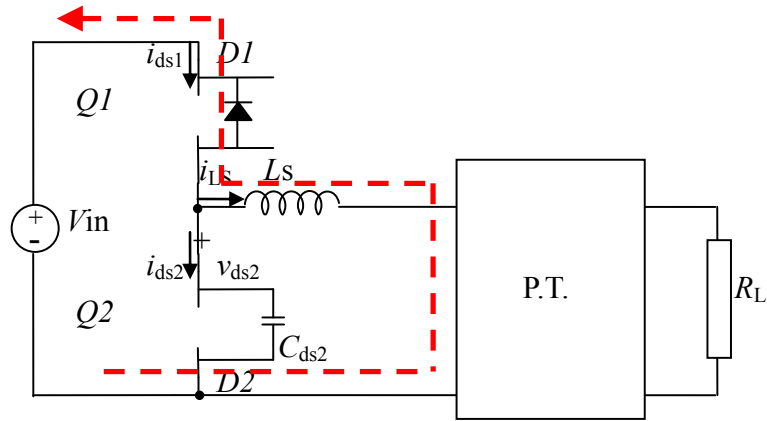


Figure 4-12. The operation of the ZVS-mode half-bridge circuit with a PT during mode

6

On the other hand, the experimental setup of PT based DC/DC converter is shown in

Figure 4-13.

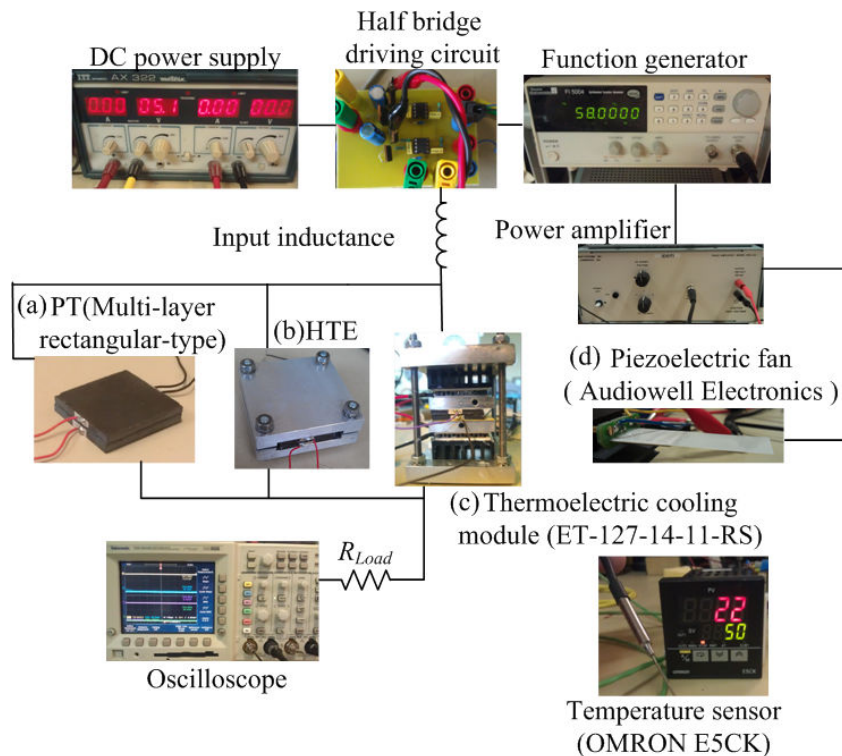
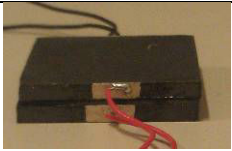




Figure 4-13. Experimental setup of PT based DC/DC converter.

In this section, we adopt the “type C” multi-layer piezoelectric transformer that works in planar vibrating mode with internal circular electrodes. Comparing to the PTs “type A” and “type B” used in Chapter 3, the dimension of the PT is different. The properties of the PT specimen and the experimental results measured by the impedance analyzer are given in Table 4-1.

Table 4-1. Picture, size and properties of the PT

 <p>PT size : 22mm*22mm*4.5mm</p>	<p>Input section</p> <p>No. of layers 4</p> <p>Thickness 0.5mm (0.5*4=2mm)</p>	<p>Output section</p> <p>No. of layers 4</p> <p>Thickness 0.5mm (0.5*4=2mm)</p>	<p>Isolation</p> <p>No. of layers 1</p> <p>Thickness 0.5mm (0.5*1=0.5mm)</p>
	<p>Input inductance</p> <p>51 <math>\mu</math>H</p>	<p>Operating frequency</p> <p>94.3 kHz</p>	<p>Unstable temperature of PT</p> <p>55 ° C</p>
<p>Material properties (PZT-QA, ELECERAM TECHNOLOGY Co., Ltd., Taiwan):</p>			
<p><math>K_p = 0.58</math> is the electromechanical coupling coefficient.</p> <p><math>Q_m = 1800</math> is the mechanical quality factor.</p> <p><math>\rho_m = 7.9</math> is the density (<math>\text{g cm}^{-3}</math>).</p> <p><math>N_p = 2200</math> is the frequency constants of the plane vibration (kHz mm).</p> <p><math>S_{11}^E = 1.14 \times 10^{-11}</math> is the compliance constant under the constant electric field, i.e. constant <math>E</math>.</p>	<p><math>d_{33} = 320 \times 10^{-12}</math> and <math>d_{31} = -140 \times 10^{-12}</math> are the piezoelectric constants (<math>\text{m V}^{-1}</math>).</p> <p><math>Y_{33} = 320 \times 10^{-12}</math> and <math>Y_{31} = -140 \times 10^{-12}</math> are the elastic constants (<math>\text{N m}^{-2}</math>).</p> <p><math>\nu = 0.16</math> is Poisson's ratio.</p> <p><math>\epsilon_{33}^S = 1420 \times 8.854 \times 10^{-12}</math> is the permittivity at constant strain condition, i.e. constant <math>S</math> (<math>\text{F m}^{-1}</math>).</p>		
<p>The experimental result obtained by impedance analyzer:</p>			

$f_t$	$f_a$	$R_0$	$L_m$	$C_m$	$C_1$	$C_2$	$N$	$T$
(KHz)	(kHz)	( $\Omega$ )	(mH)	(nF)	(nF)	(nF)	(-)	$^{\circ}\text{C}$
93.78	98.285	1.37	0.837	3.799	36.28	37.05	1	25

Furthermore, a 1 W DC power source supplies to the thermoelectric cooling module in the cooling system. Comparing to power consumption of the thermoelectric cooling module, the piezoelectric fan can be driven with a very low power requirement less than 100 mW. The properties of the thermoelectric cooling module and piezoelectric fan are given in Table 4-2 and Table 4-3.

Table 4-2. Experimental data of the thermoelectric cooling module specimen

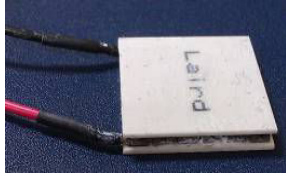
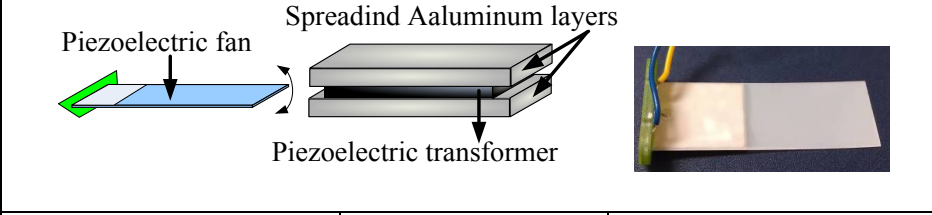
Thermoelectric cooling module size : 40mm*40mm*3.8mm		
		
Maximum intensity	Number of pairs N	Maximum power
8.4A	14	82.1W
Maximum temperature	Maximum voltage	Manufacturer code
80 $^{\circ}\text{C}$	15.7V	AND-127-14-11-RS
Operating voltage	Operating current	Operating input power
2.5V	0.7A	1.75 W

Table 4-3. Properties of the piezoelectric fan and thermoelectric cooling module

Thermoelectric cooling module size: 57mm*20mm*0.76mm (resonant frequency: 60 $\pm$ 3 Hz)
---

		
Maximum intensity	Operating voltage	Maximum power
2.5 mA	40 V	100 mW

Here, a contact temperature sensor was also used to monitoring the PT temperature in different driving conditions.

#### 4.4 COMSOL Simulation Result of Heat Generation and Temperature Rise for Multi-layer PT

In previous research [69]-[72], it is feasible to use a FEA approach to estimate temperature rise experienced in a typical ultrasonic transducer due to dielectric loss and vibration. Applying the COMSOL model, heat generation in an ultrasonic transducer due to electric potential and vibration can be determined and evaluated clearly [73]. For COMSOL analysis steps,

- First, an eigen value analysis for the PT was used to predict the exact frequency at which longitudinal mode is occurring firstly.
- Then, a frequency response analysis is performed by exciting the transducer in the axial direction by applying the voltage  $V$  to the PT. From this analysis, the strain energy density is extracted and it can be used to calculate the dielectric losses and mechanical losses by using equation (2-2) and (2-3).
- Finally, the dielectric losses density  $P_{D-Loss}$  and the mechanical losses density  $P_{M-Loss}$  are defined as heat flux inputs to the heat transfer module which is defined as an inbuilt equation, *i.e.* “Qdamp\_smsld” in COMSOL. After those heat flux inputs are applied to the PT, a thermal analysis can be

performed to find the temperature distribution of the PT with different electric potential.

- By using the COMSOL thermal model, we could compare the PT temperature distribution with or without heat transfer equipment easily.

Through the analysis step mentioned above, an Eigen value analysis for the PT and heat transfer equipment was established to predict the exact frequency as shown in Figure 4-14, *i.e.* exact frequency = 89 725 Hz, at which longitudinal mode is occurring.

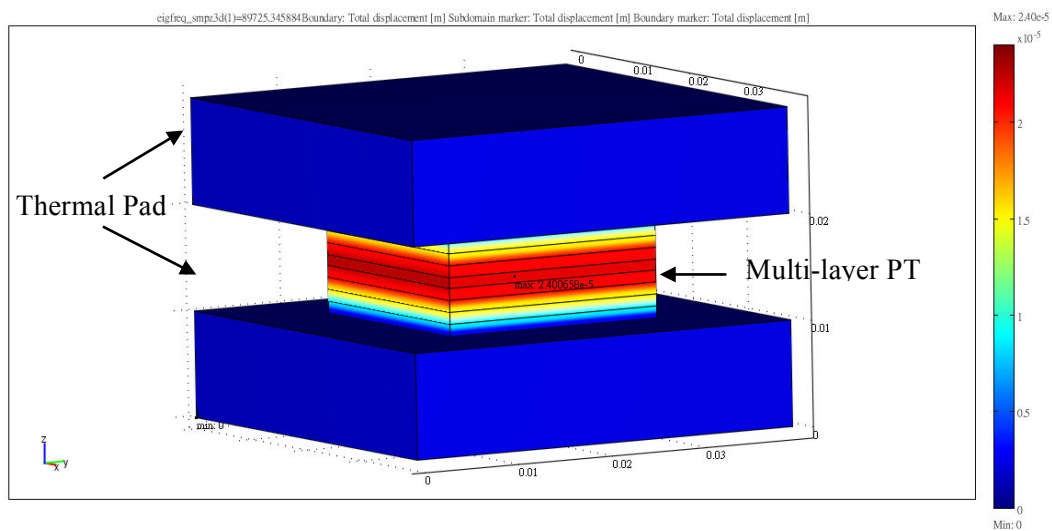


Figure 4-14. Total displacement plot at 89.73 kHz longitudinal frequency

From this analysis, the strain energy density is extracted and it can be used to calculate the dielectric losses and mechanical losses by using the COMSOL inbuilt equation “Qdamp\_smsld”. Furthermore, we can estimate the temperature rise due to internal losses under high-power conditions to predict PTs’ working temperature as shown in Figure 4-15.

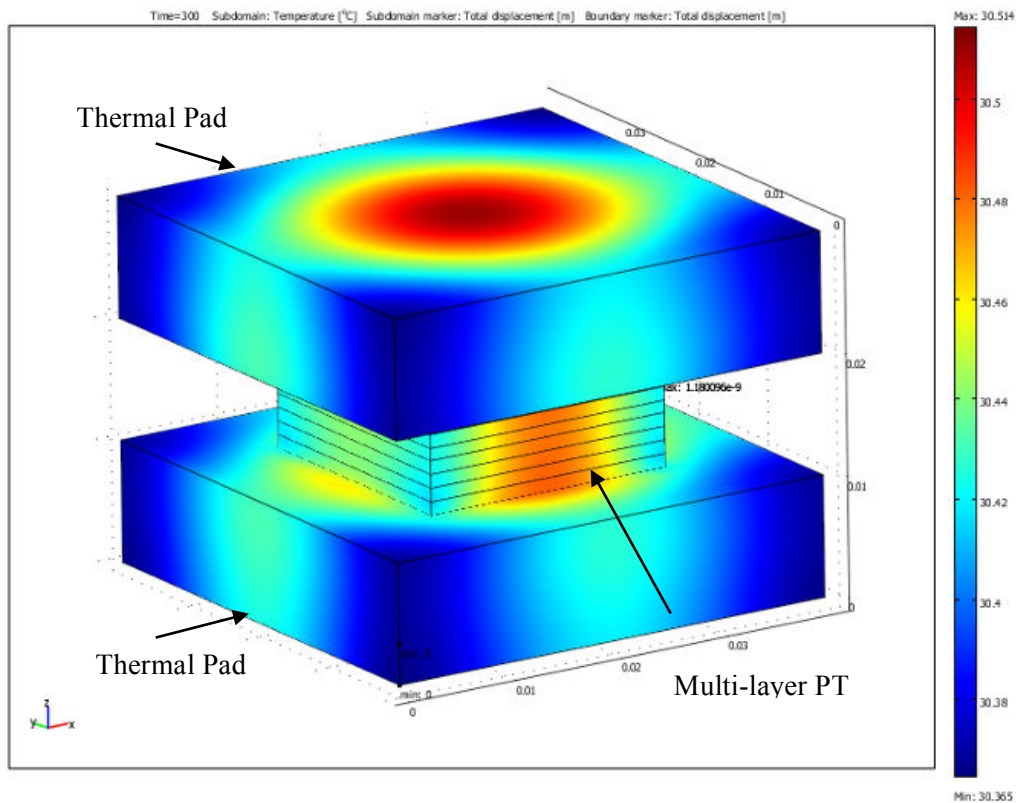


Figure 4-15. Temperature distribution of PT and HTE (Driving by a sinusoidal input voltage with a peak of 25V after 300 seconds)

In Figure 4-15, it is revealed that the maximum temperature of PT equal to 30.5°C driven by a sinusoidal input voltage with a peak of 25V after 300 seconds. The COMSOL simulation results can be used to predict working temperature of the PT and temperature distribution of the HTE system. Furthermore, through the temperature distribution between PT and heat transfer equipment based on the COMSOL simulation result provided us sufficient information to design the heat transfer equipment type.

## 4.5 Experimental Results and Discussion

To explain the relationship between vibration velocity and PT temperature, the coefficient  $\alpha$  is determined by measuring the mechanical current  $i_m$  and resistance  $R_{NL}$  and temperature for the four experimental setups. The variation of mechanical current  $i_m$  and PT temperature is obtained by applying different input voltages as shown in Figure 4-16.

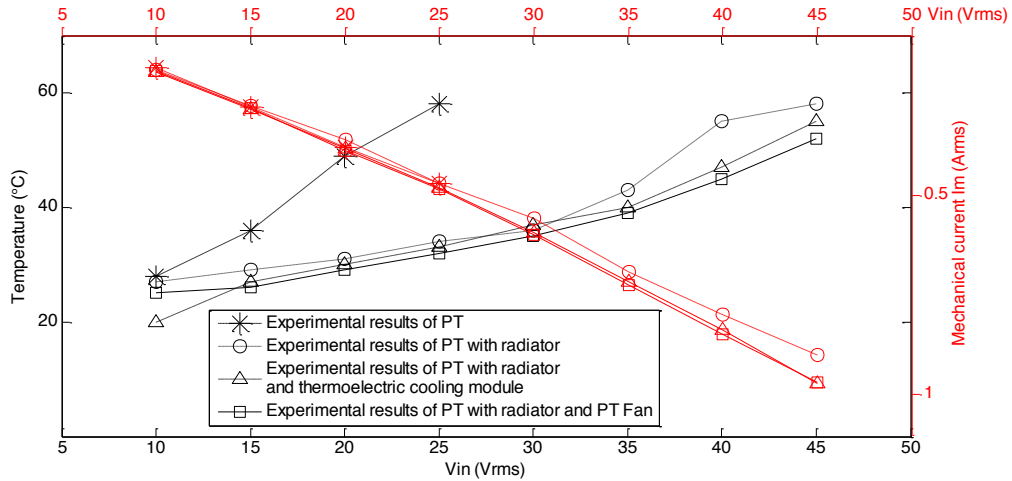


Figure 4-16. Characteristics between temperature, mechanical current and input voltage

In Figure 4-16, it can be seen that mechanical current increases with input voltage and temperature. Through applying the cooling system, for the same temperature of 55 °C, the mechanical current can increase from 0.44 A to 0.97 A as shown in Figure 4-17. At the 25–55 °C temperature range, mechanical currents which were measured with cooling system increased almost 3 times more than in the case of bared PT operation. It is clear that the resistance  $R_m$  is efficiently decreased by applying the cooling system for the same mechanical current. In addition, as the mechanical losses  $P_{m-loss}$  are a function of mechanical resistance  $R_m$ , the mechanical losses  $P_{m-loss}$  are also decreased by applying the cooling system.

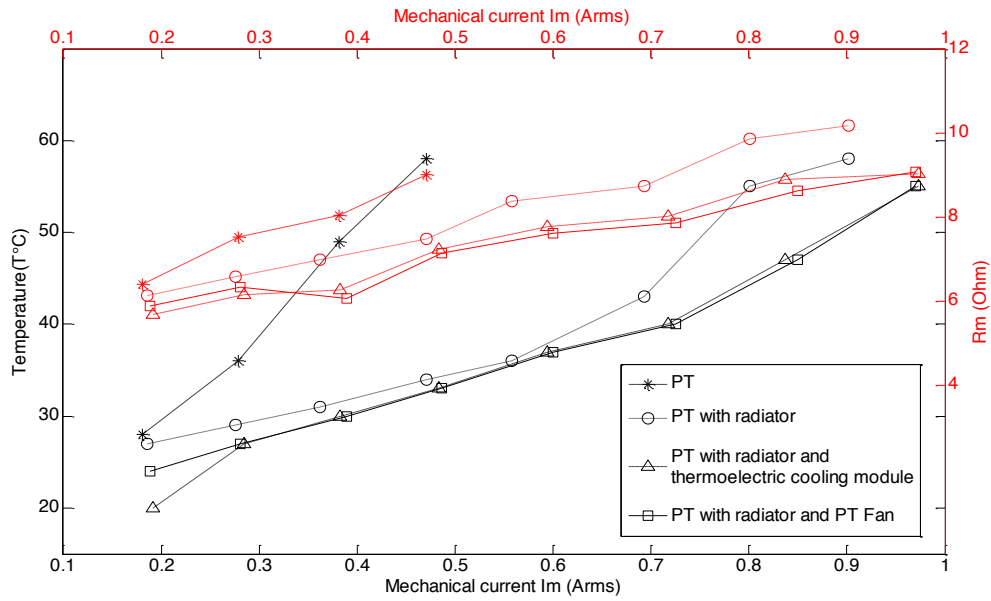


Figure 4-17. Characteristics between mechanical resistance  $R_m$ , temperature and mechanical current

Moreover, the relationship between coefficient  $\alpha$ , temperature and mechanical current can be derived from curve fitting in Figure 4-18. It is shown that the coefficient  $\alpha$  of the single PT structure is much larger than the other cases in the same temperature condition. This result clearly indicates that large coefficient  $\alpha$  leads to high PT losses at the same mechanical current.

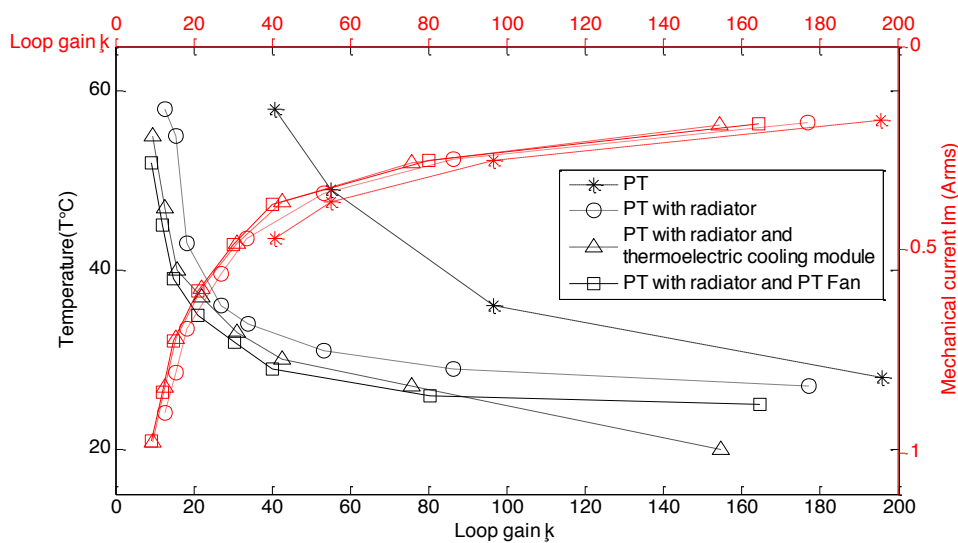


Figure 4-18. Characteristics between loop gain  $\alpha(T^{\circ}\text{C})$ , mechanical current and

temperature.

In Figure 4-19, the experimental results show that the output power of the PT with cooling system can move from 4.54 W to 13.29 W at the same temperature (55°C) with 47  $\Omega$  load value. The output power was increased at least 3 times at good efficiency (70%+) when the load was varied from 10 to 330  $\Omega$ .

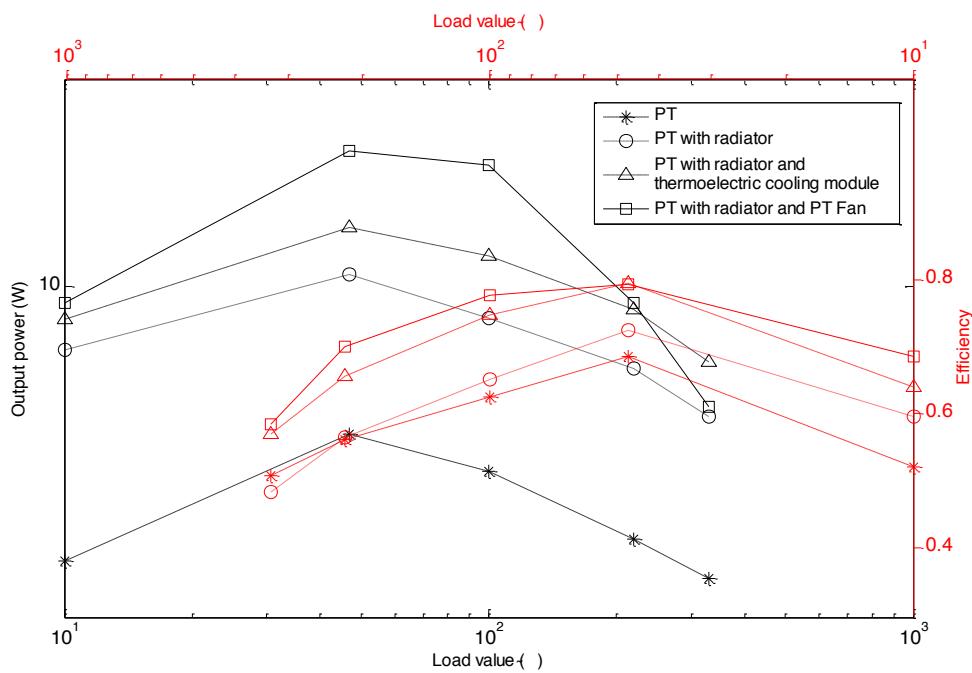


Figure 4-19. Output power and efficiency as a function of load in different cooling structures.

## 4.6 Summary

In this section, a cooling system with heat transfer equipment and piezoelectric fan was used to enhance the output power of piezoelectric transformers. According to the experimental results, all specimens remained a satisfactory efficiency even at temperature 55°C. By applying planar heat transfer equipment (HTE), the ability of heat



dissipation becomes better. The PT passing current can increase from 0.44 A to 0.97 A, and the maximum output power of the PT can also increase from 4.54 W to 13.29 W at specific temperature. Furthermore, we proposed a model that can explain the relationship between vibration velocities and temperature rises of the PT. The finite element analysis (FEA) approach by COMSOL Multiphysics was also used to predict PTs' working temperature. This study clearly indicates that it is possible to enhance the performance of the piezoelectric transformer by decreasing the loop gain  $\alpha$ . Moreover, the output current of the piezoelectric transformer in our design also increases, which implies that this technique allows the piezoelectric transformer to be used in low voltage-high current applications.

Table 4-4 shows the detail comparison between the piezoelectric fan and the thermoelectric cooling module, and it can be used to demonstrate the practicability of each device.

Table 4-4. Merit and demerit of the piezoelectric fan and the thermoelectric cooling module

Type of cooling device	Piezoelectric fan	Thermoelectric cooling module[19]
Volume and weight	+ smaller ( no redundancy necessary)	- larger (need additional radiators)
Heat sink reliability	+ stable	- unstable (heat saturated problem)
Power consumption	+ lower (100 mW)	- higher (1.75 W)
Total thickness	+ smaller (14mm collocate with HTE)	- larger (100mm collocate with radiator)
Output power capability	+ higher (13.29W with 47 $\Omega$ load )	- lower (11.45W with 47 $\Omega$ load )

Although both of the cooling method can provide the abilities to improve the output power and current of the PT, the cooling method by using piezoelectric fan provides a more reliable heat sink and needs lower power consumption. Furthermore, it is more appropriately for low-profile application.

# **Chapter 5    Application: PT-Based DC/DC Converter with Planar Heat Transfer Equipment**

## **5.1    Introduction**

The objective of this study was to increase the output current and power in a PT based DC/DC converter by adding a cooling system. Recently, the application domain of PT was extended at low voltage DC/DC converter with variable loads [14][77]. But in low voltage application, the power density of the converter is limited by the maximal value of output current. Although connecting different inductive circuits at the PT secondary terminal can increase the output current like current-doubler rectifier, the root cause of temperature build-up problem is not solved today. In this chapter a comparison between DC/DC converter with commonly used full-bridge rectifier and with PT with cooling system and DC/DC converter with current-doubler rectifier is carried out. The advantages and disadvantages of the proposed technique are investigated. In our design, the maximum output current capacity can increase 100% when the operating condition of PT temperature is kept below 55°C.

## **5.2    Converter Topologies and Control Considerations**

From previous research [60], PT-based DC/DC converter can be roughly divided into three parts including:

- Input driving circuit that can be used to excite PT vibrations
- Appropriate type of piezoelectric transformer that can be used to satisfy the application requirement
- Output interfacing circuit or network, *i.e.* rectifying circuit, which can be used to condition the output signal in desired form.

On the other hand, the "electrical load" of PTs can be basically divided into two

loads such as AC loads and DC loads according to the AC voltage/current or the DC voltage/current passing through the PTs respectively. Because of the characteristic that PT transfers the energy efficiently by the vibration but not the deformation, we can find out that the output signals from the PT are always AC signals. In practical application, PTs are often designed to operate near the resonant frequency owing to the fact that PTs transfer power efficiently near the resonance. Based on above discussions, a DC load is connected to the PT in the application of PT-based DC/DC converter and a rectifying circuit has to be inserted in between the PT output terminal and the DC load. The selection of the rectifiers is very important owing to the fact that there is no “best” choice of the rectifiers for PT basically, but only the “proper” choices [60]. We should select the most appropriate rectifier according to the application and the targeted specification. Some basic criterions to choose a proper rectifier are listed below:

- Simpler topologies of the rectifiers:

Owing to the fact that all components produce internal losses, we should utilize fewer components to induce internal loss caused by the redundant components. Considering the lower cost and lower losses, the simpler topologies of the rectifiers should be utilized.

- Higher power density:

On the demand trends of thinning tendency, the design of PT-based DC/DC converter should be appropriate for the low-profile applications. We should design the PT which can transfer power as high as possible in the same volume, *i.e.* high power density.

To analyze PT-based DC/DC converter, we adopt the previous single-mode non-linear equivalent circuit, and there are several basic assumptions in our theoretical analysis:

- 1. The mechanical current  $i_m$  is pure sinusoidal wave in the steady state.
- 2. The filtering capacitance  $C_f$  is larger enough than the output capacitor  $C_2$  of the PT, i.e.  $C_2/C_f \approx 0$ , so the load voltage  $V_L$  can be viewed as a perfect DC voltage sink.
- 3. The diode voltage drops is set 0.
- 4. The operating frequency is set near the resonant frequency. It should be noted that the resonance frequency is shifted with temperature rise, thus we assume that operating frequency don't varies in our model.

### 5.3 PT-Based Converter Circuit Diagram and Its Operation

As shown in Figure 5-1, a half-bridge circuit and an inductor were adopted as the input driving circuit to excite PT vibration. To get the DC voltage, a full-wave rectifier was connected to the PT output terminal. The filtering capacitance  $C_F$  should be sufficiently larger than the PT output capacitor  $C_2$  to guarantee the load voltage  $V_L$  can be viewed as a perfect DC voltage sink.

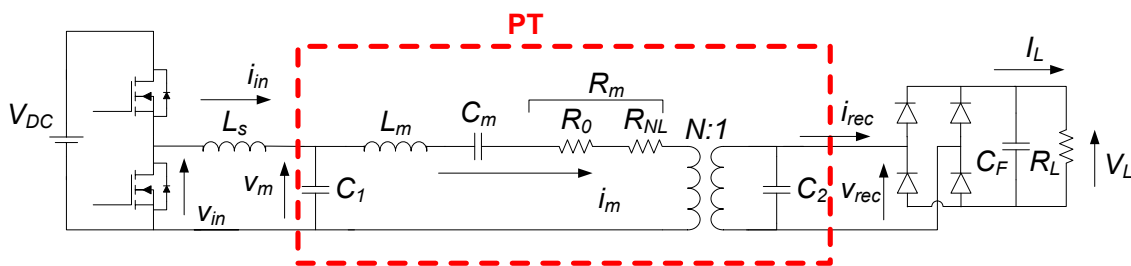


Figure 5-1. The schematic diagram of piezoelectric transformer based DC/DC converter.

Assuming that the mechanical current  $i_m$  is a sinusoidal waveform in the steady state condition, the PT model can be simplified as a current source with the clamped

capacitor  $C_2$  as shown in Figure 5-2(a). The current and voltage waveforms of the PT fed full-wave rectifier are shown in Figure 5-2(b). It should be noted that because of the large value of the filtering capacitor  $C_F$ , the PT output voltage  $v_{rec}$  is not a sine wave. These waveforms can be divided into four periods. In the first and third period, the diode is blocked, and thus the PT output capacitor is charging or discharging. In the second and fourth period, diode is conducted, and thus the rectifier voltage is roughly equal to the load voltage. The theoretical expressions of the load voltage  $V_L$ , the losses  $P_D$  and  $P_{PTLoss}$  and the load power  $P_L$  are given in Table 5-1, where  $\omega$  is the phase angle;  $\theta_b$  represents the diode block angle and  $V_D$  the diode voltage drop. Figure 5-2(c) shows our experimental waveform, which fits the characteristics of the theoretical waveforms.

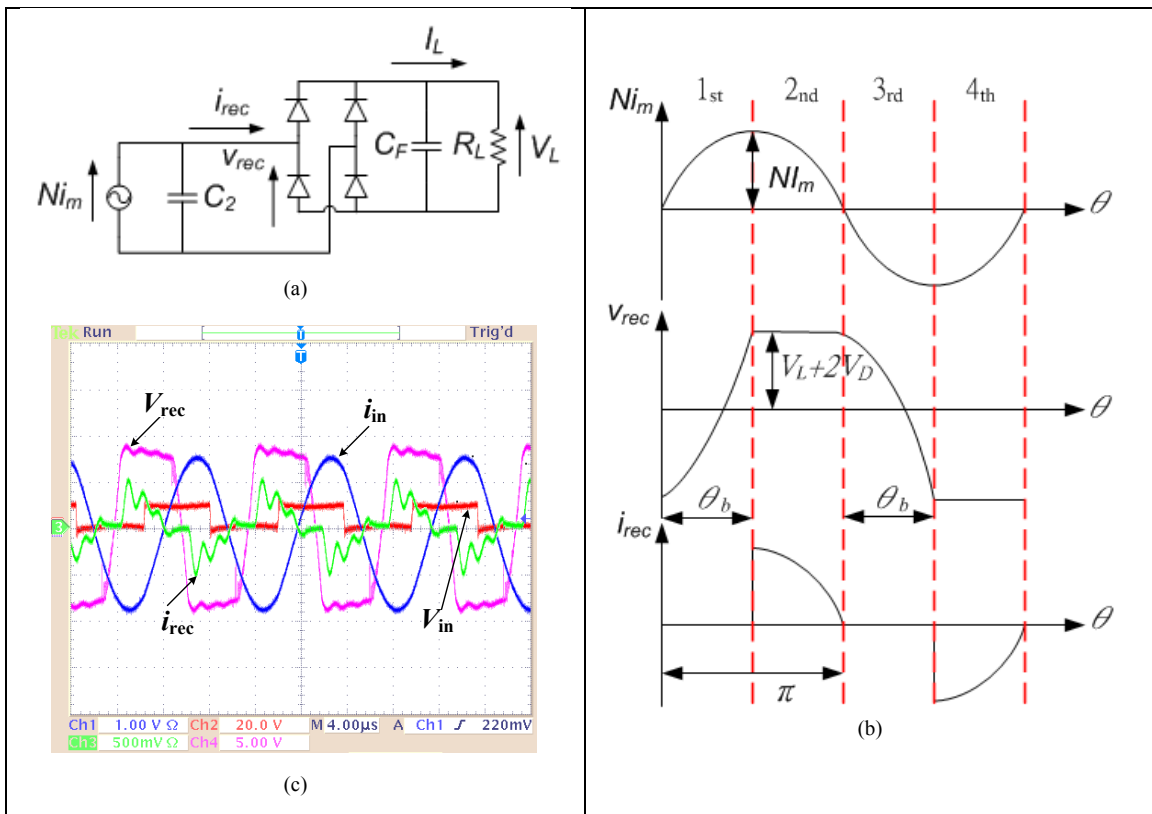


Figure 5-2. (a)The schematic diagram of PT fed full-wave rectifier (b) theoretical voltage and current waveforms of the PT fed full-wave rectifier (c) experimental waveform of PT input voltage  $v_{in}$  (blue, 20V/div), PT input current  $i_{in}$  (yellow, 1A/div),

voltage at PT output terminal  $v_{rec}$  (green, 5V/div) and current at PT output terminal  $i_{rec}$  (purple, 0.5A/div).

Table 5-1. Characteristics of the PT fed rectifier.

PT fed full-wave rectifier			
Load voltage	$V_L = \frac{2R_L(NI_m - 2\omega C_2 V_D)}{\pi + 2\omega C_2 R_L}$	Rectifier losses	$P_D = 2V_D \frac{V_L}{R_L}$
Phase angle	$\theta = \omega t$	Diode block angle	$\theta_b = \cos^{-1}\left(\frac{\pi - 2\omega C_2 R_L}{\pi + 2\omega C_2 R_L}\right)$
Optimal load condition	$R_L^* = \frac{\pi}{2\omega C_2}$	PT losses	$P_{PTloss} = I_m^2 R_m$
Load power	$P_L = \frac{V_L^2}{R_L}$	Efficiency of the converter	$\eta = \frac{P_L}{P_{PTloss} + P_D + P_L}$

Based on the Table 5-1, the efficiency of the converter can be determined by equation (5-1):

$$\eta = \frac{P_L}{P_{PTloss} + P_D + P_L} \quad (5-1)$$

Considering the input driving circuit, the ZVS (Zero Voltage Switching) condition is possible to achieve without any additional magnetic elements (no inductor) by using inductive characteristics of the PT. However, this inductor-less scheme cannot be applied to wide-range load variations [16][40]. Therefore, we include an additional series inductor  $L_s$  to achieve the ZVS condition with a wide range of load variation. The resonant circuit formed by the series inductor  $L_s$  and the input static capacitance  $C_I$  of the PT achieves a quasi sine-wave PT input voltage  $v_m$ . Moreover, this series inductor exhibits high impedance, which both limits common and differentials mode currents [18].

## 5.4 Study of PT-Based DC/DC Converter with Cooling System and Current-Doubler Rectifier

The proposed PT with cooling system is implemented in a DC/DC converter. A half-bridge circuit with inductor  $L_{in}$  was adopted as the input driving circuit to excite PT vibration [74][75]. In the following, we will compare the output current capacity and the size of two different rectifying circuits, the full-wave bridge rectifier and current-doubler, as shown in Figure 5-3. Equivalent circuit of a (a) PT fed full-wave bridge rectifier (b) PT fed current-doubler rectifier.

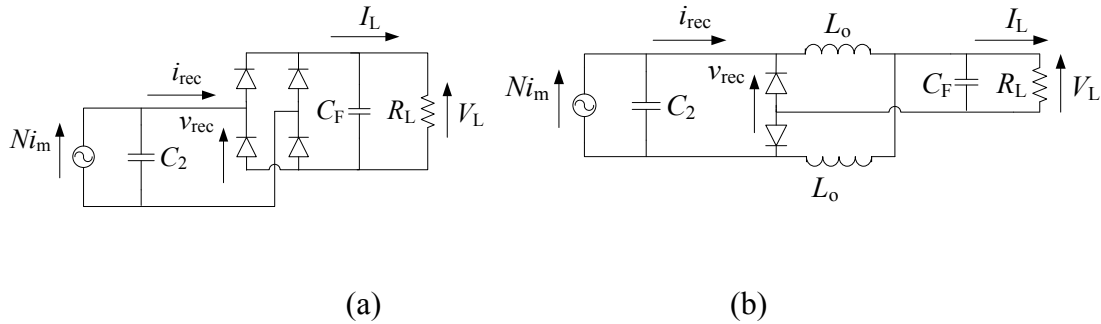


Figure 5-3. Equivalent circuit of a (a) PT fed full-wave bridge rectifier (b) PT fed current-doubler rectifier.

In Figure 5-4(a), the PT output current  $i_{rec}$  is plotted for both rectifiers with mechanical current  $i_m$ . It is assumed that both converters are operated at the maximum output voltage mode, which means the frequency and load conditions produce the maximum output voltage. The current-doubler operates in non-overlapping mode (NOM) and we assume that the load current and the  $L_o$  inductor current has negligible ripple, therefore the inductor current is clamped to the half value of the load current. The angle  $\Psi$  is the phase between the mechanical current  $i_m$  and the rectifier current  $i_{rec}$ .  $\theta_b$  is the diode block angle of the full-wave rectifier. The theoretical expressions of  $\theta_b$ ,  $\Psi$ , and

mechanical current are given in Table 5-2, where  $\omega$  is the operating angular frequency. It should be noted that the experimental result of the mechanical current could be obtained from Table 5-2.

Figure 5-4(b) shows the limit value of  $i_{rec}$ , which will cause the PT to reach present 55° C temperature limitation. The dash and the solid lines represent the higher limit value of  $i_{rec}$  for PT operated without and with cooling device respectively. To reach the same average  $i_{rec}$  current, the peak value for the current-doubler topology is smaller than for full-wave bridge topology. The current-doubler topology leads to higher output current, but nevertheless it needs the additional inductors.

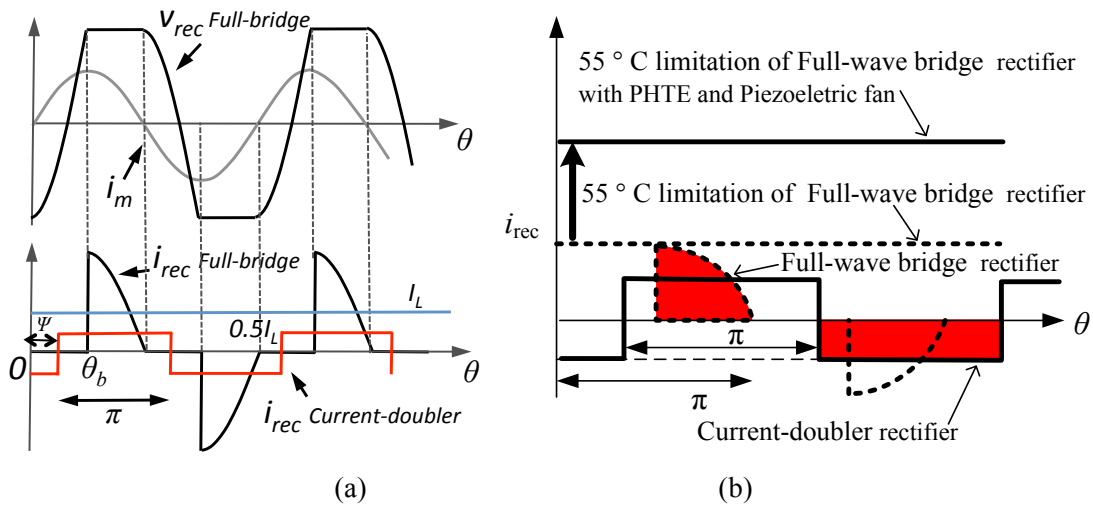


Figure 5-4. (a) Theoretical waveforms of the PT fed full-wave bridge rectifier and PT fed current-doubler rectifier (non-overlapping mode) (b) enhanced rectifier current limitation of full-wave bridge rectifier by using HTE and piezoelectric fan.

Table 5-2. Characteristics of the PT fed rectifier [14][21].

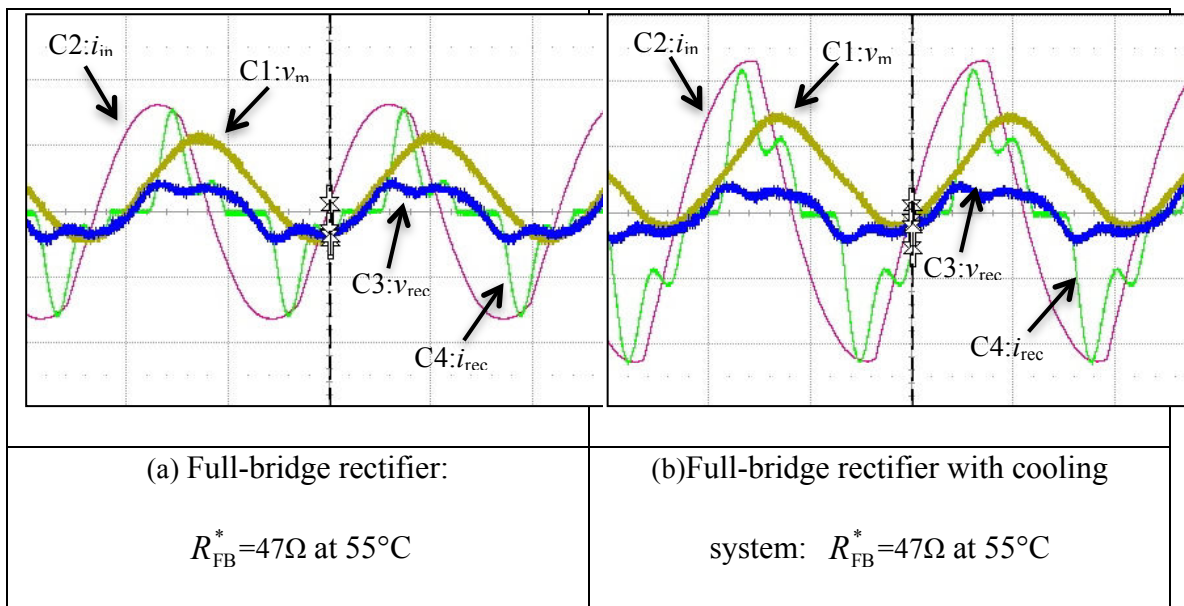
PT fed full-wave bridge rectifier			
Diode block angle	$\theta_b = \cos^{-1} \frac{(\pi - 2\omega C_2 R_L)}{(\pi + 2\omega C_2 R_L)}$	Mechanical current $i_m$	$i_m = \frac{(2\omega C_2 R_L + \pi)}{(2n_2 R_L)} V_L$
PT fed current-doubler rectifier			



Conduction angle between $Ni_m$ and $i_{rec}$ in NOM	$\psi = \tan^{-1}(4\omega C_2 R_L)$	Mechanical current $i_m$	$i_m = \frac{\pi}{4\cos\psi} I_L$
---	-------------------------------------	-----------------------------	-----------------------------------

## 5.5 Experimental Results and Discussion

Four different experimental cases are used to analyze the relationships between the input voltage, vibration velocity (mechanical current  $i_m$ ), non-linear resistance  $R_{NL}$ , coefficient  $\alpha$ , generated heat of the PT, and output power of the converters. They are (a) PT fed full-wave bridge rectifier without any add-on cooling devices, (b) PT fed full-wave bridge rectifier with HTE and piezoelectric fan, (c) PT fed current-doubler rectifier (non-overlapping mode) without any add-on cooling devices, and (d) PT fed current-doubler rectifier (non-overlapping mode) with HTE and piezoelectric fan. We first measured the experimental waveforms of the four cases in maximum output power conditions with individual optimal load resistance:  $R_{CD}^* = 10\Omega$  for current-doubler rectifier and  $R_{FB}^* = 47\Omega$  for full-wave bridge rectifier at  $55^\circ\text{C}$  temperature limitation as shown in Figure 5-5.



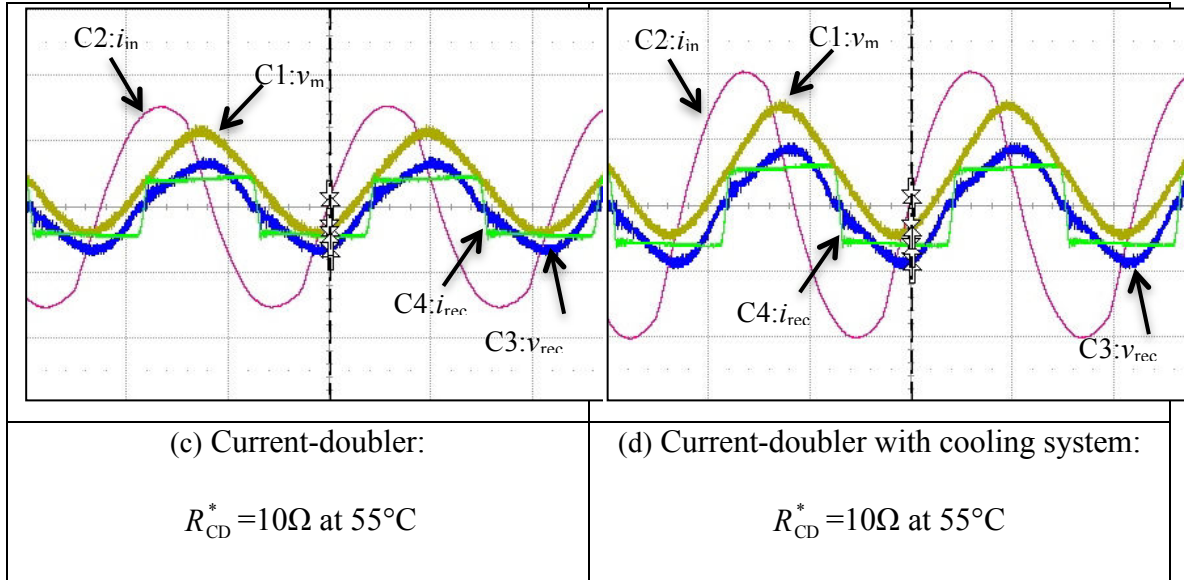
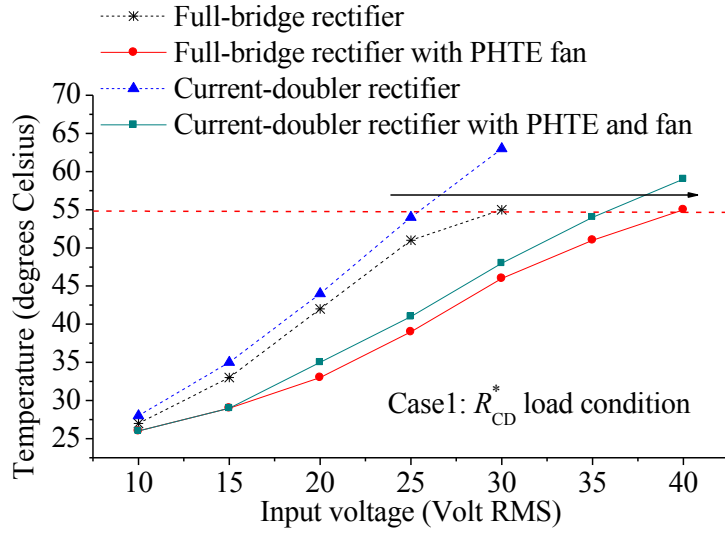


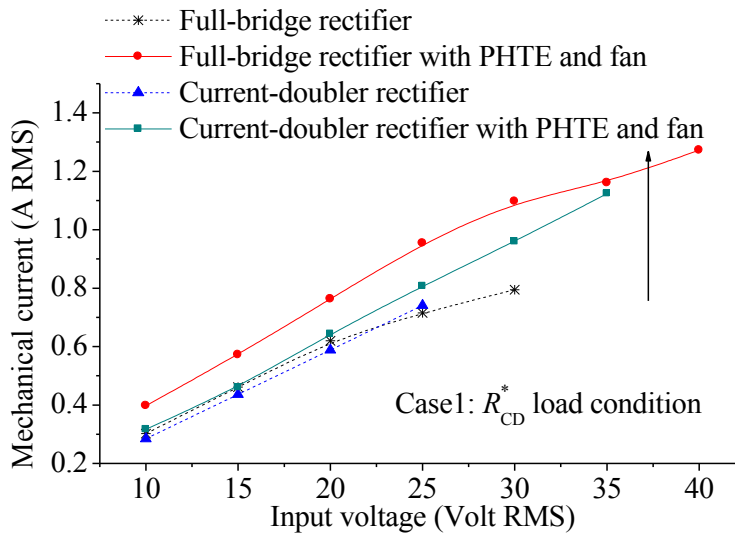
Figure 5-5. Experimental waveforms of PT input voltage  $v_m$  (C1, 50V/div), PT input current  $i_{in}$  (C2, 1A/div), voltage at PT output terminal  $v_{rec}$  (C3, 50V/div) and current at PT output terminal  $i_{rec}$  (C4, 1A/div) for (a) full-wave bridge rectifier (b) full-wave bridge rectifier with HTE and piezoelectric fan (c) current-doubler rectifier (d) current-doubler rectifier with HTE and piezoelectric fan.

In Figure 5-5, it is revealed that the capacities of PT input voltage  $v_m$  and the input current  $i_{in}$  are increased with the cooling system at the same  $55^\circ\text{C}$  temperature limitation, and thus the voltage  $v_{rec}$  and current  $i_{rec}$  at PT output terminal. The reason is owing to the fact that the capacity of applied voltage is increased [29]. The rectifying current in the case of the PT fed full-wave bridge converter is increased from 657 mA to 1069 mA at optimal load condition, and the input voltage of PT is increased from  $30.5 V_{rms}$  to  $39.5 V_{rms}$  as shown in Figure 5-6(a) and Figure 5-6 (b). On the other hand, the rectifying current in the case of the PT fed current-doubler converter is increased from 421 mA to 569 mA at optimal load condition, and the input voltage of PT is increased from  $30.2 V_{rms}$  to  $40.1 V_{rms}$  as shown in Figure 5-6(c) and Figure 5-6(d). The cooling system not only prevents the PT from overheating but it also increases the capacities of input voltage and passing current of the PT. In addition, we applied the measurement method [30] and observed that the relationships of PT's temperature and mechanical current

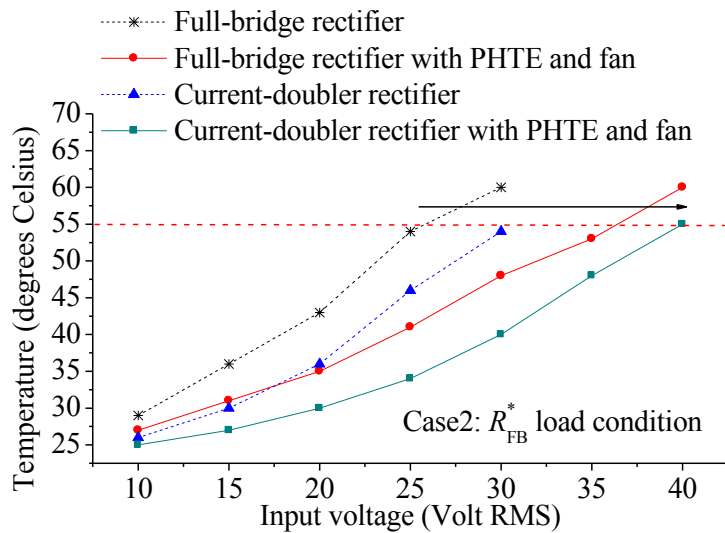
increase as a function of the input voltage as shown in Figure 5-6:



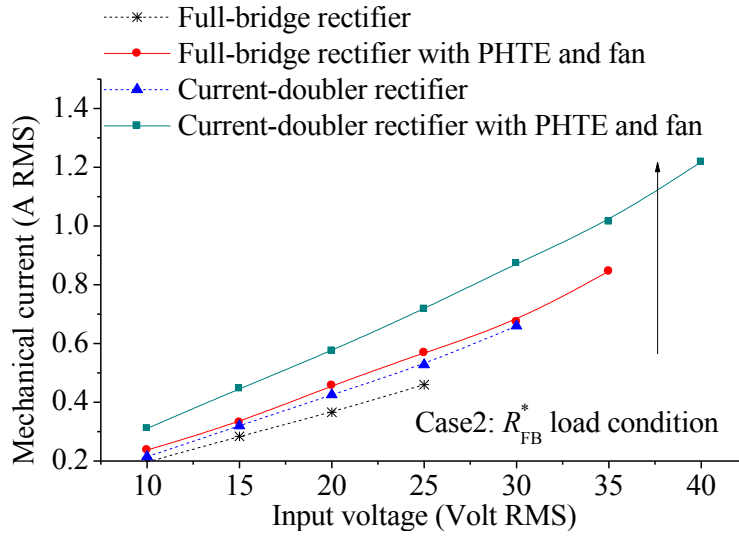
(a)



(b)



(c)



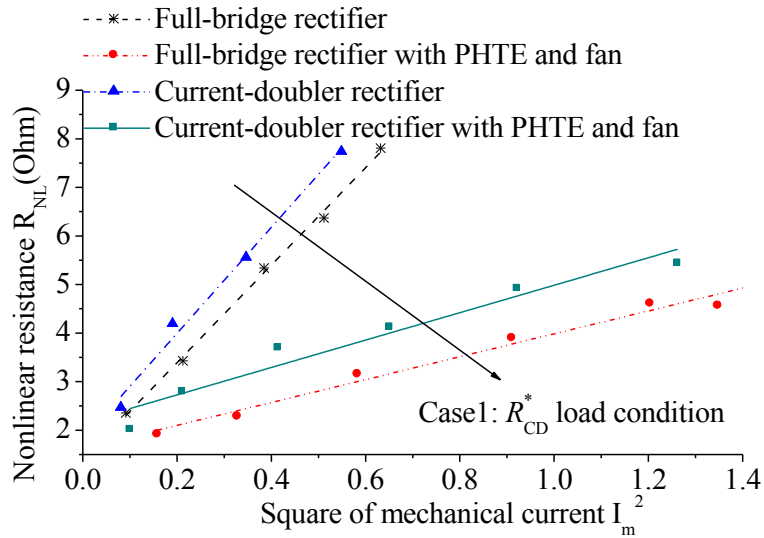
(d)

Figure 5-6. Characteristics between (a) input voltage and temperature in optimal load condition  $R_{CD}^*$  (b) input voltage and mechanical current in optimal load condition  $R_{CD}^*$  (c) input voltage and temperature in optimal load condition  $R_{FB}^*$  (d) input voltage and mechanical current in optimal load condition  $R_{FB}^*$ .

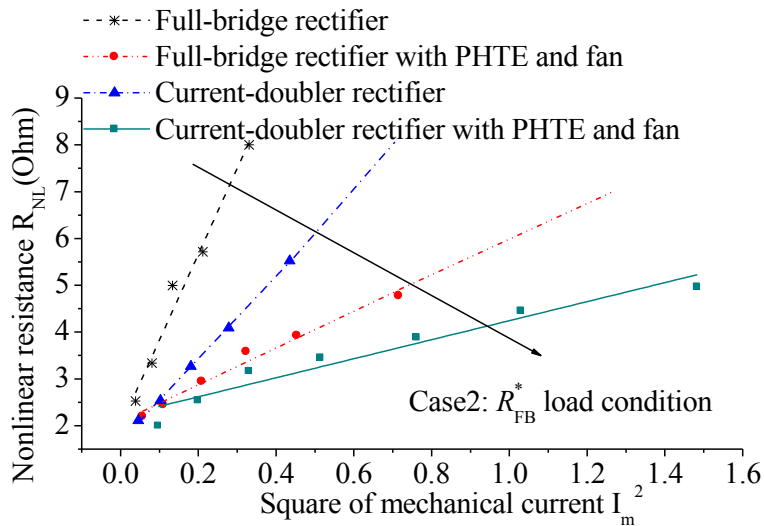
Figure 5-6(a) and Figure 5-6(c) represent the temperature rises of the PTs with various input voltages in two different optimal load conditions  $R_{CD}^*$  and  $R_{FB}^*$ . Both of the results show that the temperatures of PTs without any cooling devices achieve the temperature limitation 55 °C quickly. On the contrary, PTs with heat transfer devices can work at higher input voltage conditions (up to 40 V). In Figure 5-6(b) and Figure 5-6(d), it is also revealed that the suppression of temperature rise and nonlinear resistance allow us to increase the output current by increasing the input voltage. To have a larger output power, the mechanical resistance composed of low excitation resistance  $R_0$  and a non-linear resistance  $R_{NL}$  should be insensitive to the temperature rise [76]. The best case is that the nonlinear resistance  $R_{NL}$  is independent of temperature. To obtain the resistance  $R_{NL}$ , the power difference between the PT primary side and

secondary side  $P_{m-loss}$  and the temperature-independent resistance  $R_0$  are first measured and the resistance is calculated as:  $R_{NL} = P_{m-loss} / (i_m)^2 - R_0$ . The value of  $R_0$  is shown in Table 4-1.

To observe the non-linear resistance  $R_{NL}$  in different vibration level, the mechanical current  $i_m$  and  $P_{m-loss}$  were measured for various input voltage  $V_{in}$ . From the experimental results of  $R_{NL}$ , it is revealed that  $R_{NL}$  is a function of mechanical currents in squared as shown in Figure 5-7. Obviously, the temperature-dependent resistance  $R_{NL}$  in Figure 5-7 was efficiently reduced by using the cooling system at the same values of  $I_m^2$ . As the result, the mechanical losses can be decreased and the problem with heat generation of PT can be overcome appropriately.



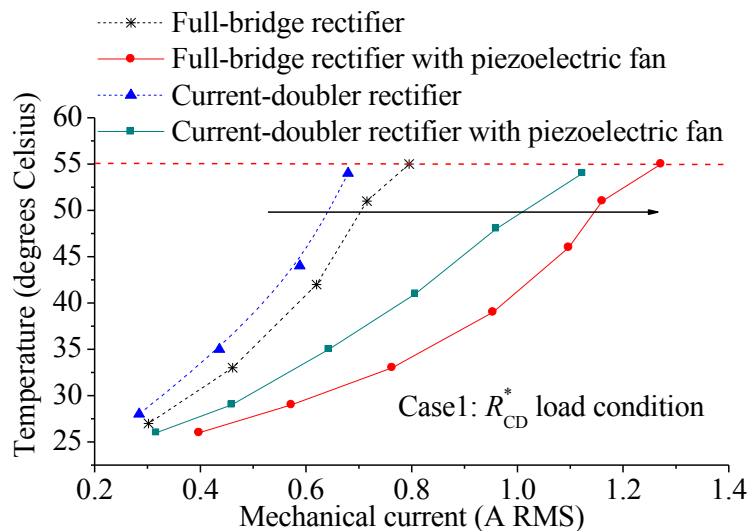
(a)



(b)

Figure 5-7. Result of the  $R_{NL}$  as a function of the square of mechanical current at different temperatures and in optimal load conditions: (a)  $R_{CD}^*$  (b)  $R_{FB}^*$

Through applying the cooling system to compare with the two rectifying circuits, for the same temperature limit of 55 °C, the mechanical current of PT connected with current-doubler rectifiers can be increased from 0.74 A to 1.12 A in optimal load condition  $R_{CD}^*$  as shown in Figure 5-8(a). On the other hand, the mechanical current of PT connected with full-bridge rectifier can be increased from 0.46 A to 0.9 A in optimal load condition  $R_{FB}^*$  as shown in Figure 5-8(b). At the 25–55 °C temperature range, mechanical currents which were measured with cooling system increased almost 2 times more than in the case of bared PT operation. It is clear that the resistance  $R_m$  is also efficiently decreased by applying the cooling system for the same mechanical current. In addition, as the mechanical losses  $P_{m-loss}$  are a function of mechanical resistance  $R_m$ , the mechanical losses  $P_{m-loss}$  are also decreased by applying the cooling system.



(a)

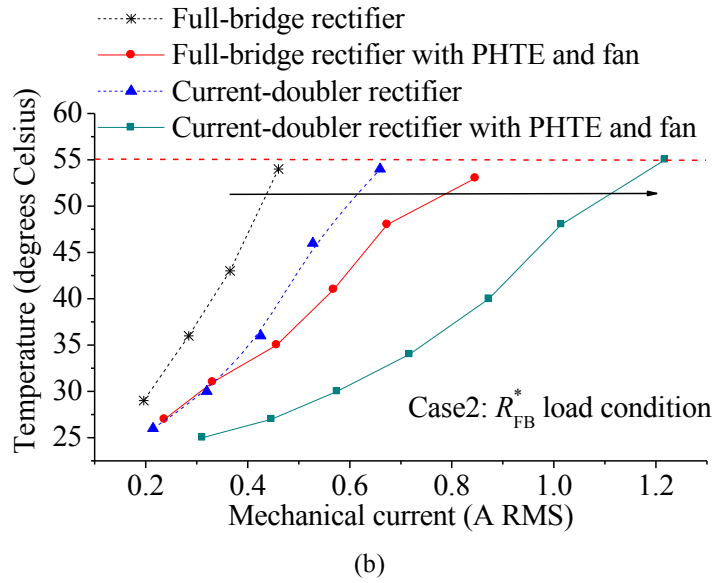
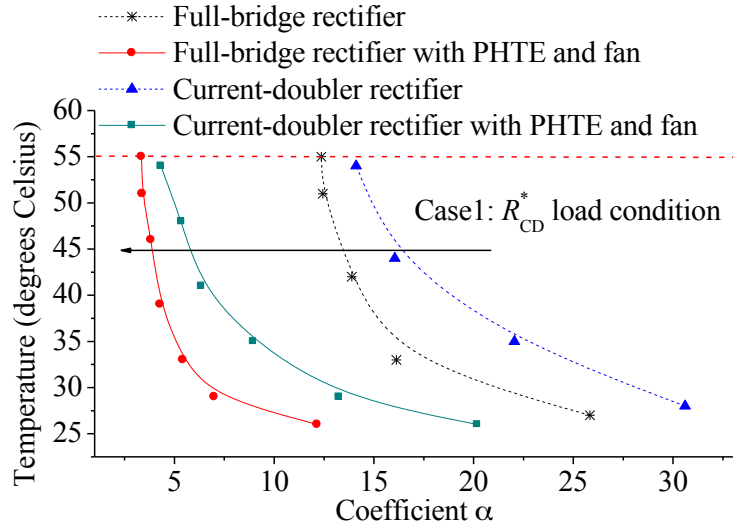
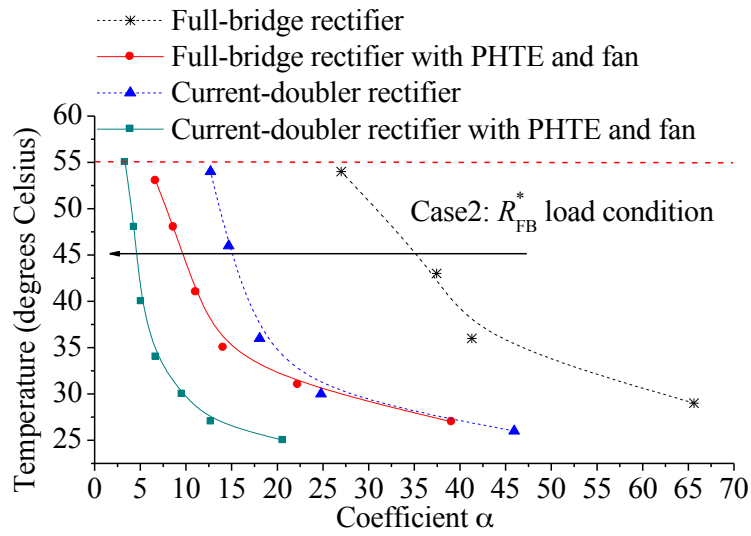


Figure 5-8. Characteristics between mechanical current and temperature. (a) in optimal load condition  $R_{CD}^*$  (b) in optimal load condition  $R_{FB}^*$

Moreover, to explain the relationship between vibration velocity and PT temperature, the coefficient  $\alpha$  is determined by measuring the mechanical current  $i_m$ , resistance  $R_{NL}$ , and temperatures based on the equation (3-6). In this dissertation, the coefficient  $\alpha$  can be seen as a thermal factor of improving output current (power) approach to the heating problem. Performance of PT-based converter can be improved through the cooling methods owing to the coefficient  $\alpha$  insensitive to the temperature rises. The relationship between coefficient  $\alpha$  and temperatures can be derived from curve fitting in Figure 5-9.



(a)



(b)

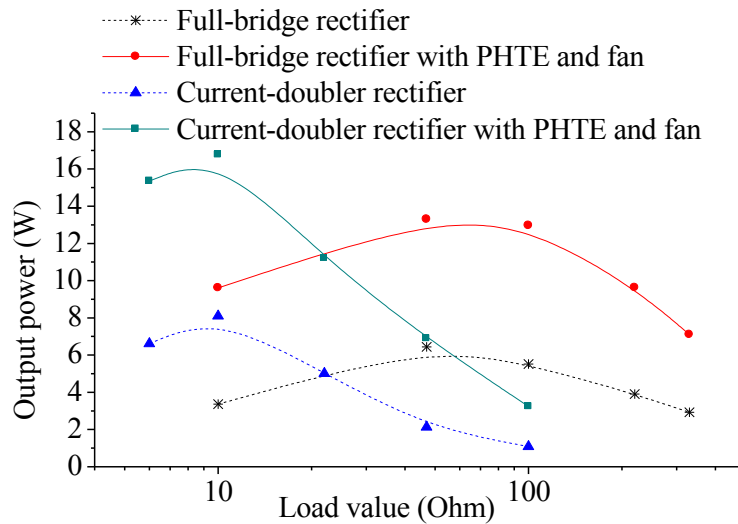
Figure 5-9. Characteristics between loop gain  $\alpha$  and temperatures (a) in optimal load

condition  $R_{CD}^*$  (b) in optimal load condition  $R_{FB}^*$

Figure 5-9 shows that the coefficient  $\alpha$  of the cases without cooling devices is much larger than the other cases in the same temperature condition. Nonlinear resistance  $R_{NL}$  increases with coefficient  $\alpha$ , this result clearly indicates that large coefficient  $\alpha$  leads to high PT losses at the same mechanical current. To increase the output power of PT, the coefficient  $\alpha$  should be decreased by using the cooling devices. In Figure 5-10(a), the experimental results show that the output power of the PT fed



full-wave bridge rectifier with cooling system can move from 6.44 W to 13.29 W at the same temperature (55°C) with 47 Ω load value (optimal load condition  $R_{FB}^*$ ). On the contrary, the output power of the PT fed current-doubler rectifier with cooling system can move from 8.1 W to 16.7 W at the same temperature (55°C) with 10 Ω load value (optimal load condition  $R_{CD}^*$ ). Therefore by using the cooling system, it is feasible to increase the passing current capacity of the PT. Accordingly, the maximum output current and the allowable output power of the PT can be substantially increased without any additional inductors. Considering the low-profile purpose, this kind of design provides a better option for enhancing the output current and performance of the PT-based DC/DC converter comparing to the method applied with current-doubler rectifier. Figure 5-10(b) also shows the design possessed good efficiency (70%+) when the load was varied from 10 to 330 Ω at temperature 55°C (temperature limitation).



(a)

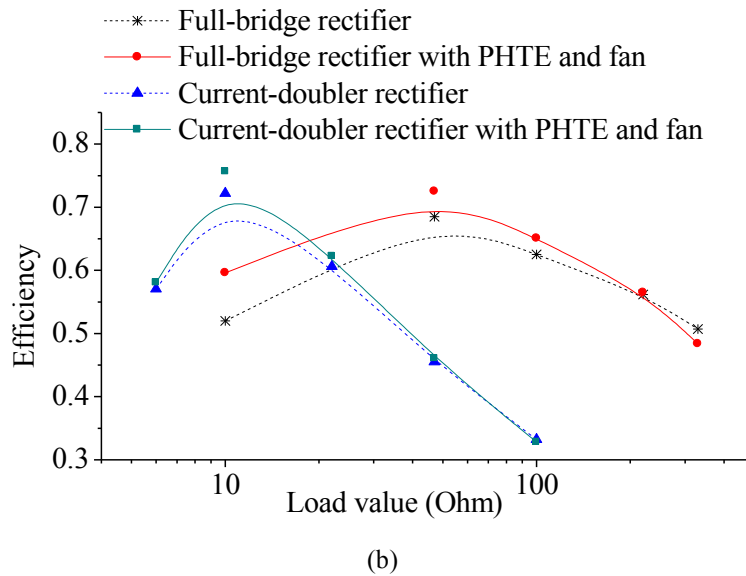


Figure 5-10. (a) Output power enhancement in different heat transfer structures (b) efficiency enhancement in different heat transfer structures

## 5.6 Summary

In this chapter, a cooling system with heat transfer equipment and piezoelectric fan was used to enhance the output power of piezoelectric transformers. According to the experimental results, all specimens remained a satisfactory efficiency even at temperature of 55°C. By applying cooling systems, the ability of heat dissipation becomes better. The PT passing current can be substantially increased under optimal load condition regardless of whether PT connected with full-wave bridge rectifier (*i.e.* from 0.46 A to 0.9 A) or current-doubler rectifier (*i.e.* from 0.74 A to 1.12 A), and thus the maximum output power of the PT-based DC/DC converter (*i.e.* increasing 100 %) at specific temperature. It should be noted that the converter system composed of PT fed full-wave bridge rectifier and cooling devices could satisfy the low-profile requirements and increase the output current (power) at the same time. This study clearly indicates that it is possible to enhance the performance of the piezoelectric transformer by decreasing the loop gain  $\alpha$ . Moreover, the output current of the piezoelectric transformer

in our design also increases, which implies that this technique allows the piezoelectric transformer to be used in low voltage-high current applications.

## Chapter 6 Summary and Conclusion

In this dissertation, we start to utilize the thermal layers consisted of graphite tape and aluminum pad to enhance the output power of a PT. It should be noted that the graphite tape is a perfect layer to decrease contact wear and transfer the heat. According to the experimental results, all specimens retained a satisfactory efficiency even at a temperature of 55°C. Due mainly to the improved ability to dissipate heat by using thermal dissipation layers, the PT passing current can be substantially increased under optimal load conditions instead of just expanding the PT's number of layers. The threshold vibration velocity, as well as the mechanical current, can be improved almost 20% when the condition of PT temperature is kept below 55°C, and thus the highest output power (an increase of 26%).

Based on the successful experimental results above, some cooling methods were used to enhance the output power of PT. According to the experimental results, all specimens kept a satisfactory efficiency even at 55°C. By applying the HTE, the mechanical current of the piezoelectric transformer can increase from 0.382 A at 2 W to 0.972 A at 9 W and the maximum output power of the piezoelectric transformers increase from 3.43 W to 9.29 W at a specific temperature. We also proposed a procedure to derive the equivalent circuit of piezoelectric transformers, especially the temperature-dependent mechanical resistance, under the conditions of high temperature and high power. This study clearly indicates that it is possible to enhance the performance of the PT by decreasing the loop gain  $\alpha(T^\circ)$  value.

Moreover, we present a theoretical-phenomenological model. The model clearly indicates that it is possible to enhance the performance of the PT by decreasing the temperature-dependent nonlinear resistance  $R_{NL}$  value and by increasing the thermal conductance  $Y$  value. This work investigates the temperature build-up problem of PT

and presents a useful method to design the piezoelectric transformers in high power applications.

As to the extension of PT-based DC/DC converter with our cooling method, the PT passing current can be substantially increased under optimal load conditions regardless of whether the PT is connected to a full-wave bridge rectifier (i.e. from 0.46 to 0.9 A) or a current-doubler rectifier (i.e. from 0.74 to 1.12 A), thus obtaining the maximum output power of the PT-based DC/DC converter (i.e. increasing 100%) at a specific temperature. It should be noted that the converter system comprising a PT-fed full-wave bridge rectifier and cooling devices could satisfy the low-profile requirements and increase the output current (power) at the same time. It should be noted that the output current of the piezoelectric transformer in our design also increases, which implies that this technique allows the piezoelectric transformer to be used in low-voltage, high-current applications.

## Chapter 7 The future works

Since the enhancement of PT's mechanical current (output power) can be fully verified by using the cooling method in this dissertation, it implies that this technique allows the piezoelectric transformer to be used in high-current and high-power applications. On the other hand, the utilization of the thermoelectric cooling module can be considered not only as the solution to the issue of temperature rising during operation but also as the thermoelectric generator for low power consumption devices with the inverse effect. Furthermore, as to the suitable design of the output rectifier stage, cooling methods can be extended to the PT-based adaptor/converter. There are several possible applications with different technological aspects, such as:

1. Devices are in great demand on high current level; for instance, the illumination power of the LED is proportional to its forward current and a single LED. That kind of system requires from 2 to 4 VDC and 1A current level. In this dissertation, a method to enhance the mechanical current of PTs was presented.
2. Devices are in great demand on high power level; for instance, there have been some significant advances in step-down PT technology, such as the Noliac ring-type PT. This annular thickness-mode device can achieve power densities of around 50W/cm<sup>3</sup> and output powers of around 50W. Combining the step-down PT technology and the cooling method in this dissertation, the power level must be improved obviously.
3. Design and implementation of thermal energy harvesting device for switching power supplies; for instance, thermoelectric cooling module can be used to collect heat energy and the collected energy will be re-used for the gate driver of the switch to save the energy of the converter.
4. Obtaining the compact and high-power AC-DC adaptor/ DC-DC converter. PT-based technology can be implemented and satisfied the modules for AC-DC adaptor

or fluorescent lamp with the suitable design of output rectifier stage and cooling methods, even the requirement of the high power demand.

## REFERENCE

- [1] Hu, J. (2003). Analyses of the temperature field in a bar-shaped piezoelectric transformer operating in longitudinal vibration mode. *Ultrasonics, Ferroelectrics and Frequency Control, IEEE Transactions on*, 50(6), 594-600.
- [2] J. Yang, "Piezoelectric transformer structural modeling—A review," *IEEE Trans. Ultrason. Ferroelectr. Freq. Control*, vol. 54, no. 6, pp.1154–1170, 2007.
- [3] A. M. Flynn and S. R. Sanders, "Fundamental limits on energy transfer and circuit considerations for piezoelectric transformers," *IEEE Transactions on Power Electronics*, vol. 17, pp. 8-14, 2002.
- [4] R. C. Buchanan, R. W. Schwartz, J. Ballato, and G. H. Haertling, *Ceramic Materials for Electronics*, (chapter 4), 3rd ed: Marcel Dekker Inc., 2004.
- [5] K. Uchino, J. H. Zheng, Y. H. Chen, X. H. Du, J. Ryu, Y. Gao, S. Ural, S. Priya, and S. Hirose, "Loss mechanisms and high power piezoelectrics," *Journal of Materials Science*, vol. 41, pp. 217-228, 2006.
- [6] Weisshaar, T. A., & Ehlers, S. M. (1990, April). Static aeroelastic behavior of an adaptive laminated piezoelectric composite wing. In *Proceedings of the 31st Structures, Structural Dynamics, and Materials Conference* (pp. 1611-1623).
- [7] Wang, B. L., & Mai, Y. W. (2003). Thermal shock fracture of piezoelectric materials. *Philosophical Magazine*, 83(5), 631-657.
- [8] Zhang, T. Y., & Gao, C. F. (2004). Fracture behaviors of piezoelectric materials. *Theoretical and applied fracture mechanics*, 41(1), 339-379.
- [9] Wang, D., Fotinich, Y., & Carman, G. P. (1998). Influence of temperature on the electromechanical and fatigue behavior of piezoelectric ceramics. *Journal of applied physics*, 83(10), 5342-5350.



- [10] S. Hirose, M. Aoyagi, Y. Tomikawa, S. Takahashi, and K. Uchino, "High power characteristics at antiresonance frequency of piezoelectric transducers," *Ultrasonics*, vol. 34, no. 2–5, pp. 213–217, 1996.
- [11] K. Uchino, J. Zheng, A. Joshi, Y.-H. Chen, S. Yoshikawa, S. Hirose, S. Takahashi, and J. W. C. de Vries, "High power characterization of piezoelectric materials," *J. Electroceram.*, vol. 2, no. 1, pp. 33–40, 1998.
- [12] K. Uchino and S. Hirose, "Loss mechanisms in piezoelectrics: How to measure different losses separately," *IEEE Trans. Ultrason. Ferroelectr. Freq. Control*, vol. 48, no. 1, pp. 307–321, 2001.
- [13] M. C. Do, *Piezoelectric Transformer Integration Possibility in High Power Density Applications*: TUDpress Verlag der Wiss., 2008.
- [14] Y. P. Liu, D. Vasic, W. J. Wu, F. Costa and C. K. Lee, 2009 Design of fixed-frequency controlled radial-mode stacked disk-type piezoelectric transformers for DC/DC converter application *Smart Materials and Structures* 18(8) 085025
- [15] N Dai, A W Lofti, G Skutt, W Tabisz and F C Lee 1994 A comparative study of high-frequency, low-profile planar transformer technologies in *Proc. IEEE APEC'94*, pp. 226–232
- [16] Y P Liu, D Vasic and F Costa 2012 Wideband ZVS half-bridge circuit for piezoelectric transformers with small inductance *Electronics Letters* 48 523-25
- [17] D Vasic, Y P Liu, D Schwander, F Costa and W J Wu 2013 Improvement of Burst-Mode Control of Piezoelectric Transformer-based DC/DC Converter *Smart Materials & Structures*, 22(5)
- [18] Y P Liu, D Vasic, F Costa and W J Wu 2010 Electromagnetic Interferences Analysis of DC/DC Converters Based on Piezoelectric Transformers *Japanese*

*Journal of Applied Physics* 49(6) 061501

- [19] D Vasic, F Costa and E Sarraute 2006 Piezoelectric Transformer for Integrated MOSFET & IGBT Gate Driver *IEEE Trans. on Power Electron.* 21 56-65
- [20] Richards, C. D., Anderson, M. J., Bahr, D. F., & Richards, R. F. (2004). Efficiency of energy conversion for devices containing a piezoelectric component. *Journal of Micromechanics and Microengineering*, 14(5), 717.
- [21] T Yamane, S Hamamura, T Zaitzu, T Minomiya, M Shoyama and Y Fuda 1998 Efficiency improvement of piezoelectric-transformer DC-DC converter in *Power Electronics Specialists Conference, 1998. PESC 98 Record. 29th Annual IEEE*, pp. 1255-1261 vol. 2
- [22] G Ivensky, S Bronstein and S Ben-Yaakov 2004 A comparison of piezoelectric transformer AC/DC converters with current doubler and voltage doubler rectifiers *IEEE Trans. on Power Electron.* 19 1446-53
- [23] D D Ebenezer, D Thomas and S M Sivakumar 2007 Non-uniform heat generation in rods with hysteretic damping *Journal of Sound and Vibration* 302 892-902
- [24] N Wakatsuki, Y Kagawa, K Suzuki and M Haba 2003 Temperature-frequency characteristics simulation of piezoelectric resonators and their equivalent circuits based on three-dimensional finite element modeling *Int. J. Numerical Modeling: Electron. Networks, Devices Fields* 16 479-492
- [25] H W Joo, C H Lee, J S Rho and H K Jung 2006 Analysis of temperature rise for piezoelectric transformer using finite-element method *IEEE Trans. Ultrason. Ferroelectr. Freq. Control* 53 1449-57
- [26] D Thomas, D D Ebenezer and S M Srinivasan 2010 Power dissipation and temperature distribution in piezoelectric ceramic slabs *J. Acoust. Soc. Am.* 128(7) 1700–1711

- [27] A Albareda, P Gonnard, V Perrin, R Briot and D Guyomar 2000 Characterization of the mechanical nonlinear behavior of piezoelectric ceramics *IEEE Trans. Ultrason. Ferroelectr. Freq. Control* 47 844-53
- [28] K Insung, K Minsoo, J Soonjong, S Jaesung and T Vo Viet 2011 Piezotransformer with ring-dot-shape for easy heat radiation and high efficiency power,” in *Int. Symp. Applications of Ferroelectrics and Int. Symp. Piezoresponse Force Microscopy and Nanoscale Phenomena in Polar Materials*, 2011, pp. 1–6.
- [29] W W Shao, L J Chen, C L Pan, Y B Liu and Z H Feng 2012 Power density of piezoelectric transformers improved using a contact heat transfer structure *IEEE Trans. Ultrason. Ferroelectr. Freq. Control* 59 3-81
- [30] Y H Su, Y P Liu, D Vasic, W J Wu, F Costa and C K Lee 2012 Power Enhancement of Piezoelectric Transformers by Adding Heat Transfer Equipment *IEEE Trans. Ultrason. Ferroelectr. Freq. Control* 59(10) 2129-2136
- [31] Su, Y. H., Liu, Y. P., Vasic, D., Costa, F., Wu, W. J., & Lee, C. K. (2013). Study of a piezoelectric transformer-based DC/DC converter with a cooling system and current-doubler rectifier. *Smart Materials and Structures*, 22(9), 095005.
- [32] Gautschi, G. (2002). *Piezoelectric sensorics: force, strain, pressure, acceleration and acoustic emission sensors, materials and amplifiers*. Springer.
- [33] R. C. Buchanan, R. W. Schwartz, J. Ballato, and G. H. Haertling, *Ceramic Materials for Electronics, (chapter 4)*, 3rd ed: Marcel Dekker Inc., 2004.
- [34] Zhang, S., Xia, R., Lebrun, L., Anderson, D., & Shrout, T. R. (2005). Piezoelectric materials for high power, high temperature applications. *Materials letters*, 59(27), 3471-3475.
- [35] Cao, W., Zhu, S., & Jiang, B. (1998). Analysis of shear modes in a piezoelectric vibrator. *Journal of applied physics*, 83(8), 4415-4420.

- [36] E L Horsley, M P Foster and D A Stone 2007 State-of-the-art Piezoelectric Transformer technology *In Proc. European Conference on Power Electronics and Applications 2007*, pp. 1-10
- [37] D. Guyomar, C. Magnet, E. Lefeuvre, and C. Richard, "Power capability enhancement of a piezoelectric transformer," *Smart Materials and Structures*, vol. 15, pp. 571-580, 2006.
- [38] S. Ben-Yaakov and S. Lineykin, "Maximum power tracking of piezoelectric transformer HV converters under load variations," *Power Electronics, IEEE Transactions on*, vol. 21, pp. 73-78, 2006.
- [39] I. Kartashev, T. Vontz, and H. Florian, "Regimes of piezoelectric transformer operation," *Measurement Science and Technology*, vol. 17, pp. 2150-2158, 2006.
- [40] R. L. Lin, "Piezoelectric Transformer Characterization and Application of Electronic Ballast (PhD Thesis)," Virginia Polytechnic Institute and State University, 2001.
- [41] A. V. Carazo, "50 Years of piezoelectric transformers. Trends in the technology," presented at Materials Research Society Symposium, Boston, MA, United States, 2003.
- [42] APC International Ltd., "Piezoelectric Constants."  
"[http://www.americanpiezo.com/piezo\\_theory/piezoelectric\\_constants.html](http://www.americanpiezo.com/piezo_theory/piezoelectric_constants.html)
- [43] R. C. Buchanan, R. W. Schwartz, J. Ballato, and G. H. Haertling, *Ceramic Materials for Electronics, (chapter 4)*, 3rd ed: Marcel Dekker Inc., 2004.
- [44] P. Laoratanakul and K. Uchino, "Designing a radial mode laminated piezoelectric transformer for high power applications," presented at IEEE International Symposium on Applications of Ferroelectrics, 2005.
- [45] S. Priya, H. Kim, S. Ural, and K. Uchino, "Erratum: High power universal

piezoelectric transformer (IEEE Transactions on Ultrasonics, Ferroelectrics and Frequency Control (Jan. 2006) 53:1 (23-29)), *IEEE Transactions on Ultrasonics, Ferroelectrics, and Frequency Control*, vol. 53, pp. 810-816, 2006.

- [46] K. Brebøl, "Piezoelectric Transformer," *U.S. Patent 6,707,235*, 2004.
- [47] J. Du, J. Hu, and K. J. Tseng, "High-power, multioutput piezoelectric transformers operating at the thickness-shear vibration mode," *IEEE Transactions on Ultrasonics, Ferroelectrics, and Frequency Control*, vol. 51, pp. 502-509, 2004.
- [48] J. S. Yang and X. Zhang, "Analysis of a thickness-shear piezoelectric transformer," *International Journal of Applied Electromagnetics and Mechanics*, vol. 21, pp. 131-141, 2005.
- [49] O.M.Stuetzer, Sandia Laboratory Report No. SC-RR-66-414.
- [50] T.Zaitso, T.Inoue, O.Ohnishi, A.Iwamoto, *2MHz Power Converter with Piezoelectric Ceramic Transformer*, Proc. of IEEE INTELEC, (1992).
- [51] O.Ohnishi, H.Kishie, A.Iwamoto, Y.Sasaki, T.Zaitso, T.Inoue, *Piezoelectric Ceramic Transformer Operating in Thickness Extensional Vibration Mode for Power Supply*, Ultrasonics Symp. Proc., pp. 483-488 (1992).
- [52] T.Zaitso, O.Ohnishi, T.Inoue, M.Shoyama, T.Ninomiya, F.C.Lee, and G.C.Hua, *Piezoelectric Transformer operating in Thickness Extensional Vibration and Its Application to Switching Converter*, IEEE PESC Record, (1994).
- [53] T.Inoue, O.Ohnishi, N.Ohde, U.S. Patent No. 5,118,982 (June 1992).
- [54] Y.Sasaki, K.Uehara, T.Inoue, U.S. Patent 5,241,236 (August 1993).
- [55] T.Zaitso, Y.Fuda, Y.Okabe, T.Ninomiya, S.Hamamura, M.Katsuno, *New Piezoelectric Converter for AC-adapter*, (IEEE APEC'97 Proc., 2, Feb. 1997) pp. 568-572.
- [56] S.Hamamura, T.Zaitso, T.Ninomiya, M.Shoyama, *Noise Characteristics of*

*Piezoelectric-Transformer DC-DC Converter*, (IEEE PESC'98 Record, May 1998) pp. 1262-1267.

- [57] S-J.Choi, K-C.Lee, B.H.Cho, *Design of Fluorescent Lamp Ballast with PFC using a Power Piezoelectric Transformer*, (IEEE Ultrasonic Symposium Proc., 1998) pp. 1135-1141.
- [58] R.P.Bishop, U.S. Patent 5,834,882 (1998).
- [59] J.A.Martin, M.J.Prieto, F.Nuño, J.Diaz, *A new full-protected control mode to drive piezoelectric transformers in DC-DC converters*, (PESC Proc., 2001).
- [60] Liu, Y. P. (2009). *Conception et mise en oeuvre de dispositifs de puissance utilisant des matériaux piézoélectriques* (Doctoral dissertation, École normale supérieure de Cachan-ENS Cachan).
- [61] Lin, C. Y. (1997). *Design and analysis of piezoelectric transformer converters* (Doctoral dissertation).
- [62] Chou, I. M., Lai, Y. Y., Wu, W. J., & Lee, C. K. (2011, March). Dependency of working temperature and equivalent constant of concentric disk-type piezoelectric transformer. In *SPIE Smart Structures and Materials+ Nondestructive Evaluation and Health Monitoring* (pp. 79771X-79771X). International Society for Optics and Photonics.
- [63] G. Ivensky, I. Zafrany, and S. S. Ben-Yaakov, "Generic operational characteristics of piezoelectric transformers," *IEEE Transactions on Power Electronics*, vol. 17, pp. 1049-1057, 2002.
- [64] Y Sasaki, M Umeda, S Takahashi, M Yamamoto, A Ochi and T Inoue 2001 High-Power Characteristics of Multilayer Piezoelectric Ceramic Transducers *Japanese Journal of Applied Physics* 40 5743-46
- [65] R. Prieto, M. Sanz, J. Cobos, P. Alou, O. Garcia, and J. Uceda, "Design

considerations of multi-layer piezoelectric transformers," in *Applied Power Electronics Conference and Exposition, 2001. APEC 2001. Sixteenth Annual IEEE*, 2001, pp. 1258-1263.

- [66] Ju, B., Shao, W., Pan, C., & Feng, Z. (2013). Polypropylene membrane decreases contact wear of piezoelectric transformer with heat transfer structure. *Electronics Letters*, 49(10), 650-651.
- [67] W. W. Shao, Z. H. Feng, J. W. Xu, C. L. Pan, and Y. B. Liu, "Radiator heightens power density of piezoelectric transformers," *Electronics Letters*, vol. 46, pp. 1662-1663.
- [68] Alonso, J. M., C. Ordiz, et al. (2008). "A novel control method for piezoelectric-transformer based power supplies assuring zero-voltage-switching operation." *IEEE Transactions on Industrial Electronics* 55(3): 1085-1089.
- [69] N. Wakatsuki, Y. Kagawa, K. Suzuki, and M. Haba, Temperature-frequency characteristics simulation of piezoelectric resonators and their equivalent circuits based on three-dimensional finite element modeling, *Int. J. Numerical Modeling: Electron. Networks, Devices Fields* 16 (2003), 479–492
- [70] H. W. Joo, C. H. Lee, J. S. Rho, and H. K. Jung, Analysis of temperature rise for piezoelectric transformer using finite-element method, *IEEE Trans. Ultrason. Ferroelectr. Freq. Control* 53 (2006), 1449-1457
- [71] N. Liu, J. Yang, F. Jin, Transient thickness-shear vibration of a piezoelectric plate of monoclinic crystals, *International Journal of Applied Electromagnetics and mechanics* 38(1) (2012), 27-37
- [72] B. Liu, Q. Jiang, J. Yang, Frequency shifts in a quartz plate piezoelectric resonator in contact with a viscous fluid under a separated electrode, *International Journal of Applied Electromagnetics and mechanics*, 35(3) (2011), 177-187

- [73] T. Rajesh, V. Benjamin and V. Ramamoorthy, Heat Generation from Dielectric Loss and Vibration using COMSOL Multiphysics, *Proc. of COMSOL Bangalore Conference*, (2010)
- [74] C S Moo, W M Chen and H K Hsieh 2003 Electronic ballast with piezoelectric transformer for cold cathode fluorescent lamps *Electric Power Applications, IEE Proceedings* 150 278-82
- [75] W C Su and C L Chen 2008 ZVS for PT Backlight Inverter Utilizing High-Order Current Harmonic *IEEE Trans. on Power Electron.* 23 4-10
- [76] S Gab-Su and C Bo-Hyung 2011 Multilayer piezoelectric transducer design guidelines for low profile magnetic-less DC/DC converter in *Power Electronics and ECCE Asia (ICPE & ECCE), 2011 IEEE 8th International Conference on*, pp. 972-976
- [77] Y.P. Liu, D. Vasic, F. Costa, W.J. Wu, and C.K. Lee, "Design Considerations of Piezoelectric Transformers with Voltage-Mode Rectifiers for DC/DC Converter Application," in *Industrial Electronics, 2008. 34th Annual Conference of IEEE*, 2008, pp. 665-670.